Oncology and Translational Medicine

Volume 8 • Number 4 • August 2022

Oncology and Translational Medicine Volume 8 • Number 4 • August 2022 pp 155-208

邮发代号：38-121
ISSN 2095-9621

GENERAL INFORMATION
≫otm.tjh.com.cn

ISSN 2095-9621
CN 42-1865/R

Oncology and Translational Medicine

肿瘤学与转化医学（英文）

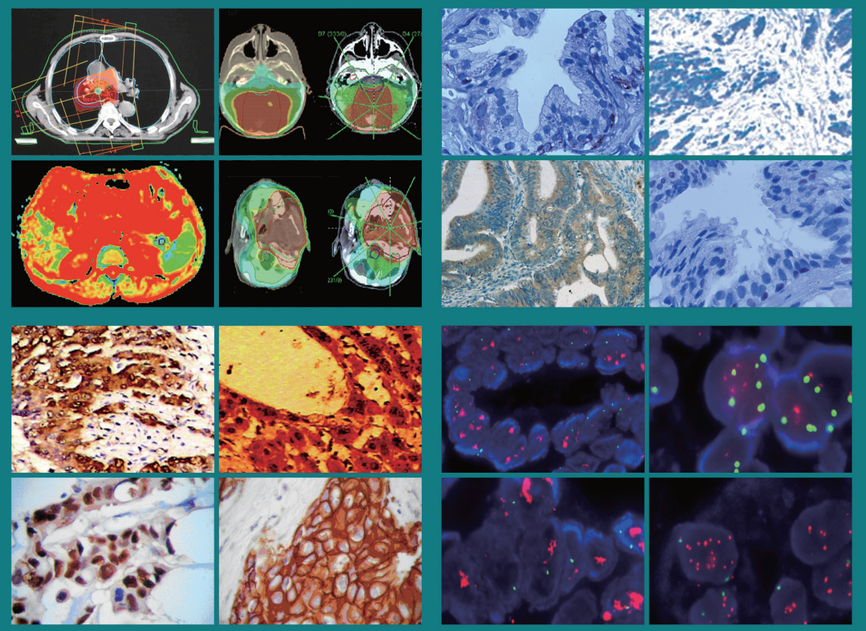

Volume 8
Number 4
August 2022

Oncology and Translational Medicine

Oncology and Translational Medicine
August 2022 Volume 8 Number 4

Contents

Oncology and Translational Medicine

Volume 8 • Number 4 • August 2022

Aims & Scope

Oncology and Translational Medicine is an international professional academic periodical. The Journal is designed to report progress in research and the latest findings in domestic and international oncology and translational medicine, to facilitate international academic exchanges, and to promote research in oncology and translational medicine as well as levels of service in clinical practice. The entire journal is published in English for a domestic and international readership.

Copyright

Supervised by

Ministry of Education of the People's Republic of China.

Administered by

Tongji Medical College, Huazhong University of Science and Technology.

Submission information

Manuscripts should be submitted to:
http://otm.tjh.com.cn
dmedizin@sina.com

Subscription information

ISSN edition: 2095-9621
CN: 42-1865/R

■ Subscription rates
Subscription may begin at any time. Remittances made by check, draft or express money order should be made payable to this journal. The price for 2022 is as follows: US $ 30 per issue; RMB ￥28.00 per issue.

Database

Oncology and Translational Medicine is abstracted and indexed in EMBASE, Index Copernicus, Chinese Science and Technology Paper Citation Database (CSTPCD), Chinese Core Journals Database, Chinese Journal Full-text Database (CJFD), Wanfang Data; Weipu Data; Chinese Academic Journal Comprehensive Evaluation Database.

Business correspondence

All matters relating to orders, subscriptions, back issues, offprints, advertisement booking and general enquiries should be addressed to the editorial office.

Mailing address
Editorial office of
Oncology and Translational Medicine
Tongji Hospital
Tongji Medical College
Huazhong University of Science and Technology
Jie Fang Da Dao 1095
430030 Wuhan, China
Tel.: +86-27-69378388
Email: dmedizin@sina.com

Printer
Changjiang Spatial Information Technology Engineering Co., Ltd. (Wuhan) Hangce Information Cartorgraphy Printing Filial, Wuhan, China
Printed in People's Republic of China

Editors-in-Chief

Managing director

Executive editors

Oncology and Translational Medicine
DOI 10.1007/s10330-021-0534-4
August 2022, Vol. 8, No. 4, P155–P164

ORIGINAL ARTICLE

Radiosensitization by microRNA30a-5p in a nude mouse model with subcutaneous lung-cancer xenograft*

Yuyan Guo[1], Yingtao Cui[1], Xing Bao[1], Yue Ke[1], Hongtao Ren[1], Jiyuan Pan[1], Liping Song[2], Hongbing Ma[1] (✉)

[1] Department of Radiation Oncology, the Second Affiliated Hospital of Xi'an Jiaotong University, Xi'an 710004, China
[2] Department of Radiation Oncology, the First Affiliated Hospital of Xi'an Jiaotong University, Xi'an 710061, China

Abstract

Objective We aimed to observe the radiosensitization effect of mir-30a-5p in a nude mouse model with subcutaneous lung-cancer xenograft and to explore the underlying mechanism.

Methods A549 cell lines with either stable upregulation or downregulation of mir-30a-5p, and their negative control, were transfected with lentivirus vectors. These cell lines were used to establish a nude mouse model with subcutaneous lung-cancer xenograft. Each group was randomly divided into irradiated and non-irradiated groups. The radiosensitization effect of mir-30a-5p *in vivo* was studied by observing xenograft growth trends and tumor weight. The mechanisms involved in this radiosensitization were investigated by detecting expressed radiosensitization-related proteins, using immunohistochemistry and Western blotting.

Results The expression level of mir-30a-5p in the lenti-mir-30a-5p group was higher than that in the negative control (lenti-GFP) group and lower in the lenti-inhibitor group ($P < 0.05$). Subcutaneous lung-cancer xenografts in the irradiation group and lenti-mir-30a-5p increased in size slowly; tumors were lighter and tumor inhibition rates were higher than those in the non-irradiation and lenti-GFP groups. In contrast, the opposite of these effects was observed in the lenti-inhibitor group. Immunohistochemistry and Western blotting indicated that ATM protein expression level was lower in the lenti-mir-30a-5p group, with or without irradiation, compared to that in the lenti-GFP group. ATM protein levels were higher in the lenti-inhibitor groups. The phosphorylation level of ATM at residue 1981 was low in the groups without irradiation and increased significantly after irradiation ($P < 0.05$). Moreover, the phosphorylation level was lower in the lenti-mir-30a-5p group and higher in the lenti-inhibitor group than that in the lenti-GFP group after irradiation ($P < 0.05$).

Conclusion Mir-30a-5p enhanced the radiosensitivity of nude mice with subcutaneous lung-cancer xenografts by inhibiting ATM phosphorylation.

Key words: Mir-30a-5p; subcutaneous xenografts; radiosensitization; ATM

Received: 15 November 2021
Revised: 2 April 2022
Accepted: 21 May 2022

Lung cancer is one of the most common malignant tumors worldwide, of which approximately 80% are non-small cell lung cancer (NSCLC) [1]. Radiotherapy is one of the primary treatments for NSCLC however, radioresistance is common during the treatment of NSCLC. This leads to a local recurrence rate up to 60%–70% and makes it difficult to achieve the expected curative effect [2]. Therefore, reducing the radioresistance of NSCLC, thereby increasing its radiosensitivity, is the key issue [3]. Various factors could be involved in regulating the radiosensitivity of cancer, such as DNA damage and repair (DDR) [4], cell cycle arrest [5], apoptosis [6], cancer stem cells

✉ Correspondence to: Hongbing Ma. Email: mhbxian@126.com
* Supported by the National Science Fund Project (No. 81872471) of the National Natural Science Foundation of China and the Science Foundation of the Second Affiliated Hospital of Xi'an Jiaotong University (No. YJ(QN)202025).

[7], autophagy [8], immunity [9–10]. Additionally, classical cell signaling pathways may be involved, including ataxia telangiectasia mutated (ATM) signal pathway [11], PI3K/AKT (phosphoinositide 3-kinase/AKT serine/threonine kinase), mitogen-activated protein kinase/extracellular regulated protein kinases (MAPK/ERK), and transforming growth factor-beta (TGF-β) signaling pathways [12–13].

Notably, microRNAs play roles in radiosensitization and can affect the radiosensitivity of cancer by modulating a variety of molecules that are involved. These molecules include DNA-dependent protein kinase catalytic subunit (DNA-PKcs), ATM [14], H2AX variant histone (H2A.X), mediator of DNA damage checkpoint 1 (MDC1), epidermal growth factor receptor (EGFR), AKT, and breast cancer susceptibility gene 1 (BRCA1) [11].

Further, mir-30a is downregulated in both NSCLC tissues and cell lines, and that it could influence cell proliferation [15], migration, invasion [16], apoptosis [17], phosphorylation, and participates in mitogen-activated protein kinase (MAPK), TGF-β, PI3K/AKT, and other pathways [11, 13]. In a previous study by our group, we found that mir-30a-5p can enhance the radiosensitivity of lung cancer cells A549 by down-regulating activating transcription factor 1 (ATF1) *in vitro* [18]. We conducted this study to further explore if mir-30a-5p can also function as a radiosensitizer *in vivo*.

Materials and methods

Animal culture

A total of 36 SPF-grade 3–5-week-old male nude mice, weighing approximately 13–20 g, were housed at a temperature of 22–24 °C and a relative humidity of 50%–70%. All the nude mice were provided by the Animal Experimental Center of the Medical Department of Xi'an Jiaotong University, China.

Cell lines and main reagents

Human lung adenocarcinoma cell line A549 and human renal epithelial cell line 293T were donated by the Transformation Center Laboratory of the First Affiliated Hospital of the Medical Department of Xi'an Jiaotong University, China. The main reagents were as follows: mir-30a-5p u vector pGMLV-MA2 and mir-30a-5p downregulation vector pGMLV-MI7 (GenePharma, Shanghai, China), QIAprep Spin Miniprep Kit (QIAGEN, Shanghai, China), T4 DNA ligase (Fermentas, USA), T4 DNA ligase buffer (Fermentas, USA), BamHI (Fermentas, USA), XhoI (Fermentas, USA), Express miRNA Extraction Kit (HaiGene CN, China), PrimeScript™ RT Master Mix (TaKaRa, Japan), Mir-X™ miRNA First-Strand Synthesis Kit (TaKaRa, Japan), SYBR Premix Ex Taq™ II (TaKaRa, Japan), SP immunohistochemical kit (Beijing Zhongshan Jinqiao Biotechnology Co. Ltd., China), and rabbit anti-goat SP kit (BOSTER Biological Technology Co. Ltd., China).

Cell culture

The human lung adenocarcinoma cell lines A549, A549 with mir-30a-5p overexpression, A549 (with mir-30a-5p downregulation) and a control cell line were cultured in RPMI-1640 medium and 293T cell line in DMEM containing 10% fetal bovine serum. The cells were incubated at 37 °C and 5% CO_2.

Lentiviral infection

Primers were synthesized to amplify the pri-miRNA sequence has-mir-30a 5'-primer: 5'-GTG TAA ACA TCC TCG ACT GGA AG-3' (Sangon Biotech, Shanghai, China), and genomic DNA was used as a template. Single-stranded DNA oligomers were synthesized with interference sequences to inhibit the processing of mir-30a-5p (Table 1) and miRNA-inhibitor primer sequences (Table 2) were synthesized by Sangon Biotech (Shanghai, China). The enzyme-digested DNA was directly connected to the lentiviral vector through the end of the endonuclease site BamH1 and Xho1. The lentiviral vector and packaging plasmid were co-transfected into 293T cells for lentiviral packaging. The original virus solution was diluted with culture medium containing 5 μg/mL polybrene, according to the appropriate MOI value. A549 cells were infected for 48 h, fluorescence was observed, and the infection

Table 1 pri-miR primer sequence

Name	Sequence
6235-F (XhoI)	5'-CCGCTCGAGCGGTAGTCTAAGTTCACTCAACTGCA-3'
6235-R (BamHI)	5'-CCGGGATCCCTGGGAAATATTGCCCTACTACG-3'

Table 2 miRNA-inhibitor primer sequence

Name	Sequence
hsa-mir-30a-inhibitor-T (BamHI)	5'-gatccGACGGCGCTAGGATCATCAACCTTCCAGTCGAGATCTGATGTTTACACAAGTATTCTGGTC ACAGAATACAACCTTCCAGTCGAGATCTGATGTTTACACAAGATGATCCTAGCGCCGTCTTTTTTg-3'
hsa-mir-30a-inhibitor-B (EcoRI)	5'-aattcAAAAAAGACGGCGCTAGGATCATCTTGTGTAAACATCAGATCTCGACTGGAAGGTTGTATTC TGTGACCAGAATACTTGTGTAAACATCAGATCTCGACTGGAAGGTTGATGATCCTAGCGCCGTCg-3'

efficiency of A549 cells was estimated.

qRT-PCR

The total RNA from cells in each group was extracted using the Express miRNA Extraction Kit (HaiGene China), according to the manufacturer's instructions. Using mRNA as a template, random primers or oligo (dT) were used to reverse transcribe cDNA. Hsa-mir-30a-5p gene sequence was queried in NCBI (GenBank No. MI0000088) and used to design primers for qRT-PCR, using Primer version 5.0 (PREMIER Biosoft International, Palo Alto, CA, USA), and synthesized by Sangon Biotech (Shanghai, China): has-mir-30a 5'-primer: 5'-GTG TAA ACA TCC TCG ACT GGA AG-3'. The expression of mir-30a-5p was detected using qRT-PCR.

Establishment of subcutaneous xenograft model

The lenti-mir-30a, lenti-inhibitor, or lenti-GFP vectors were used to infect A549 cell lines in logarithmic phase, at a final concentration of 5×10^7 cells/mL. The cells were mixed with Matrigel at a 1:1 ratio on ice. Nude mice were randomly divided into three groups, with 12 mice in each group, and injected with lenti-mir-30a A549 cells, lenti-inhibitor A549 cells, or lenti-GFP A549 cells. This was conducted subcutaneously, on the back of each nude mouse, with 0.2 mL cell suspensions. Tumorigenesis was observed every other day, and vital signs, body weight, and tumor size of nude mice were recorded.

Irradiation

When the tumor size was approximately 1.0 cm^3, the nude mice in each treatment group were randomly divided into radiation and non-radiation groups. Nude mice in the radiation group were given a total of 10 Gy 4 MV X-ray radiation at 200 cGy/d for 5 consecutive days. After irradiation, the tumor volume was measured ($V = a^2 \times b / 2$), the growth and metastasis of the tumor were observed, the nude mice were weighed every day, vital observed, and the tumor growth curves drawn. After observation, the nude mice were sacrificed, tumor tissues removed, and the tumor volume measured. Tumor tissues were fixed in 4% polyformaldehyde solution, then embedded in paraffin, and sections cut.

Immunohistochemistry

First, hematoxylin and eosin (H&E) staining was performed. Immunohistochemical staining of the paraffin sections was performed using the streptavidin-peroxidase binding method. Put the paraffin sections into a 60 °C constant temperature drying oven for 60 minutes. Then placing the sections in xylene to dewaxing. Dehydrating the paraffin sections through decreasing concentrations of ethanol, and washing in PBS. Immunostaining was undertaken using the antibodies against ATM (1:200) (Abcam) and ATM (phospho S1981) (4 μg/mL)(Abcam). The sections were placed in a humid chamber and incubated with goat serum for 15 min at 37 °C. The primary antibody was applied to the tissue sections and incubated overnight at 4 °C before incubating with the secondary antibody at 37 °C for approximately 30 min. DAB chromogenic solution (WanleiBio, China) was used to develop the color, according to the manufacturer's instructions. The sections were counter-stained via re-dyeing with hematoxylin, soaked in 1% ammonia water, dehydrated with gradient alcohol, cleared with xylene, and sealed with neutral gum seal. Microscope observation showed that ATM protein was located in the nucleus or cytoplasm. Three fields on each section were randomly selected under 400 × magnification, and the expression intensity was semi-quantitatively analyzed using IPP 6.0 image analysis software (Media Cybernetics, Georgia Avenue, USA). The expression intensity, was expressed as the average optical density value, was defined as the integrated optical density (IOD)/cumulative area.

Western blotting

Small pieces of tumor tissue were placed in protein extraction reagent (RIPA and protease inhibitors at 50:1). The tissue was homogenized at low speed until it was fully homogenized. The supernatant protein was extracted and quantified, according to the instructions of BCA protein quantitative kit. Proteins were separated according to size, by sodium dodecyl sulfate polyacrylamide gel electrophoresis. The protein was then immobilized on PVDF membrane by electroblotting before blocking to prevent non-specific protein binding. The target proteins were probed by incubating with specific primary antibodies for 12 to 16 h at 4 °C followed by incubation with a secondary antibody for 1 h at 37 °C. The antigen/antibody binding signal was then detected, using a Bio-Rad imaging system, to analyze the densitometry of the protein bands.

Ethical statement

Animal experiments were performed in accordance with the ethical guidelines for experimental animals of the Department of Medicine, Xi'an Jiaotong University, China.

Statistical analysis

All data were analyzed using SPSS 21.0 (IBM, USA), and the results are expressed as mean ± SEM. The enumeration data were analyzed by χ^2 test or Fisher's exact test, and the measurement data were tested using the group t-test. Statistical significance was set at $P < 0.05$.

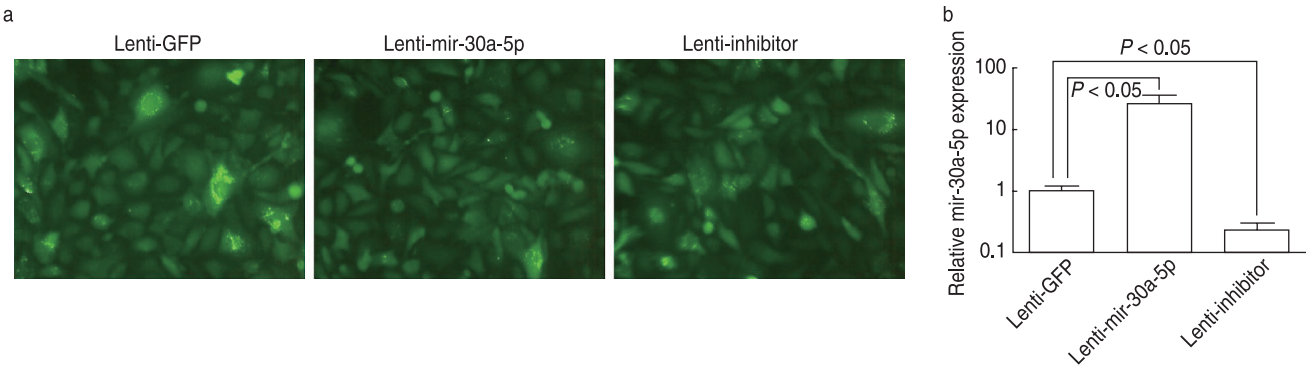

Fig. 1 Expression of mir-30a-5p in the lentivirus stable transfected A549 cell lines. (a) Green fluorescence expression (×400); (b) qRT-PCR results for expression of mir-30a-5p

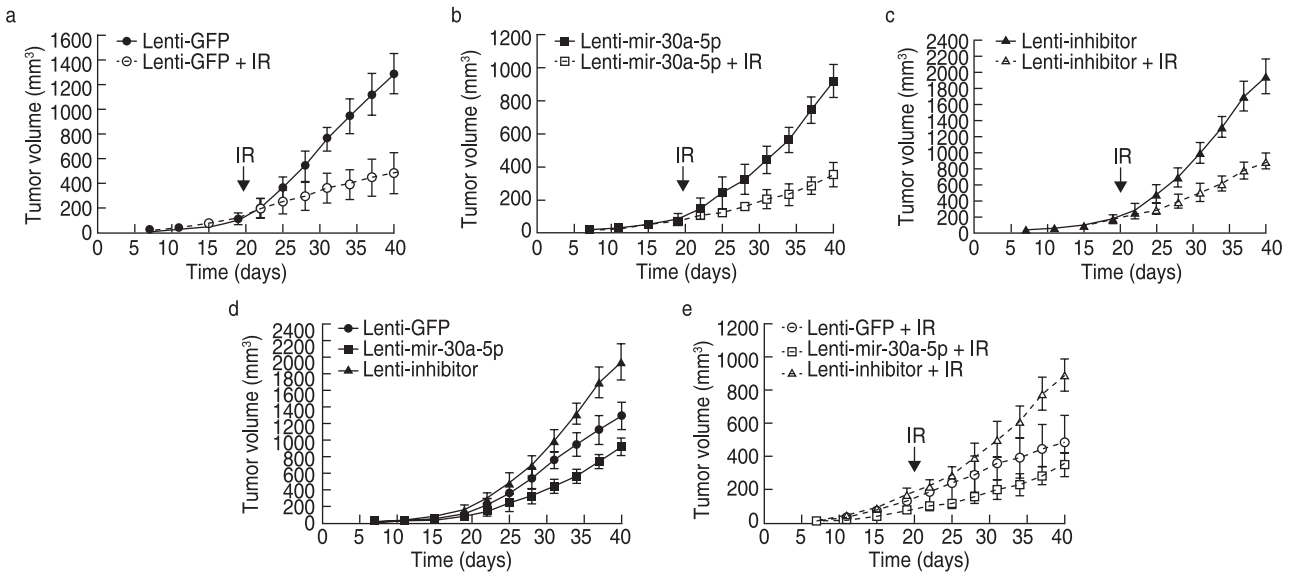

Fig. 2 Subcutaneous xenograft growth curve in different groups. (a) Lenti-GFP vs. Lenti-GFP + IR; (b) Lenti-mir-30a-5p vs. lenti-mir-30a-5p + IR; (c) Lenti-inhibitor vs. lenti-inhibitor + IR; (d) The three groups without irradiation; (e) The three groups with irradiation. IR: irradiation

Results

Lentivirus stable infected A549 cell lines were successfully constructed

The presence of green fluorescence was assessed under a fluorescence microscope (Fig. 1a). The qRT-PCR results showed that the expression level of mir-30a-5p in the lenti-mir-30a-5p group was higher than that in the lenti-GFP group ($P < 0.05$). The expression level of mir-30a-5p in the lenti-inhibitor group was lower than that in the lenti-GFP group ($P < 0.05$). This demonstrated that the lentivirus stably infected A549 cell lines with mir-30a-5p overexpression and downregulation were successfully constructed (Fig. 1b).

Radiosensitization effect of mir-30a-5p in nude mice with subcutaneous lung-cancer xenograft

The tumor volume in the different treatment groups was measured, and the tumor growth curves were drawn (Fig. 2). The results showed that when irradiation began, the volume growth trend of subcutaneous xenografts became slower, and all growth curves became smoother than those in the non-irradiated groups (Fig. 2a–2c). The volume growth trend of subcutaneous xenografts was slower, and the growth curve was smoother in the lenti-mir-30a-5p group than in the lenti-GFP group, with or without irradiation (Fig. 2d–2e). In contrast, in the lenti-inhibitor group, tumors grew faster, and the growth curve was steeper than that in the lenti-GFP group (Fig. 2d–2e).

The tumor weights in the irradiated groups were lower than those in the non-irradiated groups ($P < 0.05$). Tumor weights in the lenti-mir-30a-5p and irradiated lenti-mir-

Table 3 Tumor weight, body weight of nude mice and tumor inhibition rate in different treatment groups

	Groups	*n*	Tumor weight (g)	Body weight of nude mice (g)	Tumor inhibition rate[a] (%)	Tumor inhibition rate[b] (%)
Non-IR	Lenti-GFP	3	1.29 ± 0.28	21.83 ± 1.72	–	–
	Lenti-mir-30a-5p	3	0.92 ± 0.18	21.23 ± 1.33	27.86 ± 7.02	27.86 ± 7.02
	Lenti-inhibitor	3	1.94 ± 0.37	20.80 ± 1.30	–	–
IR	Lenti-GFP	3	0.49 ± 0.28*	16.67 ± 0.71**	–	64.47 ± 14.17
	Lenti-mir-30a-5p	3	0.35 ± 0.13*	17.10 ± 0.98*	18.75 ± 22.17	73.16 ± 3.98
	Lenti-inhibitor	3	0.89 ± 0.17*	17.17 ± 1.82*	–	30.53 ± 5.20[#]

Note: Tumor inhibition rate (%) = (tumor weight in the negative control group – tumor weight in the treatment group) / tumor weight in the negative control group × 100%; [a]: Lenti-GFP group *vs*. Lenti-mir-30a-5p group or Lenti-GFP + IR group *vs*. Lenti-mir-30a-5p + IR group; [b]: Lenti-GFP group *vs*. Lenti-GFP + IR group or Lenti-GFP *vs*. Lenti-mir-30a-5p + IR group or Lenti-GFP group *vs*. Lenti-inhibitor + IR group; *: Non-IR group *vs*. IR group, $P < 0.05$; **: Non-IR group *vs*. IR group, $P < 0.01$; [#]: Lenti-GFP + IR group *vs*. lenti-inhibitor + IR group, $P < 0.05$

Fig. 3 Tumor weight of nude mice in different treatment groups. (a) Representative picture of tumor-bearing nude mice; (b) Statistical chart tumor weight

30a-5p (lenti-mir-30a-5p + IR) groups were lower than those in the lenti-GFP groups. In contrast, both lenti-inhibitor groups showed higher tumor weights than those in the lenti-GFP groups (Fig. 3 and Table 3).

The tumor inhibition rate in the lenti-mir-30a-5p and lenti-mir-30a-5p + IR groups was 27.86 ± 7.02% and 18.75 ± 22.17%, respectively, compared to the corresponding lenti-GFP groups, indicating that overexpression of mir-30a-5p could increase the tumor inhibition rate of A549 cell line subcutaneous xenografts. Tumor inhibition rates were significantly higher in the all irradiated groups compared to the lenti-GFP group. However, inhibition rate was higher in the lenti-mir-30a-5p group ($P > 0.05$) than in the lenti-GFP + IR group, and lower in the lenti-inhibitor + IR group ($P < 0.05$) than in the lenti-GFP + IR group (Table 3).

All nude mice lost weight when irradiation began compared to the not irradiated ($P < 0.05$; Fig. 4 and Table 3).

Detecting the expression of radiosensitivity-related proteins by immunohistochemical method

H&E staining was used to confirm that tumor tissue had been obtained (Fig. 5). ATM protein expression level was lower in the lenti-mir-30a-5p group and higher in the lenti-inhibitor group than in the lenti-GFP group, with or without irradiation ($P < 0.05$; Fig. 6). The phosphorylation level of ATM at S1981 was low in the three groups without irradiation however, after

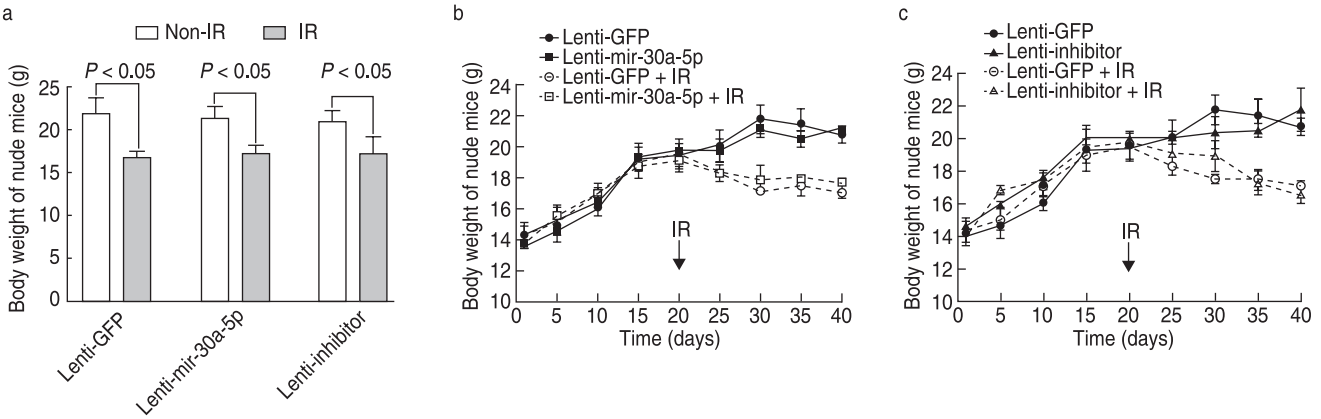

Fig. 4 Body weight of nude mice in different treatment groups. (a) Body weight of nude mice; (b) Body weight changing curve: lenti-mir-30a-5p ± IR *vs*. lenti-GFP ± IR; (c) Body weight changing curve: lenti-inhibitor ± IR *vs*. lenti-GFP + IR

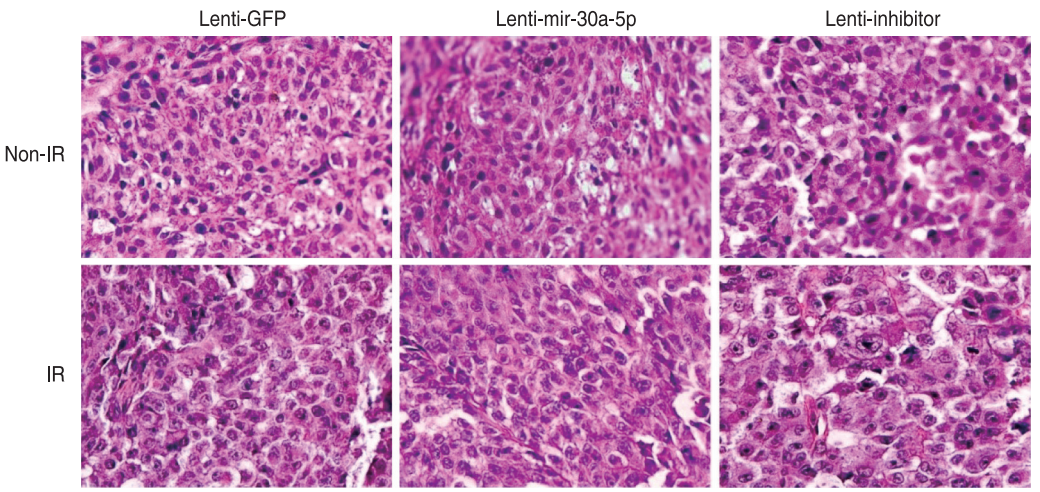

Fig. 5 H&E staining in different groups (magnification ×400)

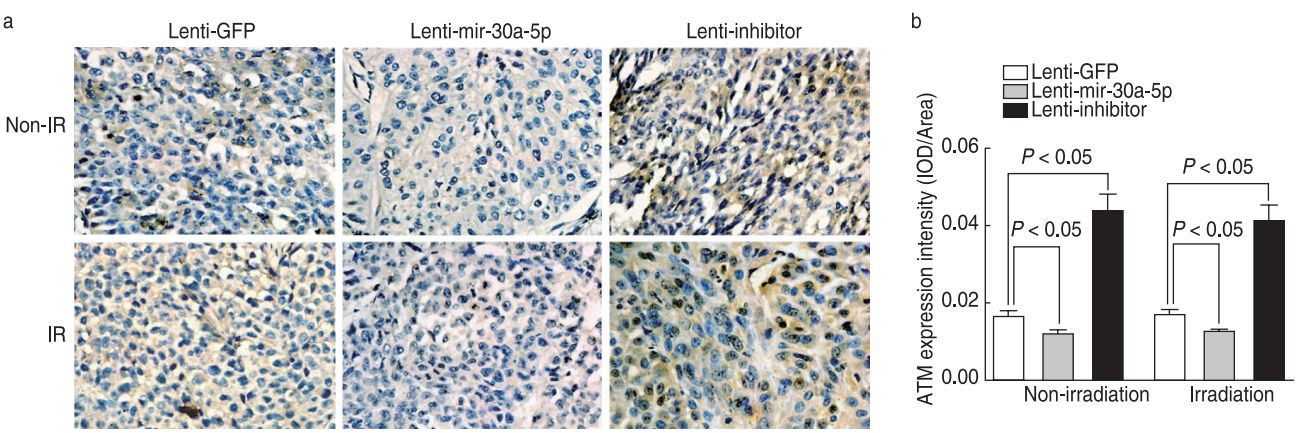

Fig. 6 ATM protein expression in different treatment groups. (a) Immunohistochemical representative image of ATM protein expression (magnification ×400); (b) Statistical chart of ATM expression intensity

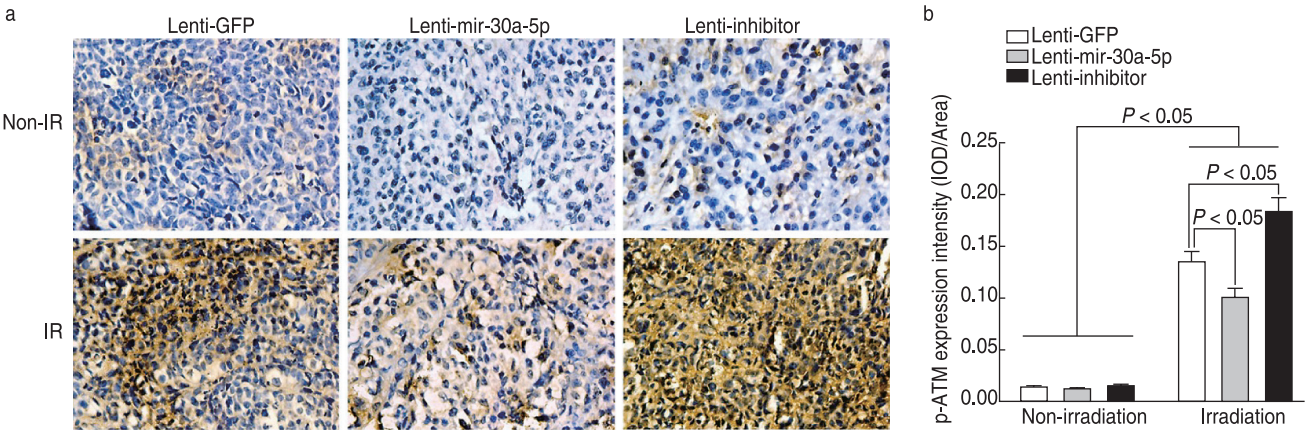

Fig. 7 Phosphorylation level of ATM at S1981 in different treatment groups. (a) Immunohistochemical representative picture of ATM phosphorylation level (magnification ×400); (b) Statistical chart of p-ATM expression intensity

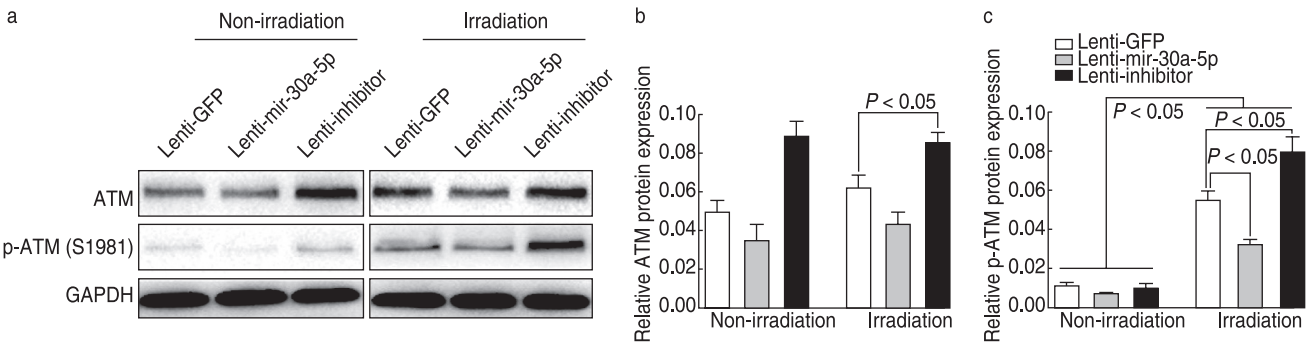

Fig. 8 ATM protein expression and phosphorylation level of ATM at S1981 in different treatment groups. (a) Representative Western blot showing ATM protein expression and its phosphorylation level; (b) Statistical chart of relative ATM protein expression; (c) Statistical chart of relative p-ATM level

irradiation, it significantly increased in all treated groups ($P < 0.05$). Moreover, it was higher in the lenti-mir-30a-5p + IR group and lower in the lenti-inhibitor + IR group than in the lenti-GFP + IR group ($P < 0.05$; Fig. 7).

Detecting the expression of radiosensitivity-related proteins by Western blotting

ATM protein expression level was lower in the lenti-mir-30a-5p group and higher in the lenti-inhibitor group than in the lenti-GFP group, with or without irradiation (Fig. 8a–8b). The phosphorylation level of ATM at S1981 was low in the three groups without irradiation however, it significantly increased ($P < 0.05$) after irradiation. It was higher in the lenti-mir-30a-5p + IR group and lower in the lenti-inhibitor + IR group compared to the lenti-GFP + IR group ($P < 0.05$; Fig. 8).

Discussion

At present, a wide variety of miRNAs have been identified that may be related to cancer progression [19–21]. Many microRNAs are important radiosensitivity regulators, which produce effects by interacting with the key factors involved in the regulation of radiosensitivity [2]. The expression level of mir-30a is diminished in many types of tumors, its expression is closely related to tumor progression and can play an inhibitory role in many types of tumors [22]. For example, gastric cancer [23], cholangiocarcinoma [15], esophageal cancer [24]. Further, mir-30a can affect tumor progression and therapeutic efficacy by regulating tumor cell proliferation [15], migration and invasion [16], EMT [25], apoptosis, and autophagy [17] (Fig. 9).

DNA is the primary target of radiation. The effect of radiation on tumors leads to the activation or inhibition of related genes, which could affect the radiosensitivity. ATM is an important effector of radiation-induced DNA damage [26]. ATM and ataxia telangiectasia and Rad3-related gene (ATR), as the core kinases in the whole process of DDR, can detect various forms of DNA damage and trigger downstream cascade reactions [11]. ATM, ATR, and DNA-PKcs are phosphatidylinositol-3 kinase-related kinase (PIKK) family members that play crucial roles in DNA damage repair [27]. ATR is activated by ultraviolet

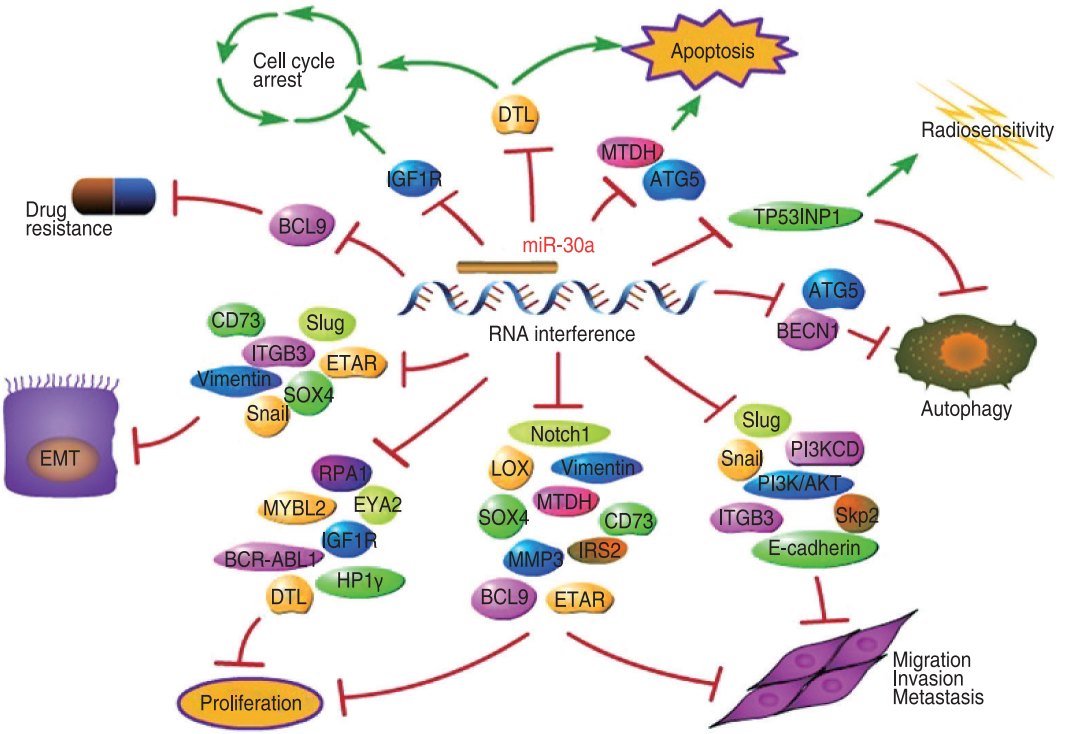

Fig. 9 Schematic diagram of the role of mir-30a in cancer

treatment or replication fork disintegration. ATM mainly affects radiation-induced DNA double-strand breaks and participates in cell reprogramming [28]. Mutations in ATM cause extreme sensitivity to radiation and increase tumor risk [14] and can also participate in the regulation of cell cycle checkpoints, DNA repair, and apoptosis [11].

DNA damage can activate the phosphorylation of serine site 1981 of ATM, which activates a series of downstream effector molecules and participates in the regulation of the cell cycle, apoptosis, and DNA damage repair [29–30], causing cells to be insensitive to radiation [11, 31]. Its downstream effectors include DNA-PK, Ku70/80, BRCA1, BRCA2, RAD51, and RAD52. These can participate in the regulation of various biological processes, such as non-homologous end-joining, homologous recombination, cell cycle checkpoints, and apoptosis regulation [12]. Poly ADP-ribose polymerase-1 is an important effect or molecule in the DDR pathway and participates in cell survival [32]. Inhibition of ATM and its downstream proteins could improve the radiosensitivity of tumors and hinder the DNA damage repair process [11, 33].

In a previous study, we confirmed the low expression levels of mir-30a-5p in A549 and H460 cell lines *in vitro*, and its radiosensitizing effect on A549 cell lines [18]. Here, we confirmed this effect by using lentivirus to construct a subcutaneous xenograft model of lung cancer in nude mice and study it *in vivo*. The results showed a slower tumor growth trend in the overexpression mir-30a-5p group after irradiation, compared to the control group. Smaller tumor volume, lower tumor weight and a higher tumor inhibition rate was observed compared to the control group. The mir-30a-5p downregulated group showed larger tumor volume, higher tumor weight and lower tumor inhibition rate than the control group. The results of immunohistochemistry and Western blotting suggested that the overexpression of mir-30a-5p could also inhibit the activation of ATM 1981 serine phosphorylation induced by radiation *in vivo*, thus improving the radiosensitivity of tumors. We plan to investigate the specific mechanism between mir-30a-5p and the ATM signaling pathway in future studies.

Some of the results in our study showed no statistical difference, which may be related to a late start time, early end time, or insufficient dose of radiation. The radiation dose and time may be the main factors affecting the experimental results. Due to limited experimental conditions, we performed whole-body irradiation of nude mice. In the radiation group, a series of systemic symptoms gradually appeared during the experiment, and the body weight of nude mice decreased significantly, which may have also interfered with the experimental results. However, there was no difference in the body weight of nude mice in the different mir-30a-5p expression groups, which also provided some theoretical support for the safety of mir-30a-5p *in vivo*.

Conclusion

These results confirmed that mir-30a-5p has a radiosensitizing effect on the A549 cell lung cancer subcutaneous xenograft model in nude mice. Mir-30a-5p enhanced the radiosensitivity of nude mice with subcutaneous lung-cancer xenografts by inhibiting ATM phosphorylation.

In further studies, the radiation dose and time can be adjusted, the *in vivo* study can be detected more accurately, a lung transplant tumor model can be constructed, and further research can be performed in lung tissue, with the help of animal imaging and other techniques.

Acknowledgments

Not applicable.

Funding

This study was supported by the National Science Fund Project (No. 81872471) of the National Natural Science Foundation of China and the Science Foundation of the Second Affiliated Hospital of Xi'an Jiaotong University (No. YJ(QN)202025).

Conflicts of interest

The authors indicated no potential conflicts of interest.

Author contributions

All authors contributed to data acquisition and interpretation and reviewed and approved the final version of this manuscript.

Data availability statement

Not applicable.

Ethical approval

Animal experiments were performed in accordance with the ethical guidelines for experimental animals of the Department of Medicine, Xi'an Jiaotong University, China.

References

1. Cao H, Wang SL, Liu YH. Antitumor and vascular effects of apatinib combined with chemotherapy in mice with non-small-cell lung cancer. Oncol Transl Med. 2021;7(3):141-147.
2. Zhao L, Bode AM, Cao Y, et al. Regulatory mechanisms and clinical perspectives of miRNA in tumor radiosensitivity. Carcinogenesis. 2012;33(11):2220-2227.
3. Lindblom E, Dasu A, Toma-Dasu I. Optimal fractionation in radiotherapy for non-small cell lung cancer – a modelling approach. Acta Oncol. 2015;54(9):1592-1598.
4. Berthel E, Ferlazzo ML, Devic C, et al. What does the history of research on the repair of DNA double-strand breaks tell us? – A comprehensive review of human radiosensitivity. Int J Mol Sci. 2019;20(21):5339.
5. Zhang T, Shen Y, Chen Y, et al. The ATM inhibitor KU55933 sensitizes radioresistant bladder cancer cells with DAB2IP gene defect. Int J Radiat Biol. 2015;91(4):368-378.
6. Tu W, Dong C, Konishi T, et al. G(2)-M phase-correlative bystander effects are co-mediated by DNA-PKcs and ATM after carbon ion irradiation. Mutat Res Genet Toxicol Environ Mutagen. 2016;795:1-6.
7. Krause M, Dubrovska A, Linge A, et al. Cancer stem cells: Radioresistance, prediction of radiotherapy outcome and specific targets for combined treatments. Adv Drug Deliv Rev. 2017;109:63-73.
8. Liang N, Zhong R, Hou X, et al. Ataxia-telangiectasia mutated (ATM) participates in the regulation of ionizing radiation-induced cell death via MAPK14 in lung cancer H1299 cells. Cell Prolif. 2015;48(5):561-572.
9. Strom T, Harrison LB, Giuliano AR, et al. Tumour radiosensitivity is associated with immune activation in solid tumours. Eur J Cancer. 2017;84:304-314.
10. Schaue D. A century of radiation therapy and adaptive immunity. Front Immunol. 2017;8:431.
11. Estiar MA, Mehdipour P. ATM in breast and brain tumors: a comprehensive review. Cancer Biol Med. 2018;15(3):210-227.
12. Zhao L, Lu X, Cao Y. MicroRNA and signal transduction pathways in tumor radiation response. Cell Signal. 2013;25(7):1625-1634.
13. Toulany M, Minjgee M, Kehlbach R, et al. ErbB2 expression through heterodimerization with erbB1 is necessary for ionizing radiation- but not EGF-induced activation of Akt survival pathway. Radiother Oncol. 2010;97(2):338-345.
14. Kerns SL, Ostrer H, Rosenstein BS. Radiogenomics: using genetics to identify cancer patients at risk for development of adverse effects following radiotherapy. Cancer Discov. 2014;4(2):155-165.
15. Zhang JW, Wang X, Li GC, et al. MiR-30a-5p promotes cholangiocarcinoma cell proliferation through targeting SOCS3. J Cancer. 2020;11(12):3604-3614.
16. Yu D, Liu H, Qin J, et al. Curcumol inhibits the viability and invasion of colorectal cancer cells via miR-30a-5p and Hippo signaling pathway. Oncol Lett. 2021;21(4):299.
17. Chen W, Li Z, Liu H, et al. MicroRNA-30a targets BECLIN-1 to inactivate autophagy and sensitizes gastrointestinal stromal tumor cells to imatinib. Cell Death Dis. 2020;11(3):198.
18. Guo Y, Sun W, Gong T, et al. miR-30a radiosensitizes non-small cell lung cancer by targeting ATF1 that is involved in the phosphorylation of ATM. Oncol Rep. 2017;37(4):1980-1988.
19. Fan T, Wang CQ, Zhang K, et al. Differentially expressed genes analysis and target genes prediction of miR-22 in breast cancer. Oncol Transl Med. 2021;7(2):59-64.
20. Zhang CL, Liu D, Tian QQ, et al. CircBAGE2 (hsa_circ_0061259) regulates CCND1 and PDCD10 expression by functioning as an miR-103a-3p 'sponge' to alter the proliferation and apoptosis of prostate cancer cells. Oncol Transl Med. 2021;7(5):221-228.
21. Hao TT, Wang CQ, Song YJ, et al. Relationship between miR-7-5p expression and ^{125}I seed implantation efficacy in pancreatic cancer and functional analysis of target genes. Oncol Transl Med. 2021;7(4):177-182.
22. Zhao JJ, Lin J, Zhu D, et al. miR-30-5p functions as a tumor suppressor and novel therapeutic tool by targeting the oncogenic Wnt/β-catenin/BCL9 pathway. Cancer Res. 2014;74(6):1801-1813.
23. Min J, Han TS, Sohn Y, et al. microRNA-30a arbitrates intestinal-type early gastric carcinogenesis by directly targeting ITGA2. Gastric Cancer. 2020;23(4):600-613.

24. Butz F, Eichelmann AK, Mayne GC, et al. MicroRNA profiling in oesophageal adenocarcinoma cell lines and patient serum samples reveals a role for miR-451a in radiation resistance. Int J Mol Sci. 2020;21(23):8898.
25. Zhang Y, Li Y. Long non-coding RNA NORAD contributes to the proliferation, invasion and EMT progression of prostate cancer via the miR-30a-5p/RAB11A/WNT/β-catenin pathway. Cancer Cell Int. 2020;20(1):571.
26. Pizzamiglio L, Focchi E, Antonucci F. ATM protein kinase: Old and new implications in neuronal pathways and brain circuitry. Cells. 2020;9(9):1969.
27. Balmus G, Pilger D, Coates J, et al. ATM orchestrates the DNA-damage response to counter toxic non-homologous end-joining at broken replication forks. Nat Commun. 2019;10(1):87.
28. Kinoshita T, Nagamatsu G, Kosaka T, et al. Ataxia-telangiectasia mutated (ATM) deficiency decreases reprogramming efficiency and leads to genomic instability in iPS cells. Biochem Biophys Res Commun. 2011;407(2):321-326.
29. Neumann J, Yang Y, Köhler R, et al. Mangrove dolabrane-type of diterpenes tagalsins suppresses tumor growth via ROS-mediated apoptosis and ATM/ATR-Chk1/Chk2-regulated cell cycle arrest. Int J Cancer. 2015;137(11):2739-2748.
30. Khoronenkova SV, Dianov GL. ATM prevents DSB formation by coordinating SSB repair and cell cycle progression. Proc Natl Acad Sci USA. 2015;112(13):3997-4002.
31. Rondeau S, Vacher S, De Koning L, et al. ATM has a major role in the double-strand break repair pathway dysregulation in sporadic breast carcinomas and is an independent prognostic marker at both mRNA and protein levels. Br J Cancer. 2015;112(6):1059-1066.
32. Menolfi D, Zha S. ATM, ATR and DNA-PKcs kinases – the lessons from the mouse models: inhibition ≠ deletion. Cell Biosci. 2020;10:8.
33. Langelier MF, Pascal JM. PARP-1 mechanism for coupling DNA damage detection to poly(ADP-ribose) synthesis. Curr Opin Struct Biol. 2013;23(1):134-143.

DOI 10.1007/s10330-021-0534-4
Cite this article as: Guo YY, Cui YT, Bao X, et al. Radiosensitization by microRNA30a-5p in a nude mouse model with subcutaneous lung-cancer xenograft. Oncol Transl Med. 2022;8(4):155-164.

Oncology and Translational Medicine
DOI 10.1007/s10330-021-0539-9
August 2022, Vol. 8, No. 4, P165–P172

ORIGINAL ARTICLE

CD14 macrophage and IL-10 levels in the peripheral blood of breast cancer patients and their diagnostic value*

Mengting Dong, Jiayu Sheng (Co-first author), Chunyang Li, Patiguli·JIAPAER, Xiaofei Li, Minjia Yuan, Xiaohong Xue, Ke Jiang (✉)

Department of Breast Diseases, Yueyang Hospital of Integrated Traditional Chinese and Western Medicine, Shanghai University of Traditional Chinese Medicine, Shanghai 200437, China

Abstract

Objective To explore the correlation between macrophages and interleukin-10 (IL-10 in the peripheral blood of breast cancer (BC) patients and the diagnostic value of joint detection.

Methods BC patients (n = 50) and healthy controls (n = 40) were prospectively recruited. The percentage of circulating cluster of differentiation 14 (CD 14) macrophage cells was analyzed by flow cytometry, and an enzyme-linked immunosorbent assay (ELISA) was used to detect IL-10 expression levels. Receiver operating characteristic (ROC) curves were used to verify the diagnostic value of the models based on the expression of CD14 macrophage cell populations and IL-10. In addition, the association between model expression and clinicopathological characteristics was investigated. Another 30 patients with BC and 30 with benign breast disease were selected to validate the IL-10 and CD14 macrophage joint detection model using the same method.

Results CD14 macrophage and IL-10 expression levels in BC patients were higher than those in healthy controls (P < 0.05). The ROC curve showed that the area under the curve (AUC) of CD14+ macrophages combined with IL-10 was 0.830, the sensitivity was 72.0%, and the specificity was 87.5%. Its diagnostic efficiency was better than all other single and joint detections. Correlation analysis of clinicopathological features showed that IL-10 and CD14+ macrophage joint detection was significantly correlated with tumor size, tumor-node-metastasis (TNM) stage, and lymph node, estrogen receptor (ER), and Ki-67 expression (P < 0.05). The validation analysis results were consistent with the test results.

Conclusion Peripheral blood macrophages can be an independent diagnostic marker for BC. Joint detection of CD14- macrophages and IL-10 suggests poor prognosis, which has unlimited potential to guide BC development and provides a new theory for studying tumor-associated macrophages in BC.

Received: 27 November 2021
Revised: 27 December 2021
Accepted: 21 May 2022

Key words: breast cancer; macrophage; IL-10; peripheral blood; diagnostic value

Breast cancer (BC) is the primary cause of cancer-associated death in women [1]. Therefore, research on the BC tumor microenvironment (TME) has recently focused on new diagnostic and treatment methods. Macrophages are the dominant immune cell population in the TME [2]. Tumor-associated macrophages (TAMs) can help cancer cells enter the blood to form new tumors. Not only that, TAMs can migrate via the lymphatic system or intravasate across intratumor capillary barriers into peripheral circulation with circulating tumor cells (CTCs) and further turn into cancer-associated macrophage-like cells (CAMLs) [3–4], meaning macrophage expression in peripheral blood may be crucial in the TME.

As a classic anti-inflammatory cytokine, interleukin-10 (IL-10) induces macrophage maturation and polarization [5]. IL-10-stimulated macrophages can further generate IL-10 and matrix remodeling factors, such as matrix metalloproteinases (MMPs), involved in tumor cell

✉ Correspondence to: Ke Jiang. Email: surgeonjk@163.com
* Supported by grants from the National Natural Science Foundation of China (No. 82104952, No. 82004240), Special project for clinical research of health industry of Shanghai Municipal Health Commission (No. 202140172), Special project of medical innovation research of Shanghai Science and Technology Commission (No. 21Y11923600) and the Shanghai Office of Traditional Chinese Medicine Development (No. ZY2018- 2020-RCPY-2009).

proliferation, migration, invasion, metastasis, and apoptosis. Additionally, IL-10 expression is closely associated with the pathological stage and prognosis [6]. Therefore, this study used the macrophage-specific marker cluster of differentiation 14 (CD14) for screening and grouping, compared and analyzed the expression levels of CD14 macrophage cell populations and IL-10 in the peripheral blood of patients in different groups, and explored the application value of CD14 macrophages and IL-10 as prognostic indicators of BC by establishing a joint detection model of CD14 macrophages and IL-10.

Materials and methods

Clinical data

We selected 50 treatment-naive patients with BC admitted to Yueyang Hospital of Integrated Traditional Chinese and Western Medicine, Shanghai University of Traditional Chinese Medicine, between January 2020 and December 2020 as the research participants. All BC diagnoses were confirmed via histological examination. Tumor-node-metastasis (TNM) classification was performed per the UICC-American Combined Committee on Cancer Staging (7th edition). None of the patients received therapy prior to blood sampling. All patients were women aged 31–72 years, with a median age of 55 years. There were 48 cases of invasive ductal carcinoma (96.0%) and two cases of invasive lobular carcinoma (4.0%). We selected 40 healthy female volunteers as normal controls and obtained written informed consent from all the patients and healthy subjects. Table 1 lists the clinicopathological features (age, TNM stage, tumor size, clinical stage, lymph node metastasis, and information on estrogen receptor (ER), progesterone receptor, and human epidermal growth factor receptor 2 (HER2) expression). Another 30 patients with BC and 30 with benign breast disease in our hospital from January 2021 to June 2021 were selected for the validation analysis. Fig. 1 illustrates the experimental design.

Main instruments and reagents

The main reagent, PM-2 K macrophage antibody, was purchased from Abcam (Cambridge, UK). Other reagents and instruments included goat anti-mouse IgG-FC SureLight (SBA company), human IL-10 enzyme-linked immunosorbent assay (ELISA) kits (Shanghai Senxiong Technology Co., Ltd.), and PerCP anti-human CD3, PE anti-human CD19, and APC anti-human CD14 antibodies from BioLegend.

Flow cytometric analysis of CD14 macrophage cells in peripheral blood

Anticoagulant whole blood (5 mL) was added to 15 mL Ficoll (Tianjin Haoyang) and centrifuged at 800 × g for 20 min, after which the white membrane layer was removed and washed once to separate peripheral blood mononuclear cells (PBMCs). The samples were blocked with 10% human plasma for 10 min. One test of PM-2 K anti-macrophage antibody (Abcam ab58822) was added to every 106 cells and incubated at 4°C for 30 min. We added 5 mL phosphate-buffered saline (PBS), centrifuged (400 × g) for 5 min, and discarded the supernatant. The cells were resuspended, and one test of goat anti-mouse LGG FC and human/bovine/horse Spads FTC (Southern Biotech 1013-02) was added to every 106 cells and incubated at 4°C for 30 min. We resuspended the antibody, added 5 ml PBS, centrifuged (400 × g) for 5 min, discarded the supernatant, and repeated the previous step. We resuspended the cells, added one test of PerCP anti-human CD3 (BioLegend 300427), one test PE anti-human CD19 (BioLegend 302207), and one test of APC anti-human CD14 (BioLegend 325608) to every 106 cells, and incubated them at 4°C for 30 min. In another tube of cells, the same type of control was added as described above. The incubated samples were washed off with unbound antibodies and analyzed by flow cytometry. A gate was set to circle the cell population of CD3–CD19 and detect PM-2k+ CD14+ and PM-2k+ CD14- macrophage levels.

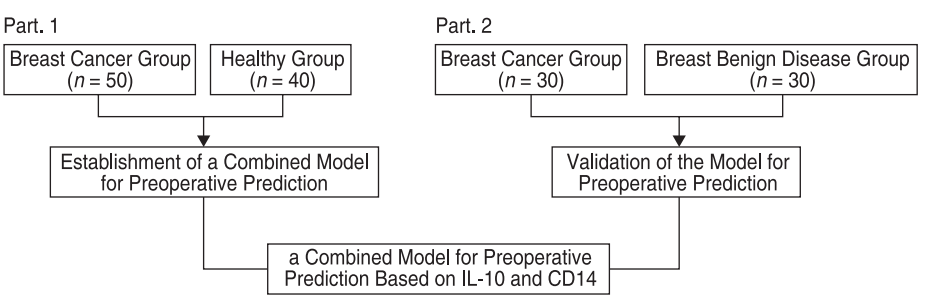

Fig. 1 Basic roadmap for the establishment and validation of IL-10 and CD14 macrophage joint detection model

Table 1 Clinicopathological features of BC group and control group [*n* (%)]

Items	BC group (*n* = 50)	Control group (*n* = 40)
Age (years, $\bar{\chi}\pm s$)	54.0±12.2	39.5±9.2
≤50	18 (36.0)	32 (80.0)
>50	32 (64.0)	8 (20.0)
Tumor size (cm, $\bar{\chi}\pm s$)	2.8±1.8	-
≤2	22 (44.0)	-
>2	28 (56.0)	-
Lymph node metastasis		
0	15 (30.0)	-
1–3	21 (42.0)	-
≥4	14 (28.0)	-
Ki-67		
>30%	29 (58.0)	-
≤30%	21 (42.0)	-
Vascular invasion		
No	33 (66.0)	-
Yes	17 (34.0)	-
TNM stage		
I	15 (30.0)	-
II	24 (48.0)	-
III	11 (22.0)	
ER		
Negative	27 (54.0)	-
Positive	23 (46.0)	-
Her-2		
Negative	20 (40.0)	-
Positive	30 (60.0)	-

Table 2 Comparison of macrophages and IL-10 expression levels between BC and control group in peripheral blood ($\bar{\chi}\pm s$)

Items (%)	BC (*n* = 50)	Control (*n* = 40)	*t*	*P*
CD14+ macrophages	4.766±1.899	2.985±1.123	5.239	0.000
CD14- macrophages	18.981±8.276	11.233±7.819	1.604	0.112
Total macrophages	16.867±8.216	13.318±8.128	2.048	0.043
IL-10(pg/mL)	17.324±5.0473	14.028±3.554	3.493	0.001

Detecting IL-10 in peripheral blood

We drew 5 mL of anticoagulant whole blood, placed it in an ethylenediaminetetraacetic acid (EDTA) anticoagulant tube, and let it stand for 1 h at 3600 × g. The serum was separated by centrifugation for 10 min and stored at -80°C until needed. ELISA was used to quantitatively detect IL-10 in the serum. The manufacturer's instructions were strictly followed.

Statistical analysis

SPSS 22.0 statistical software was used for the statistical analysis. A *t*-test was used to compare the level of peripheral blood macrophages between BC patients and healthy controls, and binary logistic regression was used to establish the joint detection formula. A receiver operating characteristic (ROC) curve was used to analyze the diagnostic efficiency of each index, and the best critical value of the test items was obtained. Clinicopathological indices, other immunohistochemical indices, molecular subtypes, and clinicopathological indices of patients with macrophages and BC were analyzed using a chi-square test and the Fisher exact probability method. Correlation analysis was performed using Spearman's rank correlation coefficient ($P < 0.05$).

Results

Comparison of peripheral blood macrophage cell populations and IL-10 expression between BC patients and healthy controls

The expression of CD14+ macrophages, CD14- macrophages, total macrophages, and IL-10 in BC patients and healthy controls was tested using a *t*-test. Although CD14- levels were higher in the BC group than in the control group, this difference was not statistically significant ($P = 0.112$). IL-10 and CD14+ were higher in the BC patients than the controls, and this difference was statistically significant ($P < 0.01$). Table 2 describes this in detail, and Fig. 2 shows the flow cytometry gating strategies.

Evaluating the diagnostic efficacy of CD14+ macrophages, CD14- macrophages, total macrophages, and IL-10 in BC

ROC curve analyses showed that the areas under the ROC curve (AUC) were 0.778, 0.596, 0.599, and 0.688, respectively. Based on the logistic regression model, we established a combined diagnosis of CD14+, CD14-, and total macrophages with IL-10 and found that the IL-10 CD14+ macrophage joint detection AUC was 0.830, which was significantly higher than the AUCs of the four indicators separately and other joint detections. It also had significant advantages because of its high sensitivity (72.0%) and specificity (87.5%) for diagnosing BC. Table 3 and Fig. 3 present the results.

Correlation analysis between clinicopathological features and CD14+ macrophages, IL-10 and CD14+ joint detection, and IL-10 and CD14- joint detection in peripheral blood

Based on the above results, we selected three detectors with relatively optimal test efficiency for the correlation analysis with clinicopathological features. The optimal cutoff values of CD14+ macrophages, IL-10 and CD14+ joint detection, and IL-10 and CD14- joint detection calculated by the ROC curve were 4.655%, 22.161%, and 29.300%, respectively. We divided the BC patients into the high score or low score groups based on the cutoff values. The results indicated that CD14+ expression

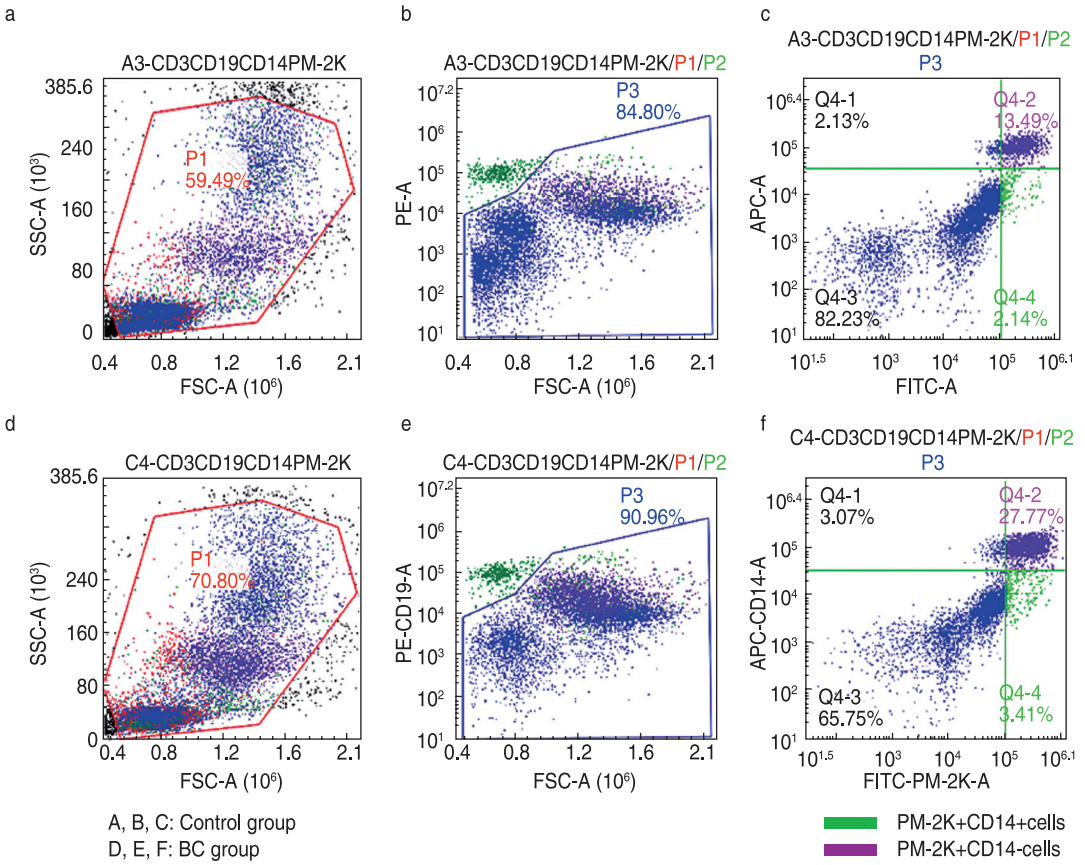

Fig. 2 Flow cytometry gating strategy for macrophages from peripheral blood of BC patients and healthy controls

Table 3 Comparison of the diagnostic value of single and combined detection of macrophages and IL-10 in breast cancer

Items	Cutoff value	AUC	95%CI	S_b	Sensitivity	Specificity
CD14+ macrophages	4.655	0.778	0.680–0.876	0.000	62.00	92.00
CD14- macrophages	19.980	0.596	0.490–0.723	0.083	34.00	66.00
Total macrophages	25.430	0.599	0.481–0.717	0.107	22.00	90.50
IL-10	19.025	0.688	0.580–0.795	0.002	40.00	82.50
IL-10 CD14+ macrophages combined detection	29.300	0.830	0.748–0.912	0.000	72.00	87.50
IL-10 CD14-macrophages combined detection	22.161	0.715	0.611–0.819	0.000	40.00	95.00
IL-10 total macrophages combined detection	17.089	0.712	0.607–0.816	0.001	62.00	65.00

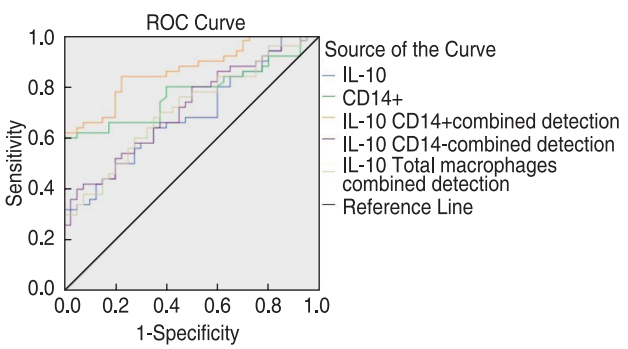

Fig. 3 Curve of CD14+ macrophages, IL-10 and their joint detections in breast cancer diagnosis

correlated with lymph node metastasis, TNM stage, and Ki-67 expression. IL-10 and CD14+ joint detection significantly correlated with tumor size, TNM stage, lymph node, ER expression, and Ki-67 expression ($P < 0.05$). IL-10 and CD14- joint detection was only related to TNM stage and lymph node metastasis. Age, vascular infiltration, and HER2 expression were not associated with any detection ($P > 0.05$) (Table 4).

Validation analysis of IL-10 and CD14+ joint detection in peripheral blood of BC patients and patients with benign breast diseases

We also collected 30 cases of breast cancer and benign breast diseases to test the diagnostic efficiency of the

Table 4 The correlation of CD14- macrophages, IL-10 and their joint detection with different clinicopathological features in BC patients [*n* (%)]

Items	CD14+ macrophages		IL-10 CD14-combined detection		IL-10 CD14+ combined detection	
	Low expression	High expression	Low expression	High expression	Low expression	High expression
Cases (*n*)	22	28	28	22	20	30
Age (years)						
≤50	9 (50.0)	9 (50.0)	12 (66.67)	6 (33.33)	9 (50.0)	9 (50.0)
>50	13 (40.6)	19 (59.4)	16 (50.00)	16 (50.00)	11 (34.4)	21 (65.6)
χ^2	0.411		1.299		1.172	
P	0.522		0.254		0.279	
r	0.091		0.161		0.153	
Tumor size (cm)						
≤2	12 (54.5)	10 (45.5)	15 (68.18)	7 (31.82)	13 (59.1)	9 (40.9)
>2	10 (35.7)	18 (64.3)	13 (46.43)	15 (53.57)	7 (25.0)	21 (75.0)
χ^2	1.773		2.366		5.966	
P	0.183		0.124		0.015	
r	0.188		0.218		0.345	
Lymph node metastasis						
0	11 (73.3)	4 (26.7)	13 (86.67)	2 (13.33)	10 (66.7)	5 (33.7)
1–3	6 (28.6)	15 (71.4)	9 (42.86)	12 (57.14)	4 (19.0)	17 (81.0)
≥4	5 (35.7)	9 (64.3)	6 (42.86)	8 (57.14)	6 (42.9)	8 (57.1)
χ^2	7.657		8.179		8.333	
P	0.022		0.017		0.016	
r	0.294		0.341		0.193	
Vascular invasion						
No	16 (48.5)	17 (51.5)	18 (54.55)	15 (45.45)	16 (48.5)	17 (51.5)
Yes	6 (35.3)	11 (64.7)	10 (58.82)	7 (41.18)	4 (23.5)	13 (76.5)
χ^2	0.792		0.083		2.911	
P	0.373		0.773		0.088	
r	0.126		-0.041		0.241	
TNM stage						
I	11 (73.3)	4 (26.7)	12 (80.00)	3 (20.00)	10 (66.7)	5 (33.7)
II+III	11 (31.4)	24 (68.6)	16 (45.71)	19 (54.29)	10 (28.6)	25 (71.4)
χ^2	7.483		5.009		6.349	
P	0.006		0.025		0.012	
r	0.387		0.317		0.356	
Her-2						
Negative	12 (60.0)	8 (40.0)	14 (70.00)	6 (30.00)	11 (55.0)	9 (45.0)
Positive	10 (33.3)	20 (66.7)	14 (45.67)	16 (53.33)	9 (30.0)	21 (70.0)
χ^2	3.463		2.652		3.125	
P	0.063		0.103		0.077	
r	0.263		-0.230		0.250	
ER						
Negative	15 (55.6)	12 (44.4)	17 (63.0)	10 (37.0)	15 (55.6)	12 (44.4)
Positive	7 (30.4)	16 (69.6)	11 (47.8)	12 (52.2)	5 (21.7)	18 (78.3)
χ^2	3.181		5.238		5.918	
P	0.075		0.022		0.015	
r	0.252		0.295		0.344	
Ki-67						
≤30	17 (58.6)	12 (41.4)	18 (62.07)	11 (37.93)	17 (58.6)	12 (41.4)
>30	5 (23.8)	16 (76.2)	10 (47.62)	11 (52.38)	3 (14.3)	18 (85.7)
χ^2	5.99		1.032		9.975	
P	0.014		0.310		0.002	
r	0.346		0.144		0.447	

Table 5 Comparison of the diagnostic value of single and combined detection of macrophages and IL-10 between patients with breast cancer and breast benign diseases

Items	AUC	95%CI	S_b	Sensitivity	Specificity
CD14+ macrophages	0.653	0.512–0.794	0.041	36.70	95.00
CD14- macrophages	0.612	0.469–0.794	0.135	98.50	26.70
Total macrophages	0.690	0.557–0.823	0.011	36.70	96.70
IL-10	0.659	0.517–0.801	0.035	46.70	90.00
IL-10 CD14+macrophages combined detection	0.779	0.660–0.896	0.000	83.30	72.30
IL-10 CD14-macrophages combined detection	0.668	0.527–0.809	0.026	40.00	96.70
IL-10 total macrophages combined detection	0.687	0.549–0.824	0.013	40.00	98.50

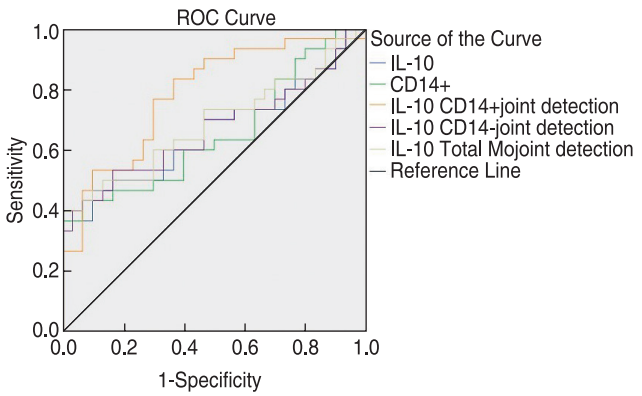

Fig. 4 Curve of CD14+ macrophages, IL-10 and their joint detections in validation analysis

above joint detection model. The analysis results of the ROC curve suggested that in the validation population with benign breast diseases as the control, the efficacy level of IL-10 and CD14+ joint detection was still higher than that of single detection and other joint detections. The AUC was 0.779, and the sensitivity and specificity were 83.3% and 72.3%, respectively. The results of the validation analysis were consistent with the test results, and the difference was statistically significant ($P < 0.001$) (Fig. 4).

Discussion

In recent years, TAMs have become well known because of their plasticity and diversity [7]. After naive monocytes in peripheral circulation are recruited to the TME, they are polarized into two phenotypes: classic M1 macrophages and alternative M2 macrophages [8]. TAMs with the M1 phenotype show proinflammatory activity and better prognosis [9], whereas the M2 phenotype is associated with increased angiogenesis and tumor aggressiveness [10–11]. M2 TAMs are also key players in tumor immune escape and angiogenesis [12]. In addition, except for macrophages in tumor tissues, TAMs were found to escape from tumor tissue, migrate via the lymphatic system, or intravasate across intratumor capillary barriers into peripheral circulation with CTCs and other blood cells, and further turn into CAMLs [13]. Therefore, future research into the BC TME should focus on the specific mechanism of M2 TAMs *in vivo*.

Of the numerous cytokines associated with the TME, IL-10 and M2 TAMs are closely related. M2 phenotype macrophages are activated in the microenvironment by IL-10, glucocorticoids, and immune complexes. They can generate auxiliary IL-10 and matrix-remodeling factors, such as MMPs [14]. Several studies have identified that IL-10 secreted by macrophages can induce endothelial cell proliferation and participate in the epithelial-to-mesenchymal transition to promote apoptosis in BC cells through their related pathways, including the Janus kinase 2 (JAK2)/signal transducer and activator of transcription 3 (STAT3) pathway [15–16]. In addition, previous research has shown that the double-labeling of IL-10 and CD14+ can screen "M2-like macrophages" in peripheral blood, which is significantly correlated with malignant clinicopathological characteristics and poor prognosis [17]. Thus, IL-10 and M2 TAMs are inextricably associated with cancer-promoting processes. CD14 macrophages and IL-10 in peripheral blood may also be critical in BC.

This study is the first to show that patients with BC have higher levels of IL-10, CD14+ macrophages, and total macrophages than healthy individuals. This implies that the *in vivo* environment, which shows the presence of more macrophages, can confer a survival advantage to tumor cells. Simultaneously, BC patients also had significantly higher IL-10 expression levels, suggesting a certain effect of M2 macrophages in BC patients. Therefore, based on these analyses, we established a joint detection model of IL-10 and CD14 macrophage expression by binary logistic regression. ROC curve analysis confirmed that the joint detection of CD14+ and IL-10 was more valuable and effective as a potential diagnostic method of BC than the single detection of IL-10 and CD14 macrophages and other joint detections (AUC = 0.830, $P < 0.001$). In the validation analysis, we found that the joint detection of CD14+ and IL-10 still showed advantageous diagnostic efficiency (AUC = 0.779,

$P < 0.001$), and the result was consistent with the test results.

This study also analyzed the relationship between macrophages and BC clinicopathological features. CD14+ macrophage expression was correlated with stage, lymph node metastasis, and high Ki-67 expression ($P < 0.05$), suggesting a significant relationship between macrophage expression in the peripheral blood and poor prognosis in BC patients. TAMs are always expressed at low levels in patients with early-stage and luminal BC and early-stage BC, whereas triple-negative BC (TNBC) mostly shows TAM overexpression [18–19]. The results of this study were consistent with these findings. The joint detection results of IL-10 and CD14+ macrophages were significantly correlated with tumor size, TNM stage, lymph node metastasis, ER expression, and Ki-67 expression ($P < 0.05$). ER-positive patients have lower macrophage expression levels in the peripheral blood. The faster tumor cells proliferate, the later the tumor stage and the stronger the expression of macrophages in the peripheral blood of BC patients. This confirmed that jointly detecting IL-10 and CD14+ macrophages could suggest tumor burden and the invasive ability of BC cancer cells, and they may be potential BC biomarkers.

However, the present study only analyzed macrophages and IL-10 in the peripheral blood, and different subtypes of macrophages were not further classified. There is a lack of intuitive data on the independence and interaction of M1 and M2 macrophages in the peripheral blood. The level difference of peripheral blood in different molecular types of breast cancer is also unclear. We need to expand the sample size to confirm this observation in future research.

In summary, this study found that the expression of total macrophages, CD14+ macrophages, and IL-10 were significantly increased in BC patients. Jointly detecting CD14+ macrophages and IL-10 can also indicate a poor prognosis, guide BC development and monitoring, and provide new ideas for research on BC-related macrophages.

Acknowledgments

Not applicable.

Funding

This study was supported by the National Natural Science Foundation of China (No. 82104952, No. 82004240), Special project for clinical research of health industry of Shanghai Municipal Health Commission(No. 202140172), Special project of medical innovation research of Shanghai Science and Technology Commission (No. 21Y11923600) and the Shanghai Office of Traditional Chinese Medicine Development (No. ZY2018-2020-RCPY-2009).

Conflicts of interest

The authors indicated no potential conflicts of interest.

Author contributions

Conception and design: K Jiang; Administrative support: X Xue; Provision of study materials or patients: J Sheng; Collection and assembly of data: M Dong, C Li, P·Jiapaer, X Li, M Yuan; Data analysis and interpretation: M Dong, K Jiang, J Sheng; Manuscript writing: all authors; Final approval of manuscript: all authors.

Data availability statement

Not applicable.

Ethical approval

The authors are accountable for all aspects of the work, ensuring that questions related to the accuracy or integrity of any part of the work are appropriately investigated and resolved. This study was performed in accordance with the Declaration of Helsinki (revised in 2013). This study was approved by the Ethics Committee of Yueyang Hospital of Integrated Traditional Chinese and Western Medicine, Shanghai University of Traditional Chinese Medicine. All the patients signed an informed consent form before inclusion in the study.

References

1. DeSantis CE, Ma J, Gaudet MM, et al. Breast cancer statistics, 2019. CA Cancer J Clin. 2019;69(6):438-451.
2. Gregory AD, Houghton AM. Tumor-associated neutrophils: new targets for cancer therapy. Cancer Res. 2011;71(7):2411-2416 .
3. Roussos ET, Balsamo M, Alford SK, et al. Mena invasive (MenaINV) promotes multicellular streaming motility and transendothelial migration in a mouse model of breast cancer. J Cell Sci. 2011;124(Pt 13):2120-2131.
4. Adams DL, Martin SS, Alpaugh RK, et al. Circulating giant macrophages as a potential biomarker of solid tumors. Proc Natl Acad Sci U S A. 2014;111(9):3514-3519.
5. Liu Q, Yang C, Wang S, et al. Wnt5a-induced M2 polarization of tumor-associated macrophages via IL-10 promotes colorectal cancer progression. Cell Commun Signal. 2020;18(1):51.
6. Hung CH, Chen FM, Lin YC, et al. Altered monocyte differentiation and macrophage polarization patterns in patients with breast cancer. BMC Cancer. 2018;18(1):366.
7. Gregory AD, Houghton AM. Tumor-associated neutrophils: new targets for cancer therapy. Cancer Res. 2011;71(7):2411-2416.
8. Zhou J, Tang Z, Gao S, et al. Tumor-associated macrophages: recent insights and therapies. Front Oncol. 2020;10:188.
9. Juncker-Jensen A, Stavrou N, Padmanabhan R, *et al*. A pro-tumorigenic mechanism of M2 tumor-associated macrophages in triple-negative breast cancer. Atlanta: AACR Annual Meeting. 2019.1175.
10. Lala PK, Nandi P, Majumder M. Roles of prostaglandins in tumor-associated lymphangiogenesis with special reference to breast cancer. Cancer Metastasis Rev. 2018;37(2-3):369-384.

11. Chen Y, Zhang S, Wang Q, et al. Tumor-recruited M2 macrophages promote gastric and breast cancer metastasis via M2 macrophage-secreted CHI3L1 protein. J Hematol Oncol. 2017;10(1):36.
12. Williams CB, Yeh ES, Soloff AC. Tumor-associated macrophages: unwitting accomplices in breast cancer malignancy. NPJ Breast Cancer. 2016;2:15025.
13. Manjunath Y, Mitchem JB, Suvilesh KN, et al. Circulating giant tumor-macrophage fusion cells are independent prognosticators in patients with NSCLC. J Thorac Oncol. 2020;15(9):1460-1471.
14. Chen Y, Zhang S, Wang Q, et al. Tumor-recruited M2 macrophages promote gastric and breast cancer metastasis via M2 macrophage-secreted CHI3L1 protein. J Hematol Oncol. 2017;10(1):36.
15. Ma L, Zheng H, Zhang T. IL-10 suppress vascular smooth muscle cell apoptosis via JAK2/STAT3 signaling pathway and its mechanism of action in atherosclerosis. Minerva Endocrinol. 2019;44(4):402-405.
16. Liu Y, Che G, Di Z, et al. Calycosin-7-O-β-D-glucoside attenuates myocardial ischemia-reperfusion injury by activating JAK2/STAT3 signaling pathway via the regulation of IL-10 secretion in mice. Mol Cell Biochem. 2020;463(1-2):175-187.
17. Hu X, Gu Y, Zhao S, et al. Increased IL-10+CD206+CD14+M2-like macrophages in alveolar lavage fluid of patients with small cell lung cancer. Cancer Immunol Immunother. 2020;69(12):2547-2560.
18. Juncker-Jensen A, Stavrou N, Padmanabhan R, *et al*. A pro-tumorigenic mechanism of M2 tumor-associated macrophages in triple-negative breast cancer. Atlanta: AACR Annual Meeting. 2019:1175.
19. Zhang WJ, Wang XH, Gao ST, et al. Tumor-associated macrophages correlate with phenomenon of epithelial-mesenchymal transition and contribute to poor prognosis in triple-negative breast cancer patients. J Surg Res. 2018;222:93-101.

DOI 10.1007/s10330-021-0539-9
Cite this article as: Dong MT, Sheng JY, Li CY, et al. CD14 macrophage and IL-10 levels in the peripheral blood of breast cancer patients and their diagnostic value. Oncol Transl Med. 2022;8(4):165-172.

Oncology and Translational Medicine
DOI 10.1007/s10330-022-0552-2
August 2022, Vol. 8, No. 4, P173–P179

ORIGINAL ARTICLE

Expression and prediction of genes related to IGF2BP3 in gastric cancer*

Yulong Li[1] (✉), Yang Yang[2], Ruifang Sun[3]

[1] Department of gastroenterology, Shaanxi Provincial People's Hospital, Xi'an 710068, China
[2] School of Public Health, Shaanxi University of Chinese Medicine, Xianyang 712046, China
[3] Department of Pathology, School of Basic Medical Sciences, Xi'anJiaotong University Health Science Center, Xi'an Jiaotong University, Xi'an 710061, China

Abstract

Objective Gastric cancer (GC) is one of the most prevalent cancers worldwide and is associated with high morbidity and mortality rates. The IGF2 mRNA-binding protein (IGF2BP) participates in a variety of cancers. The aim of this study was to analyze the expression of IGF2BP3 and explore the genes related to *IGF2BP3* in GC.

Methods Bioinformatics software was used to analyze the expression of *IGF2BP1*, *IGF2BP2*, and *IGF2BP3* in tumors, and the expression of IGF2BPs in the GSE118897 dataset. Immunohistochemistry was performed to detect the protein level of IGF2BP3 in GC samples. cBioPortal was used to query gene alteration of IGF2BP3. LinkedOmics was used to identify genes related to *IGF2BP3*.

Results Sangerbox analysis showed that the expression of all IGF2BP family members was higher in GC. cBioporta analysis showed that gene alteration of IGF2BP3 in stomach adenocarcinoma included mutation and amplificatio. LinkedOmics analysis showed that many genes were correlated with IGF2BP3, such as *PLAGL2*, *GET4*, *IGF2BP1*, *HMGA2*, *CLDN6*, *HOXC13*, *SMARCA2*, *TMEM66*, *CIRBP*, *NFIX*, *SLC25A12*, and *CYB5D2*.

Conclusion In this study, we founded that IGF2BP3 was overexpressed in GC. Furthermore, this study identified potential genes related to IGF2BP3 in GC, which should be studied further.

Received: 21 March 2022
Revised: 23 June 2022
Accepted: 10 July 2022

Key words: gastric cancer (GC); IGF2 mRNA-binding protein 3 (IGF2BP3); bioinformatics analysis

Gastric cancer (GC) is one of the most prevalent cancers worldwide and is associated with high morbidity and mortality rates. There were an estimated 1,033,700 new stomach cancer cases and 782,700 stomach cancer-related deaths in 2018 [1]. Since the symptoms of GC are not obvious, most patients are diagnosed at intermediate and advanced stages when surgery is no longer an option. The prognosis for GC is poor, with patients in the advanced stage having a mean total survival of 10–12 months [2]. Therefore, identification of novel biomarkers is vital for the early diagnosis of GC.

The conserved IGF2 mRNA-binding protein (IGF2BP) family includes the genes *IGF2BP1*, *IGF2BP2*, and *IGF2BP3*, which encode a family of RNA-binding proteins that regulate their target genes. IGF2BP proteins play important roles in development, the nervous system, and cancer, and act as essential modulator in cell growth and differentiation [3]. IGF2BP3, also known as IMP3, binds to RNA and regulates the expression of target mRNAs involved in carcinogenesis. The expression of *IGF2BP3* may serve as a predictor of bladder cancer, since the protein expression of IGF2BP3 has been associated with advanced tumor stage, grade, and recurrence [4]. *IGF2BP3* has been suggested as a poor prognostic marker in gastric tumors [5].

In this study, we used bioinformatics to analyze the expression of IGF2BPs in GC. We selected IGF2BP3 for further study and performed immunohistochemistry (IHC) to detect the protein level of IGF2BP3 in GC. Furthermore, genes related to *IGF2BP3* in GC were analyzed using LinkedOmics. Our results suggest that *IGF2BP3* represents a promising therapeutic target for GC.

✉ Correspondence to: Yulong Li. E-mail: liyulong0639@126.com
*Supported by a grant from the National Natural Science Foundation of China (No. 81802788)

Materials and methods

SangerBox analysis

SangerBox (http://sangerbox.com/) was used to detect the expression of IGF2BP1, IGF2BP2, and IGF2BP3 in tumors based on The Cancer Genome Atlas (TCGA) and the Genotype-Tissue expression project (GTEx). Differences were considered significant at $P < 0.05$, $^{*}P < 0.05$, $^{**}P < 0.01$, $^{***}P < 0.001$.

Gene Expression Omnibus (GEO) analysis

GEO (https://www.ncbi.nlm.nih.gov/geo/) was used to further assess the expression of IGF2BPs in GSE118897 dataset [6] in matched GC and normal tissues. Based on the results of these analyses, we selected *IGF2BP3* for further study.

UALCAN analysis

UALCAN (http://ualcan.path.uab.edu/) [7] was used to detect the promoter methylation expression of IGF2BP3.

IHC assays

Tissue microarrays were obtained from Shanghai Outdo Biotech Company (Shanghai, China). Each section was deparaffinized with xylene and hydrated using an alcohol gradient. The sections were then treated for endogenous peroxidase-blocking and antigen retrieval. The sections were incubated with rabbit anti-IGF2BP3 followed by incubation with a secondary antibody. For visualization, 3,3'-diaminobenzidine (DAB) and hematoxylin were used. Digital images were obtained using a Leica image analysis system.

Genetic alteration analysis

The cBioPortal (http://www.cbioportal.org/) [8] was used to determine the genetic alteration characteristics of IGF2BP3. We chose the "Quick select" section and entered "IGF2BP3" to check the results of the alteration characteristics of IGF2BP3 across TCGA tumors which were observed in the "Cancer Types Summary" module.

LinkedOmics analysis

The LinkedOmics database [9] (http://www.linkedomics.org) contains multi-omics and clinical data from 32 cancer types and 11,158 patients from TCGA. We used the LinkedOmics database to identify genes related to *IGF2BP3* in the TCGA stomach adenocarcinoma. Pearson's correlation test was used to analyze the results.

Results

Expression of *IGF2BPs* in GC

We detected the expression levels of *IGF2BPs* from TCGA and GTEx using SangerBox. The results showed that IGF2BP1, IGF2BP2, and IGF2BP3 were more highly expressed in stomach cancer than in normal tissues (Fig.1a–1c).

IGF2BP3 expression is higher in GC

GEO was used to further assess the expression of *IGF2BP* genes in the GSE118897 dataset. The results showed that *IGF2BP1* and *IGF2BP2* were more highly expressed in GC tissues than in the normal gastric mucosa. However, this difference was not statistically significant (Fig. 2a and 2b). Compared with the expression in the normal gastric mucosa, *IGF2BP3* in GC tissues was significantly overexpressed (Fig. 2c). Therefore, we selected *IGF2BP3* for further study. The level of *IGF2BP3* promoter methylation in stomach cancer was also analyzed using UALCAN. The data showed that the promoter methylation level of *IGF2BP3* was significantly lower in stomach cancer tissues than in the control tissues (Fig. 2d).

Expression of IGF2BP3 is higher in GC

We performed IHC assays to detect the protein expression of IGF2BP3 in GC. The results demonstrated that the expression of IGF2BP3 was higher in GC tissues than in paracarcinoma tissues (Fig. 3).

Mutation of IGF2BP3

Fig. 4 showed the gene alteration of IGF2BP3 in tumor samples of the TCGA cohorts. The type of gene alteration of IGF2BP3 in Stomach Adenocarcinoma included mutation and amplification.

Genes related to *IGF2BP3*

We used LinkedOmics to identify genes related with IGF2BP3 in stomach cancer. A volcano plot revealed that genes correlated with *IGF2BP3* expression (false discovery rate < 0.05; Fig. 5a). Heat maps showing genes that were positively and negatively correlated with *IGF2BP3* in stomach adenocarcinoma (TOP 50) (Fig. 5b). *PLAGL2*, *GET4*, *IGF2BP1*, *HMGA2*, *CLDN6*, and *HOXC13* positively correlated with *IGF2BP3* expression in stomach adenocarcinoma. *SMARCA2*, *TMEM66*, *CIRBP*, *NFIX*, *SLC25A12*, and *CYB5D2* negatively correlated with *IGF2BP3* expression in stomach adenocarcinoma (Fig. 5c).

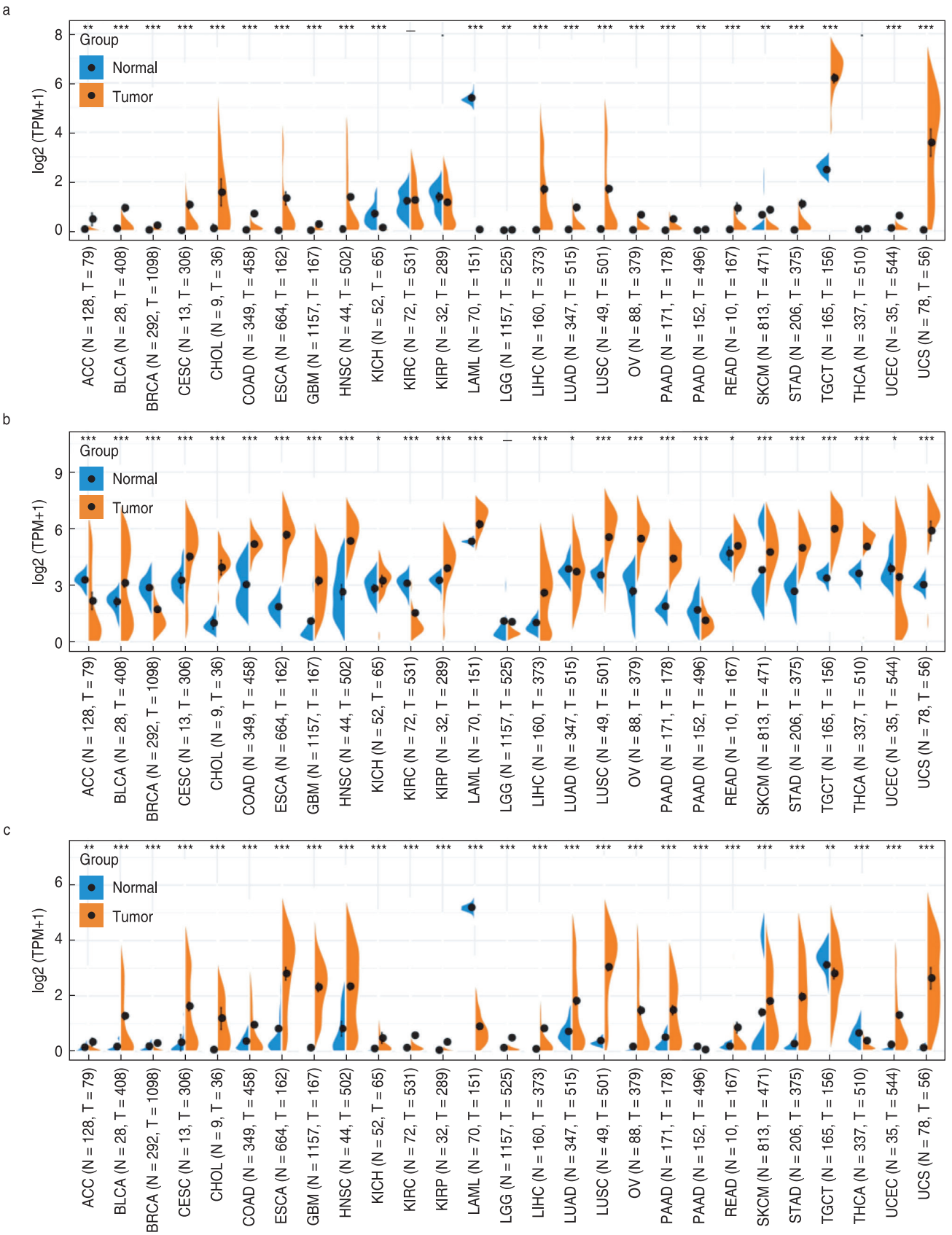

Fig. 1 Expression level of IGF2BP genes in gastric cancer
The expression of IGF2BP1 (a), IGF2BP2 (b), and IGF2BP3 (c) in tumors, analyzed using Sangerbox.

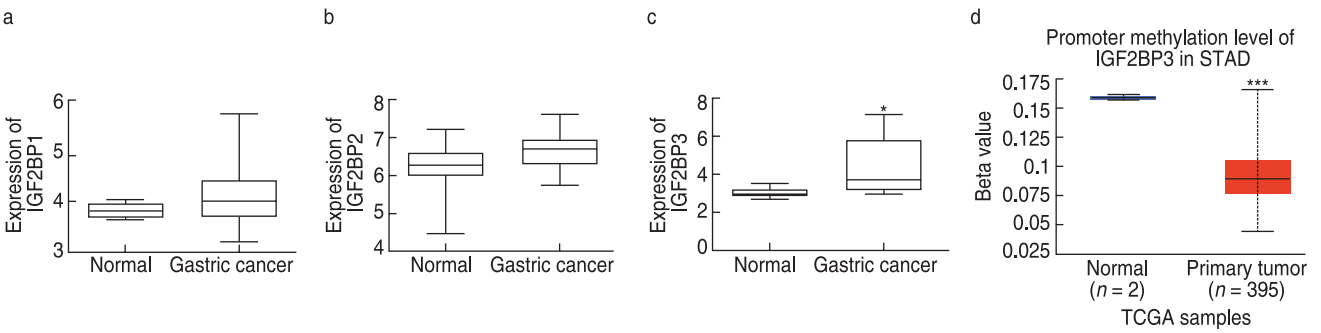

Fig. 2 *IGF2BP* gene analysis in gastric cancer, promoter methylation analysis. (a–c) Expression analysis of *IGF2BP1*, *IGF2BP2*, and *IGF2BP3* in paired gastric cancer and normal tissues in the GSE118897 dataset; (d) Promoter methylation level of *IGF2BP3* in gastric cancer. * $P < 0.05$.

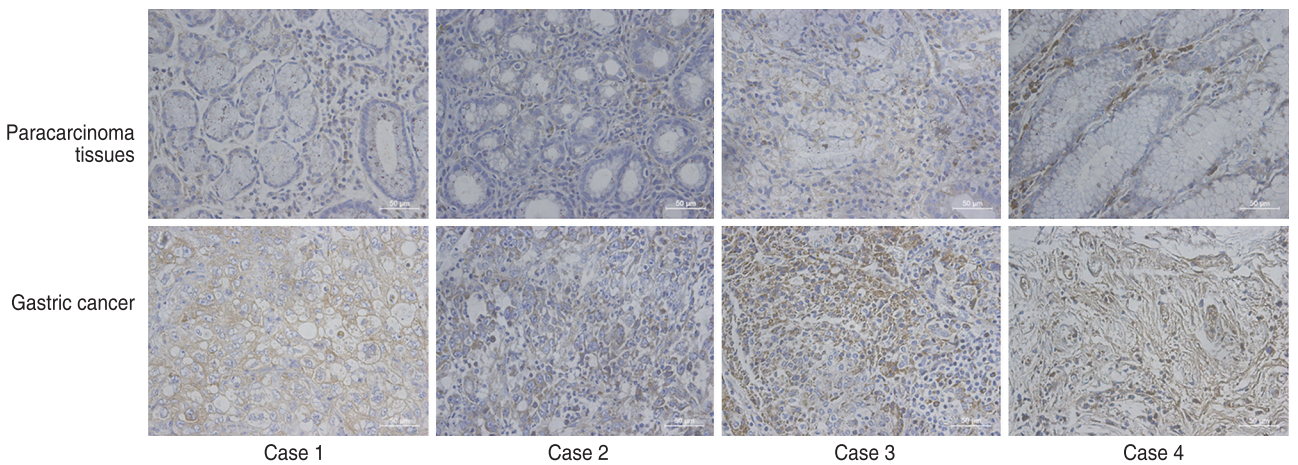

Fig. 3 Expression of *IGF2BP3* is higher in gastric cancer tissues.

Discussion

GC is a complex multifactorial disease, and genetic factors play a significant role in its development. Exploring the genes and signaling pathways related to the progression of GC could improve the early diagnosis rate and treatment options.

Recently, intensive research has demonstrated that IGF2BP3 is abnormally expressed in various tumor types, including human gliomas [10], neuroendocrine tumors of the lung [11], intrahepatic cholangiocarcinoma [12], prostate cancer [13], pediatric pilocytic and pilomyxoid astrocytoma [14], and endometrial clear cell carcinoma [15]. Zhou *et al.* [16]showed that *IGF2BP3* was dramatically overexpressed in GC tissues compared with normal gastric tissues, and higher expression of *IGF2BP3* was related to poor disease-specific survival. Collectively, these studies indicate that *IGF2BP3* may play a significant role in cancer. Therefore, assessing the expression of *IGF2BP3* and its interaction network may be useful for the diagnosis and treatment of cancer.

In recent years, the rapid development of bioinformatics methods that integrate big data has enabled advances in basic tumor research. In this study, we used bioinformatics tools to analyze the expression of *IGF2BP* genes and found that *IGF2BP3* was overexpressed in GC. We also found that the level of *IGF2BP3* promoter methylation in stomach cancer was significantly lower than that in control tissues, its elevated expression may be related to promoter hypomethylation. Additionally, heat maps showing genes positively and negatively correlated with IGF2BP3 expression in stomach adenocarcinoma. LinkedOmics showed that *PLAGL2*, *GET4*, *IGF2BP1*, *HMGA2*, *CLDN6*, and *HOXC13* were the top genes positively correlated with IGF2BP3 expression in stomach adenocarcinoma. PLAGL2 (pleomorphic adenoma gene like-2), a zinc finger PLAG transcription factor, is active in cancer progression. PLAGL2 could promote cell proliferation, migration and invasion in gastric cancer, play an important role in the stabilization of Snail1, and affect the Snail1-mediated GC cell proliferation and migration [17]. A previous study showed that *GET4* is one of the

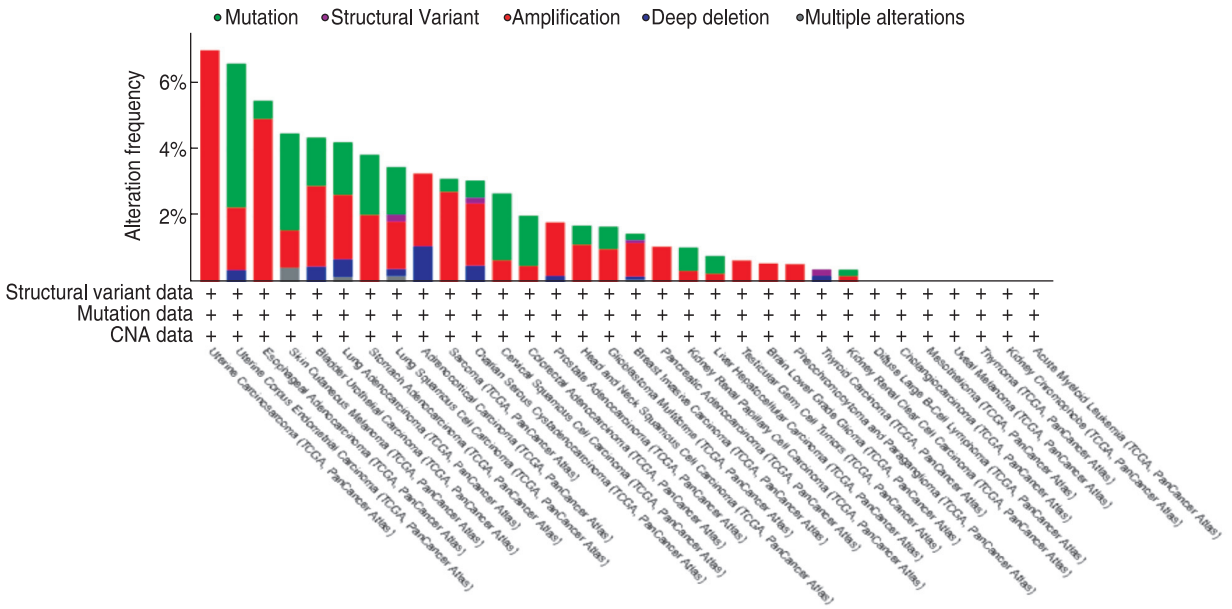

Fig. 4 Genetic alteration characteristics of IGF2BP3

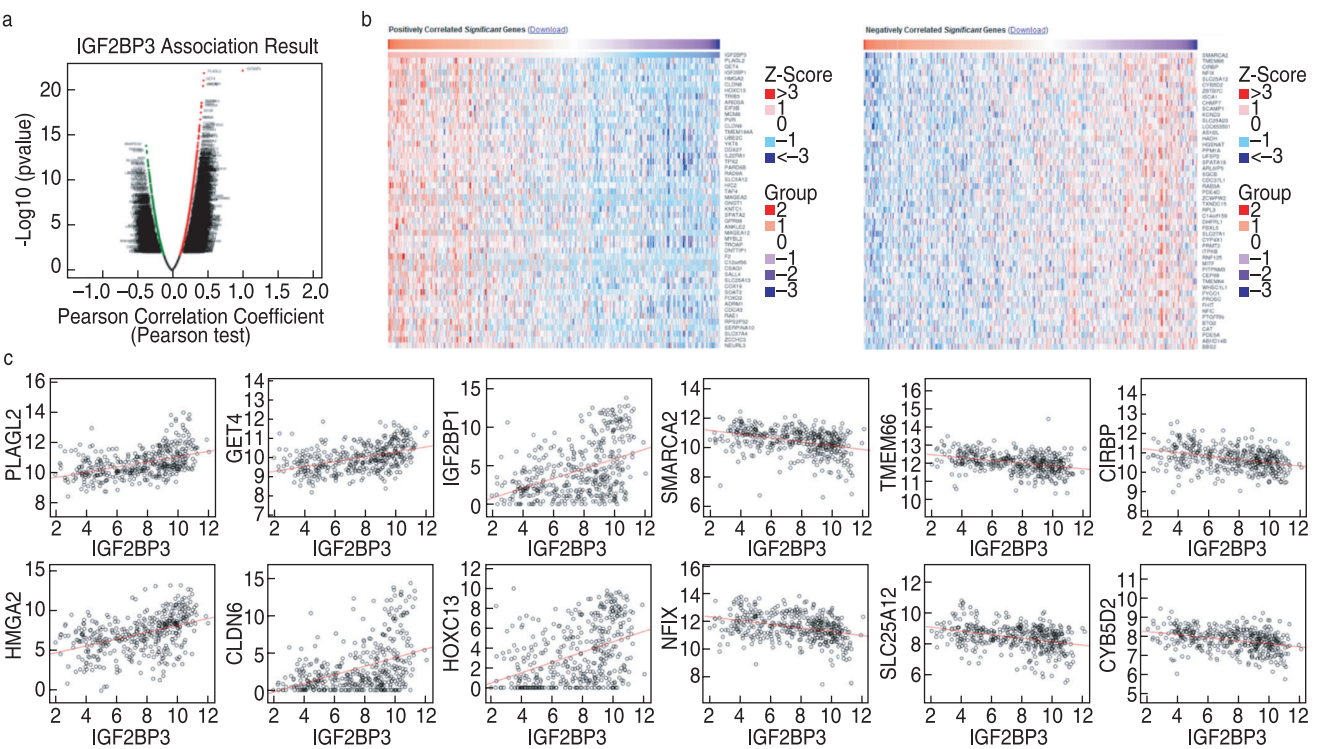

Fig. 5 Genes related to *IGF2BP3* in gastric cancer

(a) Pearson's test was performed to calculate correlations between IGF2BP3 expression and genes in gastric cancer by LinkedOmics; (b) Heat maps showing genes positively and negatively correlated with IGF2BP3 expression in stomach adenocarcinoma by LinkedOmics (TOP 50); (c) *PLAGL2*, *GET4*, *IGF2BP1*, *HMGA2*, *CLDN6*, *HOXC13*, *SMARCA2*, *TMEM66*, *CIRBP*, *NFIX*, *SLC25A12*, and *CYB5D2* were correlated with *IGF2BP3* in stomach adenocarcinoma.

genes altered in intestinal- and diffuse-type GC that were analyzed in chromosomal instability and genomically stable samples in TCGA RNA-seq data [18]. IGF2BP1 is involved in regulatory processes of long noncoding

(lnc)RNAs in GC cancer; lncRNA TRPM2-AS acted as a microRNA sponge for miR-612 and miR-612 could target IGF2BP1. Silencing the expression of IGF2BP1 inhibited GC cell proliferation and induced GC cell apoptosis; these findings reveal that IGF2BP1 has an oncogenic function in GC [19]. LncRNA GLCC1 regulates the migration and invasion of GC cells by enhancing the interaction of c-Myc/IGF2BP1 [20]. The high mobility group AT-hook 2 (HMGA2) is implicated in gastric carcinogenesis. The expression of HMGA2 significantly increased in GC samples compared with that in adenoma and normal gastric tissues. Multivariate analysis predicted that the expression of HMGA2 protein may be a useful prognostic marker for tumor recurrence [21]. Overexpression of HMGA2 induced GC cell sphere formation and migration [22]. Claudin6 (CLDN6) is a member of the tight junction family that participates in signal modulation in cancers [23]. CLDN6 expression was upregulated in both GC cell lines and tissues, and CLDN6 promoted GC proliferation and invasive ability [24]. *CLDN6* acts as a GC-promoting gene and may be a possible prognostic marker [25]. Analysis of the differentially expressed mRNAs and lncRNAs in 375 gastric adenocarcinomas and 32 adjacent non-tumor tissues on TCGA showed that lncRNA HOXC-AS3 may be a potential biomarker for gastric adenocarcinoma. HOXC-AS3 may regulate various *HOX* genes, including *HOXC13* in gastric adenocarcinoma [26]. LinkedOmics showed that *SMARCA2*, *TMEM66*, *CIRBP*, *NFIX*, *SLC25A12*, and *CYB5D2* were the top genes negatively correlated with IGF2BP3 expression in stomach adenocarcinoma. *SMARCA2* is a chromatin remodeling gene that plays vital roles in oncogenesis [27]. Somatic mutations of SMARCA2 have been reported in GC. Depletion of SMARCA2 in GC cell lines promoted cell proliferation [28]. TMEM66 may be related with multiple sclerosis and is likely a promising biomarker for multiple sclerosis [29]; nevertheless, the function of TMEM66 in cancer needs further study. CIRBP is a cold-shock protein, involved in cancers and inflammatory diseases, that regulates target mRNA. *CIRBP* is primarily thought to act as an oncogene, although it may also play a role in tumor suppression [30]. CIRBP is overexpressed in both bladder cancer tissues and cell lines, and can promote the proliferation and migration of bladder cancer cells [31]. CIRBP expression is higher in pancreatic ductal adenocarcinoma tumor tissues than in corresponding paracarcinoma tissues. CIRBP knockdown suppressed the proliferation of PANC-1 and SW1990 cancer cells, and overexpression of CIRBP promoted the proliferation of PANC-1 and SW1990 cells [32]. The role of CIRBP in gastric cancer requires further investigation. NFIX is a member of the nuclear factor I (NFI) family, which plays an important role in the development of several organs in mammals [33]. In GC, miR-625-5p targeted NFIX, and overexpression of NFIX could rescue the effect of LINC00511 silencing [34]. SLC25A12 (AGC1) is a vital component of the malate-aspartate shuttle, and SLC25A12 can affect pulmonary metastasis [35]. SLC25A12 was reactivated in HepG2 cells via CREB recruitment and histone acetylation. Silencing SLC25A12 inhibits the proliferation of HepG2 cells by regulating the cell cycle [36]. The expression of SLC25A12 is aberrant in acute myeloid leukemia (AML); it is overexpressed in AML patients compared with healthy people, and the expression of SLC25A12 is related to shorter event-free survival and overall survival of AML patients. SLC25A12 is a potential prognostic biomarker for AML [37]. CYB5D2 suppresses the proliferation of MCF7 cells and is a potential tumor suppressor in breast cancer [38]. CYB5D2 inhibits the invasion of HeLa cells. The expression of CYB5D2 was reduced in cervical squamous cell carcinomas [39]. Some of these predicted genes, which may be related to IGF2BP3, have been reported to play essential roles in gastric cancer. Overall, our results may be a starting point for further research on the function of IGF2BP3 in GC.

Acknowledgments

Not applicable.

Funding

This work was supported by the National Natural Science Foundation of China (No. 81802788)

Conflicts of interest

The authors indicated no potential conflicts of interest.

Author contributions

All authors contributed to data acquisition. All authors reviewed and approved the final version of this manuscript.

Data availability statement

The data that support the findings of this study are available from Yulong Li .

Ethical approval

This study was approved by the Ethics Committee of Shanghai Outdo Biotech Company.

References

1. Ferlay J, Colombet M, Soerjomataram I, et al. Estimating the global cancer incidence and mortality in 2018: GLOBOCAN sources and methods. Int J Cancer. 2019;144(8):1941-1953.
2. Digklia A, Wagner AD. Advanced gastric cancer: Current treatment landscape and future perspectives. World J Gastroenterol. 2016;22(8):2403-2414.
3. Bell JL, Wachter K, Muhleck B, et al. Insulin-like growth factor 2 mRNA-binding proteins (IGF2BPs): post-transcriptional drivers of cancer progression?. Cell Mol Life Sci. 2013;70(15):2657-2675.

4. Yang F, Zhou Q, Meng L, et al. IMP3 is a biomarker for non-muscle-invasive urothelial carcinoma of the bladder associated with an aggressive phenotype. Medicine (Baltimore). 2019;98(27):e16009.
5. Wang L, Li HG, Xia ZS, et al. IMP3 is a novel biomarker to predict metastasis and prognosis of gastric adenocarcinoma: a retrospective study. Chin Med J. 2010;123(24):3554-3558.
6. Yang Z, Li C, Yan C, et al. KIF14 promotes tumor progression and metastasis and is an independent predictor of poor prognosis in human gastric cancer. Biochim Biophys Acta Mol Basis Dis. 2019;1865(8):181-192.
7. Chandrashekar DS, Bashel B, Balasubramanya SAH, et al. UALCAN: A portal for facilitating tumor subgroup gene expression and survival analyses. Neoplasia. 2017;19(5):649-658.
8. Cerami E, Gao J, Dogrusoz U, et al. The cBio cancer genomics portal: an open platform for exploring multidimensional cancer genomics data. Cancer Discov. 2012;2(5):401-404.
9. Vasaikar SV, Straub P, Wang J, et al. LinkedOmics: analyzing multi-omics data within and across 32 cancer types. Nucleic Acids Res. 2018;46(D1):D956-D963.
10. Del Gobbo A, Vaira V, Ferrari L, et al. The oncofetal protein IMP3: a novel grading tool and predictor of poor clinical outcome in human gliomas. Biomed Res Int. 2015;2015:413897.
11. Del Gobbo A, Vaira V, Guerini Rocco E, et al. The oncofetal protein IMP3: a useful marker to predict poor clinical outcome in neuroendocrine tumors of the lung. J Thorac Oncol. 2014;9(11):1656-1661.
12. Gao Y, Yang M, Jiang Z, et al. IMP3 expression is associated with poor outcome and epigenetic deregulation in intrahepatic cholangiocarcinoma. Hum Pathol. 2014;45(6):1184-1191.
13. Szarvas T, Tschirdewahn S, Niedworok C, et al. Prognostic value of tissue and circulating levels of IMP3 in prostate cancer. Int J Cancer. 2014;135(7):1596-1604.
14. Barton VN, Donson AM, Birks DK, et al. Insulin-like growth factor 2 mRNA binding protein 3 expression is an independent prognostic factor in pediatric pilocytic and pilomyxoid astrocytoma. J Neuropathol Exp Neurol. 2013;72(5):442-449.
15. Fadare O, Liang SX, Crispens MA, et al. Expression of the oncofetal protein IGF2BP3 in endometrial clear cell carcinoma: assessment of frequency and significance. Hum Pathol. 2013;44(8):1508-1515.
16. Zhou Y, Huang T, Siu HL, et al. IGF2BP3 functions as a potential oncogene and is a crucial target of miR-34a in gastric carcinogenesis. Mol Cancer. 2017;16(1):77.
17. Wu L, Zhao N, Zhou Z, et al. PLAGL2 promotes the proliferation and migration of gastric cancer cells via USP37-mediated deubiquitination of Snail1. Theranostics. 2021;11(2):700-714.
18. Tanabe S, Quader S, Ono R, et al. Molecular network profiling in intestinal- and diffuse-type gastric cancer. Cancers (Basel). 2020;12 (12):3833.
19. Xiao J, Lin L, Luo D, et al. Long noncoding RNA TRPM2-AS acts as a microRNA sponge of miR-612 to promote gastric cancer progression and radioresistance. Oncogenesis. 2020;9(3):29.
20. Yang DL, Dong LF, Qiu YB, et al. An oncogenic lncRNA, GLCC1, promotes tumorigenesis in gastric carcinoma by enhancing the c-Myc/IGF2BP1 interaction. Neoplasma. 2021;68(5):1052-1062.
21. Jun KH, Jung JH, Choi HJ, et al. HMGA1/HMGA2 protein expression and prognostic implications in gastric cancer. Int J Surg. 2015;24(Pt A):39-44.
22. Sun J, Sun B, Zhu D, et al. HMGA2 regulates CD44 expression to promote gastric cancer cell motility and sphere formation. Am J Cancer Res. 2017;7(2):260-274.
23. Qu H, Jin Q, Quan C. CLDN6: From traditional barrier function to emerging roles in cancers. Int J Mol Sci. 2021;22(24):13416.
24. Yu S, Zhang Y, Li Q, et al. CLDN6 promotes tumor progression through the YAP1-snail1 axis in gastric cancer. Cell Death Dis. 2019; 10(12):949.
25. Kohmoto T, Masuda K, Shoda K, et al. Claudin-6 is a single prognostic marker and functions as a tumor-promoting gene in a subgroup of intestinal type gastric cancer. Gastric Cancer. 2020;23(3):403-417.
26. Fu T, Ji X, Bu Z, et al. Identification of key long non-coding RNAs in gastric adenocarcinoma. Cancer Biomark. 2020;27(4):541-553.
27. Horton RK, Ahadi M, Gill AJ, et al. SMARCA4/SMARCA2-deficient Carcinoma of the Esophagus and Gastroesophageal Junction. Am J Surg Pathol. 2021;45(3): 414-420.
28. Takeshima H, Niwa T, Takahashi T, et al. Frequent involvement of chromatin remodeler alterations in gastric field cancerization[J]. Cancer Lett. 2015;357(1):328-338.
29. Taha S, Aljishi M, Alsharoqi I, et al. Differential upregulation of the hypothetical transmembrane protein 66 (TMEM66) in multiple sclerosis patients with potential inflammatory response. Biomed Rep, 2015;3(1):98-104.
30. Kim YM, Hong S. Controversial roles of coldinducible RNAbinding protein in human cancer (Review). Int J Oncol. 2021;59(5):91.
31. Lu M, Ge Q, Wang G, et al. CIRBP is a novel oncogene in human bladder cancer inducing expression of HIF-1alpha. Cell Death Dis. 2018;9:1046.
32. Chen X, Xie H, Wang X, et al. CIRBP Knockdown Attenuates Tumourigenesis and Improves the Chemosensitivity of Pancreatic Cancer via the Downregulation of DYRK1B. Front Cell Dev Biol. 2021;9(10):667551.
33. Li Y, Sun C, Tan Y, et al. Transcription levels and prognostic significance of the NFI family members in human cancers. Peer J. 2020;8:e8816.
34. Chen Z, Wu H, Zhang Z, et al. LINC00511 accelerated the process of gastric cancer by targeting miR-625-5p/NFIX axis. Cancer Cell Int. 2019;26(19):351.
35. Alkan HF, Vesely PW, Hackl H, et al. Deficiency of malate-aspartate shuttle component SLC25A12 induces pulmonary metastasis. Cancer Metab. 2020;8(1):26.
36. Infantino V, Dituri F, Convertini P, et al. Epigenetic upregulation and functional role of the mitochondrial aspartate/glutamate carrier isoform 1 in hepatocellular carcinoma. Bio Biophys Acta Mol Basis Dis. 2019;1865(1):38-47.
37. Liu YC, Yin CL, Chen Q, et al. Prognostic value of SLC25A12 expression in patients with acute myeloid leukemia based on integrated analysis of multi-dimensional clinical data. Zhongguo Shi Yan Xue Ye Xue Za Zhi. 2020;28(2):377-384.
38. Ojo D, Rodriguez D, Wei F, et al. Downregulation of CYB5D2 is associated with breast cancer progression. Sci Rep. 2019;9(1): 6624.
39. Xie Y, Shen YT, Kapoor A, et al. CYB5D2 displays tumor suppression activities towards cervical cancer. Biochim Biophys Acta. 2016;1862(4):556-565.

DOI 10.1007/s10330-022-0552-2
Cite this article as: Li YL, Yang Y, Sun RF. Expression and prediction of genes related to IGF2BP3 in gastric cancer. Oncol Transl Med. 2022;8(4):173-179.

Oncology and Translational Medicine
DOI 10.1007/s10330-022-0548-8

August 2022, Vol. 8, No. 4, P180–P185

ORIGINAL ARTICLE

CEA levels predict tumor response to neoadjuvant chemoradiotherapy in locally advanced rectal cancer*

Lili Shen[1] (✉), Chao Li[2], Jingwen Wang[3], Jin Fan[3], Ji Zhu[3] (✉)

[1] Department of Oncology, Nantong Haimen People's Hospital, Haimen Hospital of Nantong University, Nantong 226100, China
[2] Department of Radiotherapy, Huashan Hospital, Fudan University, Shanghai 200032, China
[3] Department of Radiation Oncology, Fudan University Shanghai Cancer Center, Shanghai 200032, China

Abstract

Objective The aim of this study was to evaluate the impact of serum carcinoembryonic antigen (CEA) in the prediction of pathological complete response (pCR) in locally advanced rectal cancer (LARC) patients treated with neoadjuvant chemoradiotherapy (nCRT).

Methods A total of 925 LARC patients who underwent nCRT followed by TME between March 2006 and February 2018 were enrolled at Fudan University Shanghai Cancer Center. Using logistic regression models, we investigated the associations between serum CEA levels and pathological complete remission (pCR). Further stratified analyses were performed according to different CEA thresholds.

Results We found that pre-nCRT CEA and post-nCRT CEA were negatively correlated with pCR ($P < 0.001$). Stratified analyses revealed that when the CEA cutoff value was set to 5 ng/mL, 10.6% of patients with post-nCRT CEA levels > 5 ng/mL achieved pCR. Meanwhile, when the CEA cutoff value was set to 10 ng/mL, only 6.8% of the patients with post-nCRT CEA levels > 10 ng/mL achieved pCR.

Conclusion In summary, pre- and post-nCRT CEA levels ≤ 5 ng/mL were favorable predictors of pCR in LACR patients, and the "watch and wait" strategy is not recommended for patients with post-nCRT CEA levels > 10 ng/mL.

Received: 21 March 2022
Revised: 20 April 2022
Accepted: 14 July 2022

Key words: locally advanced rectal cancer (LARC); carcinoembryonic antigen (CEA); neoadjuvant chemoradiotherapy; pathological complete response (pCR)

Rectal cancer is one of the leading causes of mortality and morbidity worldwide, and its growing incidence reflects the consequences of a modification in lifestyle behaviors [1]. According to NCCN clinical practice guidelines [2], the standard treatment for locally advanced rectal cancer (LARC) includes neoadjuvant chemoradiotherapy (nCRT) followed by total mesorectal excision (TME). However, prior studies have shown inconsistent treatment responses to neoadjuvant CRT, ranging from a pathological complete response (pCR) to the total resistance. Previous studies [3–7] have shown that rectal cancer patients with pCR after neoadjuvant chemoradiotherapy and surgical resection of the primary lesion have better long-term outcomes than patients who lack significant remission or non-remission, and pCR rates of 10%-30% have been reported in some studies [8–10]. However, a method to identify patients who can benefit the most from nCRT remains to be found. This stratification could be used to identify patients in whom "watch and wait" management may be a significant treatment option. "Watch and wait" is a novel alternative to TME after a clinical complete response (cCR) to nCRT with the promise of improved quality of life and comparable cure effect [11]. In addition, the NCCN guidelines suggest that "watch and wait" management may be considered for patients with a cCR and no evidence of residual disease. Therefore, it is important to explore predictive factors of pCR before surgery in LARC patients to support decision-making in organ preservation strategies.

In recent years, a number of studies have explored the importance of pre- and post-nCRT carcinoembryonic antigen (CEA) levels on pCR and come to different conclusions. Some studies [12–15] have reported that a lower pre-treatment CEA level is associated with a higher pCR

✉ Correspondence to: Lili Shen. Email: shenlilimao2012@163.com; Ji Zhu. Email: leoon.zhu@gmail.com.
* Supported by a grant from the Scientific research project of Nantong Municipal Health Commission (No. QA2019049)

rate, while others have shown that the predictive value is only significant in non-smokers [16–17]. Other studies have shown that a lower pre-nCRT CEA level is not correlated with pCR [18–19], while post-nCRT CEA is negatively correlated with pCR [20–22]. Furthermore, several studies have suggested that patients with elevated pre-nCRT CEA levels may not be suitable for the "watch and wait" strategy [23]. However, only limited research focusing on the correlation between pre- and post-treatment CEA and pCR in the Asian population has been performed. Therefore, this retrospective study was performed to evaluate the predictive value of pre- and post-treatment CEA levels after neoadjuvant chemoradiotherapy in LARC patients. These findings can be used to distinguish LARC patients who are suitable for the "watch and wait" strategy based on the CEA levels.

Materials and methods

Study participants

Between March 2006 and February 2018, a total of 1130 patients with locally advanced rectal cancer received nCRT at Fudan University Shanghai Cancer Center. The inclusion criteria of this study were as follows: (1) distance from the anal verge ≤ 12 cm; (2) histopathological diagnosis of adenocarcinoma; (3) clinical stage T3-4 and/or N+ with MRI or ERUS; (4) no evidence of distant metastasis shown on computed tomography (CT) of the chest and abdomen; (5) receiving a long-course CRT followed by radical resection within 6-10 weeks after the end of CRT; (6) available pre- and post-nCRT CEA data. Pre-nCRT CEA level was defined as the CEA value measured within one week before nCRT, while post-nCRT CEA level is the CEA value measured within one week before surgery.

Treatment

All the patients underwent intensity-modulated radiation therapy (IMRT) ranging from 44 to 55 Gy in 20 to 25 fractions, concurrent with capecitabine-based chemotherapy, including capecitabine alone, capecitabine plus oxaliplatin, and capecitabine plus irinotecan. A TME was performed 6-10 weeks after completion of CRT. The pathological evaluation was defined according to the 8th American Joint Committee on Cancer (AJCC) Manual [24]. PCR was defined as complete regression of both the primary lesion and the regional lymph nodes.

Statistical analysis

Patient's demographic and clinical-pathological features, including age, gender, Body Mass Index (BMI), distance from the anal verge, clinical T- and N-stage, pathological T- and N-stage after TME, CRT regimen, type of surgery, and CEA values of pre- and post-CRT were retrieved from the patient's medical records.

Continuous variables were reported as mean and standard deviations, and categorical variables were shown as frequencies or percentages. Fisher's exact and Pearson's chi-square tests were used to determine correlations between categorical variables. Logistic regression models identified the predictors of endpoint pCR. For all analyses, a P-value of < 0.05 was considered significant. Statistical analyses were performed using SPSS 26.0 software.

Results

Baseline characteristics

A total of 925 patients were recruited for this retrospective study (Fig. 1 and Table 1). Overall, 29 patients (3.1%) had a clinical T2 primary tumor, 748 (80.9%) had a clinical T3 primary tumor, and 148 (16%) had a clinical T4 primary tumor. Further, 64 patients (6.9%) had a clinical N0 and 861 (93.1%) had a clinical N+, indicating lymphatic metastasis. Tumor pathological staging after TME was evaluated, and 194 patients (21.0%) achieved pCR, as shown in Table 2. Serum CEA levels were collected at two different time periods, one week before nCRT and one week before surgery. In total, 408 patients had pre-nCRT CEA levels greater than 5 ng/mL, while 217 patients had post-nCRT CEA levels greater than 5 ng/mL, while 103 patients had levels > 10 ng/mL.

Multivariate analysis of pCR

A logistic regression model was used to analyze the potential factors influencing pCR (Table 3). The findings revealed that patients with pre-nCRT CEA levels ≤ 5 ng/mL were more likely to achieve a pCR (RR = 0.596, $P < 0.001$). Similarly, post-nCRT CEA levels were negatively correlated with the pCR rate (RR = 0.438, $P < 0.001$). Other factors, including age, sex, BMI, clinical T-category, clinical N-category, and distance from the anal verge, were not significantly associated with pCR.

Stratified analysis of the effect of CEA after nCRT on pCR

The 5 ng/mL and 10 ng/mL cutoff values were set to stratify the patients based on their post-nCRT CEA level. There were 217 patients with CEA greater than 5 ng/mL (Table 4), whose pCR rate was 10.6%. Among the remaining 708 patients, 24.2% achieved pCR. There were 103 patients with CEA greater than 10 ng/mL (Table 4), in whom only 6.8% achieved pCR, while the corresponding rate was 22.7% in the remaining patients. The differences in complete response rate between subgroups were statistically significant.

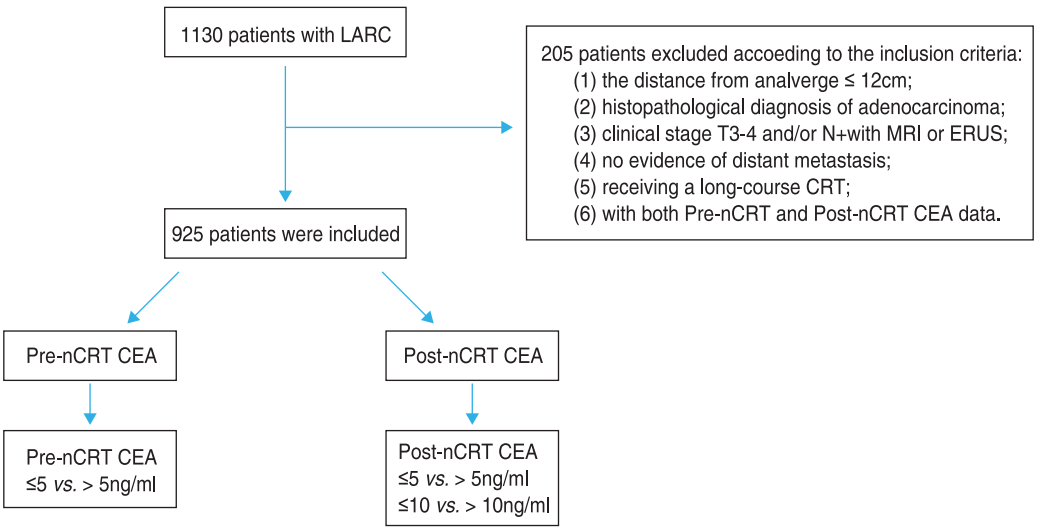

Fig. 1 Stages of this research. Between March 2006 and February 2018, a total of 1130 patients with locally advanced rectal cancer received nCRT at Fudan University Shanghai Cancer Center. In this period, 925 patients met the inclusion criteria for this retrospective analysis, with available pre- and post-nCRT CEA levels.

Discussion

In this study, CEA expression levels were significantly associated with pCR in LARC patients, indicating their use in predicting patient response to nCRT. Patients with pre-nCRT CEA level > 5 ng/mL had a lower pCR (P< 0.001). Similarly, a higher post-nCRT CEA level was negatively correlated with higher pCR (CEA cutoff value set to 5 ng/mL, RR = 0.438, P< 0.001; CEA cutoff value set to 10 ng/mL, RR = 0.300, P < 0.001, respectively). The pCR rate of patients with CEA level > 5 ng/mL was 10.6%, while the pCR rate of the remaining patients with CEA level ≤ 5 ng/mL was 24.2%. Meanwhile, patients with a CEA level greater than 10 ng/mL had a very low pCR rate of 6.8%, while that in the remaining patients was 22.7%. There was no significant correlation between age, sex, BMI, clinical T-category, clinical N-category, and location from the anal verge with pCR.

In this study, the 21.0% pCR rate obtained is consistent with data reported in other studies (10%–30%) [8–10]. CRT and TME result in a poor-quality of life due to adverse reactions to TME. The idea of the "watch and wait" method was first proposed by Habr-Gama [11] and is based on the idea that treatment strategy for LARC patients should be chosen based on the stages after neoadjuvant therapy. Studies have shown that LARC patients who received cCR after chemoradiotherapy have better long-term follow-up results with a "watch and wait" strategy. However, other studies have reported that only 36% of patients clinically evaluated as cCR achieve pCR after surgery. Therefore, precise diagnosis of cCR patients is important. Herein, we performed a large sample study to explore the predictive ability of curative characteristics of nCRT treatment efficacy and to define predictive factors of complete remission.

Recently, studies have discussed the correlation between CEA and treatment evaluation in rectal cancer. Joye I *et al.* [15] reports that the pre-treatment CEA mean level is statistically significant with pCR to nCRT (P = 0.04). Yinuo Tan *et al.* [13] reported that the pCR rate was 22% in patients with pre-treatment CEA levels < 5 ng/mL and 18% in patients with pre-treatment CEA levels ≥ 5 ng/mL. Kleiman *et al.* [19] demonstrate that post-CRT CEA levels are significantly lower in LARC patients with pCR (1.7 *vs.* 2.4 mg/L, P< 0.01). These studies indicate that both pre- and post-CRT CEA levels are strong predictors of achieving pCR in LARC. Similarly, we found that low pre- and post-nCRT CEA levels are significant predictors of pCR. Furthermore, when stratified according to the post-nCRT CEA level (10 ng/mL), the difference in pCR rate between subgroups is significant (6.8% *vs.* 22.7%). Therefore, the "watch and wait" strategy is not recommended if the LARC patients' post-nCRT CEA level is greater than 10 ng/mL after chemoradiotherapy.

Fewer studies have combined the predictive value of the CEA level with the "watch and wait" strategy. This has been associated with a lack of accuracy and sensitivity of CEA in predicting the efficacy of nCRT in LARC. Other studies have identified other predictors of the curative effect of nCRT in LARC. Monguzzi L *et al.* [25] reported that the apparent diffusion coefficient (ADC) value of magnetic resonance diffusion-weighted imaging (DW-MRI) could be used to predict the pathological grade of nCRT. Jia H *et al.* [26] reported a panel of metabolites used to predict pathological response to nCRT in LARC. Zhang J *et al.* [27] also found that the LARC assigner 3 classification

Table 1 Baseline characteristics.

Items	*n*	%
Total	925	100.0
Age (years)		
≤ 55	440	47.6
> 55	485	52.4
Sex		
Male	634	68.5
Female	291	31.5
BMI		
< 18	38	4.1
18–25	640	69.2
≥ 25	208	22.5
Unknown or missing	39	4.2
Clinical T-categary		
cT2	29	3.1
cT3	748	80.9
cT4	148	16.0
Clinical N-categary		
cN0	64	6.9
cN+	861	93.1
Location from anal verge (cm)		
≤ 5	501	54.2
> 5	424	45.8
CRT regimen		
Cap + RT	354	38.3
CapOx + RT	295	31.9
CapIri + RT	276	29.8
Pre-nCRT CEA level[a]		
≤ 5	517	55.9
> 5	408	44.1
Post-nCRT CEA level[b] (cutoff = 5)		
≤ 5	708	76.5
> 5	217	23.5
Post-nCRT CEA level[b] (cutoff = 10)		
≤ 10	822	88.9
> 10	103	11.1

Note:
[a] Pre-nCRT CEA level was defined as the CEA value within one week before nCRT.
[b] Post-nCRT CEA level was defined as the CEA value within one week before surgery.
Abbreviation: BMI, Body Mass Index; CRT, chemoradiotherapy; RT, radiotherapy; N+, lymphatic metastasis.

could predict outcomes in LARC patients, and tumors identified as low-risk based on this classification had a better prognosis.

This study had several limitations. First, this retrospective study used data from only a single cancer center, which may have led to selection bias. Second, we only reported a correlation between CEA levels and a pCR, but other associated serum tumor markers were not completely collected. Lastly, our study did not analyze the prognosis of patients who chose nonsurgical treatment based on the CEA value.

Table 2 Surgical type and pathological results.

Items	*n*	%
Total	925	100.0
Surgery		
Miles	415	44.9
Dixon	458	49.5
Hartmann	52	5.6
pCR		
Yes	194	21.0
No	731	79.0
ypT		
ypT0	215	23.2
ypT1	33	3.6
ypT2	246	26.6
ypT3	413	44.6
ypT4	18	1.9
ypN		
ypN0	587	63.5
ypN1	263	28.4
ypN2	75	8.1

Note: yp, pathological staging after neoadjuvant therapy.

Table 3 Relative risk for pCR.

Items	RR	*P* value
Age (> 55 *vs.* ≤ 55)	0.867	0.277
Sex (Female *vs.* Male)	0.976	0.858
BMI (≥ 25 *vs.* < 25)	1.250	0.261
Clinical T (cT4 *vs.* cT2-3)	0.958	0.970
Clinical N (cN+ *vs.* cN0)	1.039	0.977
Location from anal verge (> 5 cm *vs.* ≤ 5cm)	0.958	0.755
Pre-nCRT CEA level (> 5 *vs.* ≤ 5)	0.596	< 0.001
Post-nCRT CEA level (> 5 *vs.* ≤ 5)	0.438	< 0.001
Post-nCRT CEA level (> 10 *vs.* ≤ 10)	0.300	< 0.001

Note: RR, risk ratio

Table 4 Correlation between Post-nCRT CEA level and pCR.

Items	PCR		Non-PCR		*P* value
	n	%	*n*	%	
Using 5 ng/mL as Cut-off value of CEA					< 0.001
≤ 5 ng/mL	171	24.2	537	75.8	
> 5 ng/mL	23	10.6	194	89.4	
Using 10 ng/mL as Cut-off value of CEA					< 0.001
≤ 10 ng/mL	187	22.7	635	77.3	
> 10 ng/mL	7	6.8	96	93.2	

Note: CEA refers to Post-nCRT CEA.

Conclusion

This study demonstrated that high serum CEA level is an independent predictor for a lower rate of pCR in locally advanced rectal cancer patients. This could facilitate patient selection and aid clinicians to identify patients who may benefit most from watch-and-wait strategies. However, further prospective, randomized large-scale studies are warranted to combine predictive

factors to develop a multi-factor prediction model with a more accurate prediction of complete remission.

Acknowledgments

Not applicable.

Funding

Supported by a grant from the Scientific research project of Nantong Municipal Health Commission (No. QA2019049).

Conflicts of interest

The authors indicated no potential conflicts of interest.

Author contributions

All authors contributed to data acquisition, data interpretation, and reviewed and approved the final version of this manuscript.

Data availability statement

Not applicable.

Ethical approval

It has passed the ethical examination of our hospital.

References

1. Siegel RL, Miller KD, Fuchs HE, et al. Cancer statistics, 2021. CA Cancer J Clin. 2021;71(1):7-33.
2. Benson AB, Venook AP, Al-Hawary MM, et al. NCCN Guidelines Insights: Rectal Cancer, Version 6.2020. J Natl Compr Canc Netw. 2020;18(7):806-815.
3. Belluco C, Forlin M, Olivieri M, et al. Long-term outcome of rectal cancer with clinically (EUS/MRI) metastatic mesorectal lymph nodes treated by neoadjuvant chemoradiation: role of organ preservation strategies in relation to pathologic response. Ann Surg Oncol. 2016;23(13):4302-4309.
4. Hasan S, Renz P, Wegner RE, et al. Microsatellite instability (MSI) as an independent predictor of pathologic complete response (PCR) in LIDB) Analysis. Ann Surg. 2020;271(4):716-723.
5. Hu Y, Wei J, Chang H, et al. The high pCR rate of sandwich neoadjuvant treatment in locally advanced rectal cancer may translate into a better long-term survival benefit: 5-year outcome of a Phase II clinical trial. Cancer Manag Res. 2018;10:4363-4369.
6. Jalilian M, Davis S, Mohebbi M, et al. Pathologic response to neoadjuvant treatment in locally advanced rectal cancer and impact on outcome. J Gastrointest Oncol. 2016;7(4): 603-608.
7. Petrelli F, Coinu A, Cabiddu M, et al. Correlation of pathologic complete response with survival after neoadjuvant chemotherapy in bladder cancer treated with cystectomy: a meta-analysis. Eur Urol. 2014;65(2):350-357.
8. Maas M, Nelemans PJ, Valentini V, et al. Long-term outcome in patients with a pathological complete response after chemoradiation for rectal cancer: a pooled analysis of individual patient data. Lancet Oncol. 2010;11(9):835-844.
9. Zeng W, Liang J, Wang Z, et al. Clinical parameters predicting pathologic complete response following neoadjuvant chemoradiotherapy for rectal cancer. Chin J Cancer. 2015;34(10):468-474.
10. Zhu J, Liu F, Gu W, et al. Concomitant boost IMRT-based neoadjuvant chemoradiotherapy for clinical stage II/III rectal adenocarcinoma: results of a phase II study. Radiat Oncol. 2014;9:70.
11. Habr-Gama A, Perez RO, Nadalin W, et al. Operative versus nonoperative treatment for stage 0 distal rectal cancer following chemoradiation therapy: long-term results. Ann Surg. 2004;240(4):711-718.
12. Peng H, Wang C, Xiao W, et al. Analysis of Clinical characteristics to predict pathologic complete response for patients with locally advanced rectal cancer treated with neoadjuvant chemoradiotherapy. J Cancer. 2018;9(15):2687-2692.
13. Tan Y, Fu D, Li D, et al. Predictors and risk factors of pathologic complete response following neoadjuvant chemoradiotherapy for rectal cancer: a population-based analysis. Front Oncol. 2019;9: 497.
14. Tomono A, Yamashita K, Kanemitsu K, et al. Prognostic significance of pathological response to preoperative chemoradiotherapy in patients with locally advanced rectal cancer. Int J Clin Oncol. 2016; 21(2):344-349.
15. Joye I, Debucquoy A, Fieuws S, et al. Can clinical factors be used as a selection tool for an organ-preserving strategy in rectal cancer? Acta Oncol. 2016;55(8):1047-1052.
16. Wallin U, Rothenberger D, Lowry A, et al. CEA – a predictor for pathologic complete response after neoadjuvant therapy for rectal cancer. Dis Colon Rectum. 2013;56(7):859-868.
17. Yang J, Ling X, Tang W, et al. Analyses of predictive factors for pathological complete remission in neoadjuvant therapy for locally advanced rectal cancer. J BUON. 2019;24(1):77-83.
18. Kalady MF, Campos-Lobato LFD, Stocchi L, et al. Predictive factors of pathologic complete response after neoadjuvant chemoradiation for rectal cancer. Ann Surg. 2009;250(4):582-589.
19. Kleiman A, Al-Khamis A, Farsi A, et al. Normalization of CEA levels post-neoadjuvant therapy is a strong predictor of pathologic complete response in rectal cancer. J Gastrointest Surg. 2015;19(6):1106-1112.
20. Armstrong D, Raissouni S, Hiller JP, et al. Predictors of pathologic complete response after neoadjuvant treatment for rectal cancer: a multicenter study. Clin Colorectal Cancer. 2015;14(4):291-295.
21. Kim HJ, Choi G, Park JS, et al. Clinical significance of thrombocytosis before preoperative chemoradiotherapy in rectal cancer: predicting pathologic tumor response and oncologic outcome. Ann Surg Oncol. 2015;22(2):513-519.
22. Perez RO, Juliao GPS, Habr-Gama A, et al. The role of carcinoembriogenic antigen in predicting response and survival to neoadjuvant chemoradiotherapy for distal rectal cancer. Dis Colon Rectum. 2009;52(6):1137-1143.
23. Probst CP, Becerra AZ, Aquina CT, et al. Watch and wait? – Elevated pretreatment CEA Is associated with decreased pathological complete response in rectal cancer. J Gastrointest Surg. 2016;20(1): 43-52.
24. Amin MB, Greene FL, Edge SB, et al. The eighth Edition AJCC Cancer Staging Manual: continuing to build a bridge from a population-based to a more "personalized" approach to cancer staging. CA Cancer J Clin. 2017;67(2): 93-99.
25. Monguzzi L, Ippolito D, Bernasconi DP, et al. Locally advanced rectal cancer: value of ADC mapping in prediction of tumor response to radiochemotherapy. Eur J Radiol. 2013;82(2):234-240.
26. Jia H, Shen X, Guan Y, et al. Predicting the pathological response to neoadjuvant chemoradiation using untargeted metabolomics in locally advanced rectal cancer. Radiother Oncol. 2018;128(3):548-556.

27. Zhang J, Shen L, Deng Y, et al. A novel LARCassigner3 classification predicts outcomes in patients with locally advanced rectal cancer treated with neoadjuvant chemoradiotherapy: a retrospective training and validation analysis. Cancer Manag Res. 2019;11:4153-4170.

DOI 10.1007/s10330-022-0548-8
Cite this article as: Shen LL, Li C, Wang JW, et al. CEA levels predict tumor response to neoadjuvant chemoradiotherapy in locally advanced rectal cancer. Oncol Transl Med. 2022;8(4):180-185.

Oncology and Translational Medicine
DOI 10.1007/s10330-022-0562-2

August 2022, Vol. 8, No. 4, P186–P190

ORIGINAL ARTICLE

Risk factors of lymph node metastasis in rectal neuroendocrine tumors*

Donghong Liang[1], Zhennan Niu[1], Xiaofang Sun[1], Changjuan Meng[2], Zhuang Liu[1] (✉)

[1] Department of Endoscopy, Xingtai Third Hospital, Xintai 054099, China
[2] Department of Pathology, Xingtai Third Hospital, Xintai 054099, China

Abstract

Objective The aim of this study was to investigate the risk factors of lymph node metastasis in rectal neuroendocrine neoplasms (RNENs).

Methods We enrolled 168 patients with RNENs as the research object, and their clinicopathological and survival data were collected. The risk factors affecting lymph node metastasis were analyzed retrospectively, and independent risk factors affecting prognosis were evaluated.

Results Analysis showed that age, tumor diameter, tumor function, grade, and T stage were correlated with lymph node metastasis ($P < 0.05$). Multiple logistic regression analysis showed that tumor size, grade, and T stage were independent risk factors for lymph node metastasis in patients with RNENs. Kaplan–Meier analysis showed that the 5-year overall survival (OS) of patients with lymph node metastasis was 40.0% (10/25), and that of patients without lymph node metastasis was 93.0% (133/143). The prognosis of RNENs patients with lymph node metastasis along with patients with large tumor diameter and high grade was poor. Cox multivariate analysis showed that tumor diameter (HR = 1.985, $P = 0.008$), grade (HR = 3.416, $P = 0.004$), T stage (HR = 2.413, $P = 0.014$), and lymph node metastasis (HR = 3.119, $P = 0.000$) were independent risk factors affecting the prognosis of patients with RNENs.

Conclusion Tumor size, grade, and T stage are the main risk factors for lymph node metastasis and prognosis in patients with RNENs. These risk factors should be fully evaluated before surgery.

Received: 21 March 2022
Revised: 15 May 2022
Accepted: 20 July 2022

Key words: rectal neuroendocrine tumor; lymph node metastasis; risk factors

Neuroendocrine neoplasms (NENS) are heterogeneous tumors of peptidergic neurons that originate from neuroendocrine cells and exert a neuroendocrine function. They can produce a variety of different hormones resulting in different symptoms [1]. In recent years, the incidence of NENS originating from the gastroenteric pancreas system and lungs is increasing [2]. The incidence rate of rectal neuroendocrine neoplasm (RNENs) is the highest in the gastrointestinal tract. As diagnostic technology continues to improve, the incidence rate of RNENs has increased by nearly ten-fold [3] in the past 30 years. Many factors affect the prognosis of patients with RNENs, among which lymph node metastasis is an important risk factor. Therefore, the determination of lymph node metastasis or related high-risk factors in patients is of utmost importance in the selection of clinical treatment strategy [4]. However, the relevant factors related to lymph node metastasis of RNENs have not been fully understood. Therefore, this study retrospectively analyzed the clinical data of 168 patients with RNENs. This study explored the risk factors affecting lymph node metastasis, in order to provide a strong basis for the treatment and prognosis of such patients.

Materials and methods

Research object

Overall, 168 patients with NENS who were treated in our hospital from January 2002 to January 2019 were selected as the research objects. The inclusion criteria were: (1) Patients who underwent pathological as well as immunohistochemical examination and were histologically diagnosed with RNENS. (2) Patients who underwent radical resection. (3) Patients with initial diagnosis and treatment. The exclusion criteria were: (1) Endoscopic treatment or local anal resection. (2)

✉ Correspondence to: Zhuang Liu. Email: futuanfu52831@163.com
* Supported by a grant from the Xingtai Key Research and Development Plan Project (No. 2020zc277).

Concurrent severe liver, kidney, and lung damage or serious mental illness. (3) Concurrent benign and malignant tumors of the rectum. (4) Incomplete clinical or follow-up data. The demographic data, clinicopathological characteristics, and treatment plans of patients were collected through the electronic medical record system. Patient survival data was obtained from outpatient examination and follow-up via telephone. The median age of 168 patients with RNENs was 48 years, with a range of 20 to 78 years. There were 67 patients over 50 years old, 101 patients under 50 years old, 108 male patients (%), and 60 male patients (%). Excluding two patients on different treatment plans, all other patients received radical rectal surgery, endoscopic resection, anal resection and somatostatin analogs. All patients received surgical treatment, and all patients had negative margins. According to the proliferative activity of the tumor, gastrointestinal, and pancreatic neuroendocrine tumors were classified as G1 (low-grade, mitotic image number 1/10, high-power field or Ki-67 index ≤ 2%), G2 (medium-grade, mitotic image number 2–20/10, high-power field or Ki-67 index 3%–20%), G3 (high-grade, mitotic image number > 20/10, high-power field or Ki-67 index > 20%).

Follow-up

All patients received regular follow-up, including physical examination. Tests were conducted to check whole blood cell count, and serum carcinoembryonic antigen (CEA) levels. When necessary, the patients underwent imaging examinations such as abdominal ultrasound and chest radiography. When recurrence was suspected, CT or MRI was performed.

statistical analysis

All data were analyzed using the SPSS20.0 software. The counting data were expressed as the frequency (example), and chi square test was used. A logistic multivariate model was used to analyze the risk factors of lymph node metastasis. Kaplan–Meier and log rank survival curves were used to compare the survival rates. Multivariate Cox regression analysis was used for survival analysis. Differences were considered significant at $P < 0.05$.

Results

Clinicopathological features of patients

Among the 168 patients, 115, 18, 16, and 19 had stage I, II, III and IV RNENs, respectively. Tumor invasion reached the mucosa and submucosa (T1) in 128 patients. Tumors invaded the muscularis propria in 18 cases (T2), and the external muscularis in 22 cases. Grade G1, G2, and G3 was found in 124, 34, and 10 cases, respectively. The average tumor size was 1.28 ± 0.60 cm, of which 132 cases were < 1 cm and 36 cases were greater than 2 cm. Approximately 29 patients with functional tumors developed intermittent flushing and diarrhea, and 25 patients had lymph node metastasis. The rate of lymph node metastasis was 14.9%. All patients received regular follow-ups. The average follow-up time was 38 months. The longest follow-up time was 138 months, and the shortest follow-up time was 3 months. 20 patients died, which accounted for 11.9% of all patients.

Single factor analysis of lymph node metastasis

Univariate analysis showed that age, tumor diameter, tumor function, grade, and T stage were correlated with lymph node metastasis ($P < 0.05$). Higher age, larger tumor diameter, higher functional tumor, grade, and T stage, were associated with higher risk of lymph node metastasis in patients with RNENs (Table 1).

Multivariate analysis of lymph node metastasis

Multiple logistic regression analysis revealed that tumor size, grade, and T stage were independent risk factors for lymph node metastasis in patients with RNENs (Table 2).

Prognostic analysis of patients with different clinical characteristics

Among 168 patients, 25 succumbed to the disease. The overall survival rate was 85.1% (143/168). Kaplan–

Table 1 A univariate analysis of the affected lymph node metastasis

Index	*n*	Lymphatic metastasis		χ^2	*P*
		Positive (*n*=25)	Negative (*n*=143)		
Gender				0.176	0.674
Female	108	17	91		
Male	60	8	52		
Age (years)				19.717	0.000
≤ 50	101	5	96		
> 50	67	20	47		
Tumor diameter (cm)				77.309	0.000
< 1	132	3	129		
≥ 1	36	22	14		
Functional tumor				4.467	0.035
Yes	29	8	21		
No	139	17	122		
WHO Grade				56.505	0.000
G1	124	7	117		
G2	34	9	25		
G3	10	9	1		
T stage				85.859	0.000
T1	128	3	125		
T2	18	5	13		
> T2	22	17	5		

Table 2 Multivariate analysis affecting lymph node metastasis

Index	β	SE	Wald	df	*P*	95%CI
Gender	0.241	0.262	0.829	1	0.551	0.542–1.98
Tumor diameter	0.524	0.485	5.141	1	0.000	1.146–4.632
Functional tumor	0.498	0.362	1.256	1	0.412	1.035–3.791
Grade	0.320	0.208	14.965	1	0.000	1.369–2.216
T stage	0.265	0.277	14.846	1	0.000	1.965–2.470

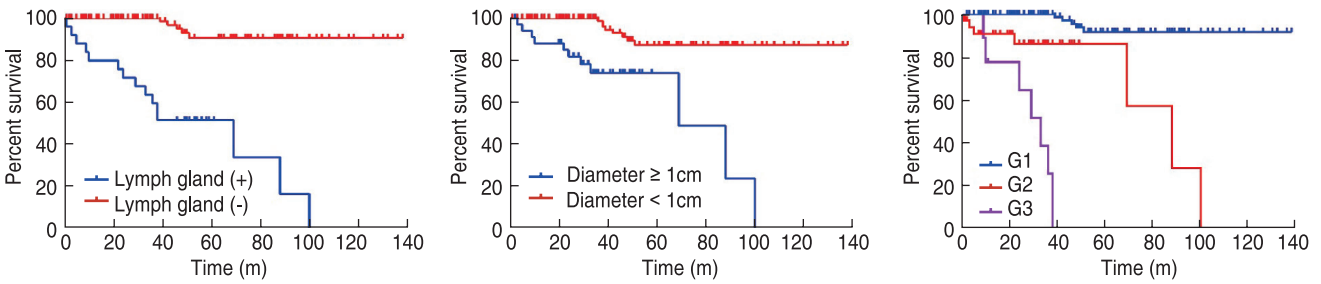

Fig. 1 Analysis of the prognosis of patients with different clinical characteristics

Meier analysis showed that the 5-year OS of patients with lymph node metastasis and without lymph node metastasis was 40.0% (10/25) and 93.0% (133/143) respectively. The difference between the two groups was statistically significant ($\chi^2 = 29.64$, $P = 0.00$), and the prognosis of RNEN patients with lymph node metastasis was significantly worse. Nevertheless, when the tumor diameter was large ($\chi^2 = 22.75$, $P = 0.000$), the grade was higher ($\chi^2 = 121.70$, $P = 0.000$; Fig. 1).

Cox univariate and multivariate analysis affecting the prognosis of patients

Cox univariate and multivariate analysis revealed that tumor diameter (HR = 1.985, $P = 0.008$), grade (HR = 3.416, $P = 0.004$), T stage (HR = 2.413, $P = 0.014$), and lymph node metastasis (HR = 3.119, $P = 0.000$) were independent risk factors affecting the prognosis of patients with RNEN (Table 3).

Discussion

According to the surveillance, epidemiology, and end results (SEER) data, the incidence rate of RNENs increased from 1.09/10 million in 1973 to 5.25/10 million in 2004, with an incidence rate that increased every year. Studies in Taiwan and Japan show that the highest incidence of RNENs in Asian people is in the digestive tract. The incidence rate of [5] is the highest. Surgery, which includes radical resection, endoscopic resection, or transanal resection, is the most important treatment for RNENs. It is believed that G1 grade early RNENs can be treated by endoscopic resection; however, once lymph node metastasis occurs, radical surgical resection should be performed [6]. Therefore, understanding the high-risk factors of lymph node metastasis will help clinicians to choose the best surgical method.

In this study, 25 of 168 patients had lymph node

Table 3 Cox univariate and multivariate analysis affecting patient outcomes

Items	Univariate analysis			Multiplicity analysis		
	HR	95%CI	*P*	HR	95%CI	*P*
Gender	1.036	0.897–1.320	0.326	-	-	-
Age	1.130	0.964–1.254	0.489	-	-	-
Tumor diameter	2.512	1.820–3.336	0.013	1.985	1.316–2.765	0.008
functional tumor	1.236	0.874–1.521	0.117	-	-	-
Grade	3.154	2.870–3.461	0.005	3.416	2.794–3.852	0.004
T stage	2.203	1.754–2.965	0.032	2.413	1.978–3.021	0.014
Lymphatic metastasis	3.846	2.143–5.089	0.001	3.119	2.541–5.135	0.000

metastasis, where the lymph node metastasis rate was 14.9%. The 5-year survival rate with lymph node metastasis and without lymph node metastasis was 40.0% (10/25) and 93.0% (133/143) respectively. The survival rate indicated that the prognosis of patients with RNENs complicated with lymph node metastasis was significantly poor. Hence, there is a necessity of preoperative lymph node metastasis status evaluation in treatment selection. The lymph node metastasis rates of G1, G2, and G3 tumors were 5.6%, 26.4%, and 90.0% respectively. Li *et al.* [7] found that the lymph node metastasis rates of G1, G2 and G3 patients were 2.92%, 20.0%, and 66.67% respectively, which was similar to that in our results. In multivariate analysis, grade was an independent risk factor for lymph node metastasis. In addition, there was a significant difference in the rate of lymph node metastasis between G1 and G2 patients, which suggested that patients above G2 are more likely to have regional lymph node metastasis. The 5-year survival rates of patients with grade G1, G2, and G3 were 94.4%, 79.9%, and 19%, respectively. The 5-year survival rate of patients with grade G2 or above was significantly lower than patients with grade G1. The survival rate indicated that the prognosis of patients with grade G2 or above is worse than patients with grade G1. The prognosis may be related to the higher risk of lymph node metastasis in patients with grade G2 or above.

The depth of tumor invasion is also a key factor affecting the prognosis of patients with RNEN [8]. Studies have shown that the depth of tumor invasion is a predictor of lymph node metastasis [9]. Shields *et al.* found that the 5-year survival rate of T1 and T2 differed by approximately 10% [10]. At present, it is believed that when the tumor invades the muscularis propria, the risk of lymph node metastasis is significantly increased. Furthermore, the prognosis is far worse than patients where tumor invasion is limited to submucosa. The lymph node metastasis rates of T1, T2, and above T2 were 2.3%, 27.8%, and 77.3% respectively. The depth of tumor invasion is an independent risk factor for lymph node metastasis of RNEN. When the tumor invades greater than T2, the risk of lymph node metastasis increases significantly, radical surgery should be performed in such cases.

This study presented that tumor size is also an important factor affecting the risk factors and prognosis of lymph node metastasis in RNEN. The European neuroendocrine tumor society guidelines suggest that when lymph node metastasis does not occur, endoscopic tumor resection or transanal resection can achieve the effect of radical surgery with good long-term survival [11]. The guidelines of the national comprehensive cancer network also suggest that when the lesion is less than 2 cm in diameter, endoscopic resection or anal resection is sufficient radical treatment [7]. However, Japanese scholars believe that when the tumor diameter is > 1 cm, radical surgery including lymph node dissection must be performed, as research has shown that RNEN with diameter > 1 cm have the same risk of lymph node metastasis as colorectal adenocarcinoma [12]. Further studies have reported that the lymph node metastasis rates of tumors with diameter > 2 cm and 1.0–2.0 cm are 50% and 23.5% respectively. Moreover, the lymph node metastasis rate of tumors with a diameter <1 cm is less than 2% [13], which indicated that the lymph node metastasis rate of tumors with a diameter <1 cm is very low. Hence, for tumors with a diameter <1 cm, endoscopic resection, or anal resection is satisfactory. In addition, tumors with a diameter > 2 cm should undergo radical surgery, such as anterior rectal resection or abdominal resection. Nonetheless, the optimal criteria to decide on the surgical procedure when the tumor diameter is between 1-2 cm remains unclear. In this study, tumor size was an independent risk factor for lymph node metastasis. There was a significant difference in the rate of lymph node metastasis between patients with tumor diameter < 1 cm and patients with tumor diameter of 1–2 cm. Patients with tumor diameter of 1 = 2 cm or > 2 cm are more likely to have regional lymph node metastasis. Thus, taking the research mentioned above into account, we postulate that patients with tumor diameter > 2 cm require radical surgery. Nevertheless, tumors with a diameter of 1–2 cm require careful treatment. Our study showed that 11 patients with lymph node metastasis and tumor diameter of 1–2 cm had tumor infiltration to T2 or deeper or grade G2 or G3. The data from these 11 patients suggested that other high-risk factors, such as tumor infiltration depth or grade, should be considered before surgery. Therefore, according to our results, we suggest that when the tumor diameter is 1–2 cm, has invaded T2 or deeper, or when it is grade G2 or G3 at the same time, radical surgery should be performed.

In conclusion, this study found that tumor size, grade and depth of tumor invasion were independent risk factors for lymph node metastasis of RNENs. When the depth of tumor invasion reaches beyond the muscularis propria, the tumor is classified as grade G2 or G3. Additionally, when the diameter is > 2 cm, the risk of lymph node metastasis increases significantly. In such cases, radical surgery is recommended. However, this study has some limitations which should be considered: (1) this study was a retrospective study, where the timespan for patient selection was large, which inevitably led to a certain sample bias. (2) The sample size is small. (3) This study is a descriptive report where all the patients received surgical treatment. Additionally, there was a lack of control group without surgical intervention.

Acknowledgments

Not applicable.

Funding

Supported by a grant from the Xingtai Key Research and Development Plan Project (No. 2020zc277).

Conflicts of interest

The authors indicated no potential conflicts of interest.

Author contributions

Not applicable.

Data availability statement

Not applicable.

Ethical approval

Not applicable.

References

1. Cavalcanti E, Armentano R, Valentini AM, et al. Role of PD-L1 expression as a biomarker for GEP neuroendocrine neoplasm grading. Cell Death Dis. 2017;8(8):3004.
2. Wang Y, Chen Y, Li X, et al. Loss of expression and prognosis value of alpha-internexin in gastroenteropancreatic neuroendocrine neoplasm. BMC Cancer. 2018;18(1):1-12.
3. Shi H, Jiang C, Zhang Q, et al. Clinicopathological heterogeneity between primary and metastatic sites of gastroenteropancreatic neuroendocrine neoplasm. Diagnostic Pathol. 2020;15(1):1-10.
4. Sciarra A, Missiaglia E, Trimech M, et al. Gallbladder mixed neuroendocrine non neuroendocrine neoplasm(MiNEN) arising in intracholecystic papillary neoplasm: clinicopathologic and molecular analysis of a case and review of the literature. Endocrine Pathol, 2020;31(1):84-93.
5. Watzka FM, Fottner C, Miederer M, et al. Surgical therapy of neuroendocrine neoplasm with hepatic metastasis: patient selection and prognosis. Langenbeck's archives Surgery. 2015;400(3):349-358.
6. Tai WM, Tan SH, Tan DMY, et al. Clinicopathologic characteristics and survival of patients with gastroenteropancreatic neuroendocrine neoplasm in a multi-ethnic asian institution. Neuroendocrinology, 2019;108(4):265-277.
7. Li P, Wu F, Zhao H, et al. Analysis of the factors affecting lymph node metastasis and the prognosis of rectal neuroendocrine tumors. Int J Clin experimental Pathol. 2015;8(10):13331.
8. Scharf M, Petry V, Daniel H, et al. Bone metastases in patients with neuroendocrine neoplasm: frequency and clinical, therapeutic, and prognostic relevance. Neuroendocrinology. 2018;106(1):30-37.
9. Al Natour RH, Saund MS, Sanchez VM, et al. Tumor size and depth predict rate of lymph node metastasis in colon carcinoids and can be used to select patients for endoscopic resection. J gastrointestinal Surg. 2012;16(3):595-602.
10. Shields CJ, Tiret E, Winter DC, et al. Carcinoid tumors of the rectum: a multi-institutional international collaboration. Ann Surg. 2010;252(5): 750-755.
11. Ramage JK, De Herder WW, Delle Fave G, et al. ENETS consensus guidelines update for colorectal neuroendocrine neoplasms. Neuroendocrinology. 2016;103(2):139-143.
12. Tsukamoto S, Fujita S, Yamaguchi T, et al. Clinicopathological characteristics and prognosis of rectal well-differentiated neuroendocrine tumors. Inter J Colorectal Dis. 2008;23(11):1109-1113.
13. Colonoscopy Study Group of Korean Society of C. Clinical characteristics of colorectal carcinoid tumors. J Korean Society Coloproctology. 2011;27(1):17-20.

DOI 10.1007/s10330-022-0562-2
Cite this article as: Liang DH, Liu ZN, Sun XF, et al. Risk factors of lymph node metastasis in rectal neuroendocrine tumors. Oncol Transl Med. 2022;8(4):186-190.

Oncology and Translational Medicine
DOI 10.1007/s10330-021-0510-0
August 2022, Vol. 8, No. 4, P191–P195

ORIGINAL ARTICLE

Association of 2-methoxyestradiol levels with the occurrence and development of endometrial cancer in humans*

Huanhuan Zhao[1], Junyu Li[1], Yan Liu[2], Li Li[1] (✉)

[1] Department of Obstetrics and Gynecology, The Forth Hospital, Hebei Medical University, Shijiazhuang 050011, China
[2] Department of Pharmacy, Hebei Medical University, Shijiazhuang 050017, China

Abstract

Objective The aim of the study was to determine the association of urinary levels of estradiol (E_2) and 2-methoxyestradiol (2-$MeOE_2$) with the occurrence and development of endometrial cancer.

Methods In this case-control study, 24-h urine specimens were collected from 28 postmenopausal patients with endometrial cancer and 28 postmenopausal healthy female controls. The concentration of 2-$MeOE_2$ was determined using liquid chromatography-mass spectrometry with hollow fiber liquid-phase microextraction. The concentration of E_2 was determined using an enzyme-linked immunosorbent assay.

Results Estrogen levels were different between the patients with endometrial cancer and controls. The relative quantity of E_2 in the case group was higher than that in the control group ($P < 0.05$), whereas that of 2-$MeOE_2$ was lower in the case group than that in the control group ($P < 0.05$). The ratio of E_2-to-2-$MeOE_2$ in the case group was significantly higher than that in the control group ($P < 0.05$).

Conclusion The results of this study indicate an imbalance of estrogen metabolites in endometrial carcinogenesis. Reduced 2-$MeOE_2$ levels and elevated E_2-to-2-$MeOE_2$ ratio may be used as potential biomarkers for the risk assessment of estrogen-induced endometrial cancer.

Received: 23 July 2021
Revised: 6 April 2022
Accepted: 21 June 2022

Key words: endometrial cancer; 2-methoxyestradiol (2-$MeOE_2$); estradiol (E_2); urine; high-performance liquid chromatography-mass spectrometry (HPLC-MS)

Endometrial cancer is estrogen-dependent. It is believed that exposure to estrogens in the absence of progesterone increases the risk of developing endometrial cancer [1]. Estradiol (E_2) is a sex hormone with strong biological activity, valuable in diagnosing and discriminating endocrine and gynecologic diseases. Estrogen metabolites are closely related to the occurrence and development of tumors [2]. An important metabolite of E_2, 2-methoxyestradiol (2-$MeOE_2$), is produced by cytochrome P450 1B1 and catechol-O-methyltransferase (COMT) [3]. During the last decade, 2-$MeOE_2$ has received considerable attention owing to its anticancer activity. Phase I and II clinical trials have revealed that orally administered 2-$MeOE_2$ is well tolerated by patients with grade 2 and grade 3 toxicities [4–7]. It is believed that 2-$MeOE_2$ acts directly on tumor growth by reducing cell proliferation, inducing apoptosis, and inhibiting angiogenesis [8]. A previous study has shown that 2-$MeOE_2$ inhibited the growth of endometrial cancer cells by inducing apoptosis and cell cycle arrest [9]. Therefore, it would be interesting to elucidate the mechanism of action of 2-$MeOE_2$.

Quantitative measurement of endogenous 2-$MeOE_2$ may play an important role in elucidating the mechanism underlying endometrial carcinogenesis; however, the low content of 2-$MeOE_2$ in the human body limits its measurement. Current methods for measuring endogenous catechol estrogens involve radioimmunoassay [10], enzyme immunoassay [11], high-performance liquid chromatography (HPLC) [12], liquid chromatography coupled with mass spectrometry [13], and gas chromatography-mass spectrometry [14]; however,

✉ Correspondence to: Li Li. Email: lily_lucky1@163.com
* Supported by the Hebei Province Medical Science Research Key Project (No. 20210276).

there are no inexpensive and convenient methods to measure 2-MeOE$_2$ levels. This study used hollow fiber liquid-phase microextraction (HF-LPME) and high-performance liquid chromatography-mass spectrometry (HPLC-MS) to improve sensitivity.

Materials and methods

Reagents and materials

The analytical reference 2-MeOE$_2$ was purchased from Sigma-Aldrich (Beijing, China). Ethinyl estradiol (IS) with a purity > 98% was obtained from the National Institute for Control of Pharmaceutical and Biological Products (Beijing, China). HPLC-grade methanol (Fisher, Pittsburgh, PA, USA) was used for the HPLC analysis and urine sample preparation. Analytic-grade n-octyl alcohol (Tianjin Heng Xing Corporation, Hebei, China) was used to prepare urine extracts. A polyvinylidene difluoride (PVDF; Foshan, Guangzhou, China) hollow fiber membrane was used for HF-LPME. An Agilent 1200 liquid chromatography system (Agilent, Santa Clara, CA, USA) was used for all the analyses. An enzyme-linked immunosorbent assay (ELISA) kit for E$_2$ was purchased from Shanghai BlueGene Biotech Co., Ltd. (Shanghai, China).

Urine sample collection

This hospital-based case-control study of endometrial cancer was conducted at the Fourth Hospital of Hebei Medical University (Hebei, China). The study patients had newly diagnosed endometrial adenocarcinoma, which was confirmed by pathological examination postoperatively. Twenty-eight patients with endometrial cancer (45–74 years of age) were included in the study. Patients who received medical treatment 3 months before study enrollment and those with a history of cigarette smoking were excluded. Twenty-eight healthy women (46–65 years old) were included as controls. Healthy women underwent complete examinations, including ultrasonic examination of the liver, kidney, abdomen, and uterus at the Fourth Hospital of Hebei Medical University (Hebei, China). Serum tumor markers were negative in healthy women. All studies were conducted according to the protocols approved by the Ethics Committee of the Fourth Hospital of Hebei Medical University (Hebei, China). Informed consent was obtained from all the patients and healthy controls.

Twenty-four-hour urine samples were collected in 1-L bottles containing 1 g of ascorbic acid to prevent oxidation. None of the women received exogenous estrogens. The urine volume was recorded immediately after collection. Aliquots of urines were stored at –20 °C until analysis.

Instruments and chromatographic and mass spectrometry conditions

All chromatographic analyses were performed using an Agilent 1200 liquid chromatography system. Chromatographic separation was performed on a Kromasil C18 column [150 mm × 4.6 mm (I.D.), particle size: 5 mm; Agilent]. The column temperature was maintained at 25 °C. Chromatographic separation was achieved isocratically using a mobile phase [water and methanol (8:92), v/v] supplemented with 0.1% acetic acid. The flow rate was set at 1 mL/min, and the injection volume was 10 μL. The total analysis time was 7 min for each run. Detection was performed using a 3200 QTRAPTM system (Applied Biosystems, Foster City, CA, USA) with a hybrid triple quadrupole linear ion trap mass spectrometer equipped with Turbo V sources and Turbo Ionspray interface. The instrument was operated using an electrospray ionization source in positive mode. Multiple reaction monitoring mode was used for quantification (Fig. 1). All instruments were controlled and synchronized using the Analyst

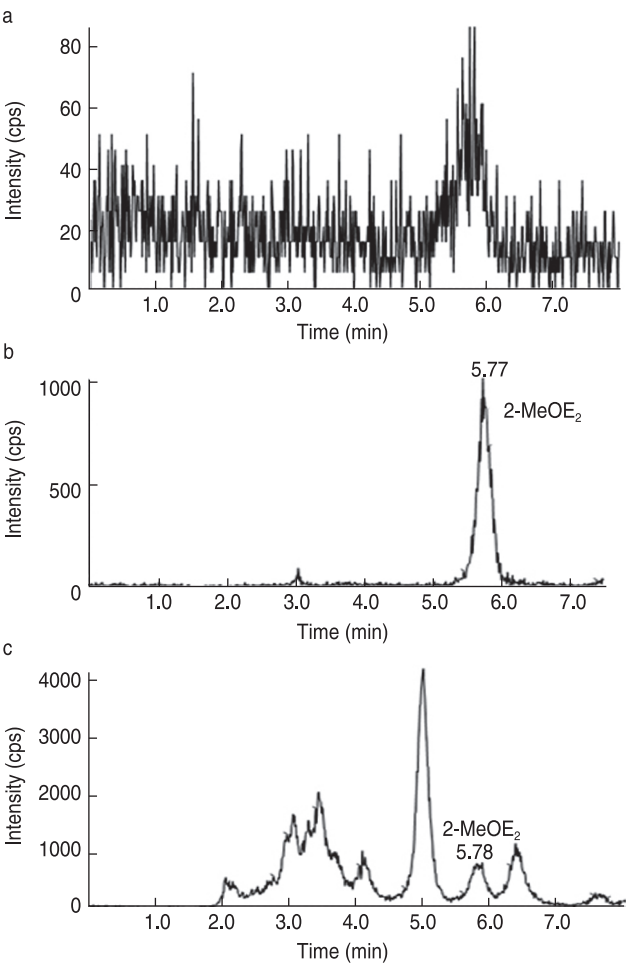

Fig. 1 Mass-spectrogram of 2-MeOE$_2$. (a) Control; (b) Artificial human urine; (c) Urine of patients with endometrial cancer

software (version 1.4.2; Applied Biosystems/MDS Sciex, Beijing, China).

Hydrolysis, extraction, and derivatization procedure

Because 2-MeOE$_2$ is mostly present in urine as glucuronide conjugate and small amounts of sulfate conjugate, a hydrolysis step was included. To a 140-mL aliquot of urine, 5.6 g of NaOH was added, followed by boiling for 10 min and centrifugation at 450 × g for 10 min. The precipitate was discarded, and concentrated hydrochloric acid was added to acidify the residual solution (pH 3.0). The residual solution was then diluted with water to a final volume of 140 mL.

The optimization procedure was conducted using 20 ng/mL of standard solutions. Extraction and preconcentration procedures were performed as previously described. At the end of the extraction, the hollow fiber extraction device was removed from the bottle, all sealed ends were carefully cut, and the organic acceptor phase solvent was carefully withdrawn into the microsyringe. Subsequently, 100 μL of methanol was slowly flushed through the lumen to simultaneously transfer analytes in the acceptor and membrane phases into a clean and dry polytef insert tube. The entire elution solution was evaporated to dryness at 90 °C under nitrogen gas.

Sodium bicarbonate buffer (100 μL, pH 9.0) and 100 μL of dansyl chloride solution (1 mg/mL in acetone) were added to the dried samples. After vortexing, the sample was heated at 60 °C for 5 min to form 2-MeOE$_2$ and dansyl chloride derivatives, respectively.

Ethinyl 2-MeOE$_2$ was dissolved in HPLC-grade methanol to produce an IS solution at a concentration of 143 pg/mL. To validate the method, three concentrations of the standard solution added to 2-MeOE$_2$ (10, 100, and 400 pg/mL) were used to prepare control urine samples.

Determination of E_2 using ELISA

The concentration of E_2 was measured using a microplate reader (VersaMax, Shanghai, China), according to the manufacturer's instructions. A standard curve was established to calculate E_2 concentrations in the samples.

Statistical analysis

Statistical analysis was performed using the SPSS 13.0 software package (SPSS Inc., Chicago, IL, USA). The results are expressed as medians. A comparison of the two groups was performed using a non-parametric test when the variance was uneven. Statistical significance was set at $P < 0.05$.

Results

Linearity, LOD, LOQ, and recovery

The linear range was 1.714–685.2 pg/mL, with a correlation coefficient of 0.996 using a weighted linear regression method. The calibration equation was as follows: A = 1.91 C + 2.91, where C is the concentration of 2-MeOE$_2$ (pg/mL). The SD of the slope and intercept were 0.0009 and 0.0004, respectively. The limits of quantification (LOQ) and limits of detection (LOD), defined as signal-to-noise ratios (S/N) of 10 and 3, respectively, were separately determined by five-fold replicate analysis. The LOD and LOQ were 0.14 pg/mL and 1.4 pg/mL, respectively.

Intra- and inter-day precision and stability

Table 1 presents the results of the accuracy and recovery of the proposed method. We measured the intra- and inter-day precision at various concentrations to assess the repeatability and reproducibility of the newly developed method. The relative standard deviations (RSD) of the intra-day precision of the three concentrations were 8.4%, 6.5%, and 7.2%, respectively (Table 1). Moreover, we evaluated the inter-day precision of the method by assessing sample concentrations at high, middle, and low linearity ranges over 6 consecutive days. The RSD values of the inter-day precision were 6.2%, 4.8%, and 5.6%, respectively (Table 1).

To evaluate freeze-thaw stability, samples were subjected to freezing for 24 h at –20 °C and thawed at room temperature (25–28 °C) for three cycles. The stability at freezing was assessed by storing the samples at –20 °C for 48 h, whereas the stability at room temperature (25–28 °C) was assessed by placing the samples at room temperature (25–28 °C) for 6 h. All RSD values for sample stability were < 7.8%.

Analysis of human urine samples (Table 2)

Concentrations of E_2 and 2-MeOE$_2$ in human urine

The distributions of E_2 and 2-MeOE$_2$ concentrations were abnormal. The median E_2 concentration in the case group was 3.38 ng/mL, whereas that in the control group was 2.34 ng/mL. The median 2-MeOE$_2$ levels in the case and control groups were 3.38 pg/mL and 9.85 pg/mL, respectively.

Table 1 Results of recovery rate and precision of the method (n = 6)

Concentration (pg/mL)	Relative recovery (%)	Inter-day RSD (%)	Intra-day RSD (%)
13.7	90.4	6.2	8.4
137.0	98.9	4.8	6.5
685.6	95.2	5.6	7.2

Table 2 Median concentration and quantity of E_2 and 2-$MeOE_2$ at 24 h in the urine of patients with endometrial cancer and healthy controls

Groups	Concentration		Content at 24 h		
	E_2 (ng/mL)	2-$MeOE_2$ (pg/mL)	E_2 (mg)	2-$MeOE_2$ (ng)	E_2/2-$MeOE_2$
Control (n = 28)	2.34	9.85	2.70	12.01	2.31
Case (n = 28)	3.38	3.38	4.40	6.77	9.91
P	< 0.05	< 0.05	< 0.05	< 0.05	< 0.05

Note: Performed by a non-parametric test

Levels of E_2 and 2-$MeOE_2$ at 24 h

The distributions of E_2 and 2-$MeOE_2$ levels at 24 h were abnormal. The median E_2 levels at 24 h in the case and control groups were 4.40 mg and 2.70 mg, respectively. The median 2-$MeOE_2$ levels in the case and control groups were 6.77 ng and 12.01 ng, respectively.

Comparison of E_2/2-$MeOE_2$ in patients and controls

2-$MeOE_2$ is a product of E_2 hydroxylation and methylation. The E_2/2-$MeOE_2$ ratio at 24 h was calculated. The E_2/2-$MeOE_2$ ratio at 24 h was abnormal. The E_2/2-$MeOE_2$ ratio was significantly higher in the case group (9.91) than that in the control group (2.31; $P < 0.05$).

Discussion

Urinalysis is widely used clinically because it is a simple procedure that provides critical information about disease processes and facilitates disease diagnosis, treatment, and prognosis. Although the urinary levels of 25 androgens and corticoids and 16 estrogens have been quantitatively determined using gas chromatography-mass spectrometry-selected ion monitoring [15], the measurement of 2-$MeOE_2$ concentration remains unresolved. We used HF-LPME and HPLC-MS to successfully measure 2-$MeOE_2$ levels. This method is simple, effective, and sufficient to determine 2-$MeOE_2$ levels in humans.

The exact endogenous 2-$MeOE_2$ concentrations in tissues are unknown, and the serum concentrations of 2-$MeOE_2$ are frequently reported in combination with 2-methoxyestrone. The reported plasma concentrations of 2-$MeOE_2$ in men, non-pregnant women, and pregnant women are 10–35 pg/mL, 18–138 pg/mL, and 216–10 690 pg/mL, respectively [16–17]. Recently, an analytical method developed to detect different methoxyestrogens reported the total concentration of 2-$MeOE_2$ in the serum to be (10.6 ± 7.91) pg/mL, and (2.5 ± 0.57) pg/mL in the luteal and follicular phases in pre- and postmenopausal women, respectively [18]. The concentration of the unconjugated form of 2-$MeOE_2$ was approximately half of the above values. In this study, the concentration of 2-$MeOE_2$ was measured in urine. The median 2-$MeOE_2$ level was 9.08 pg/mL in the control group, which is similar to the serum level reported previously.

2-$MeOE_2$ is endogenously formed from estradiol and has been reported to be a potent antiangiogenic and antitumor agent [19]. Regarding *in vitro* antiproliferative properties, the majority of 60 cell lines from human tumor cell lines are sensitive to 2-$MeOE_2$ with inhibitory concentrations between 0.08 and 5.0 μM [20]. The median 2-$MeOE_2$ concentration in the case group was 6.77 pg/mL, which was significantly lower than that of the control group. To exclude the influence of urine volume, 2-$MeOE_2$ levels at 24 h were compared. Thus, the reduction in 2-$MeOE_2$ was associated with a reduction in anticancer activity, which can be explained by the change in COMT.

Many tissues can actively produce 2-$MeOE_2$ because COMT is a ubiquitous enzyme found in different organs, such as the liver, kidney, intestine, stomach, spleen, brain, pancreas, and lungs [21]. Both COMT protein expression and activity are reduced in endometrial cancer tissues [22]. It is reasonable to assume that a decrease in 2-$MeOE_2$ levels is a risk factor for endometrial cancer.

The level of E_2 was measured using ELISA. E_2 is also associated with the occurrence of endometrial cancer [23]. Thus, the relative quantity of E_2 in the case group was significantly higher than that in the control group ($P < 0.05$). The E_2/2-$MeOE_2$ ratio in the case group (9.91) was significantly higher than that in the control group (2.31; $P < 0.05$). E_2 can induce endometrial cancer, whereas 2-$MeOE_2$ acts against endometrial cancer. Thus, the E_2/2-$MeOE_2$ ratio could be used as an indicator to identify patients with endometrial cancer in a high-risk population.

Acknowledgments

We would like to thank the Department of Gynecology and Institute of Hebei Cancer Research of the 4th Hospital of Hebei Medical University, China. We are particularly grateful to Ye Jiang for his excellent technical assistance. We are also grateful to the patients and women without cancer who participated in this study.

Funding

This work was supported by the Hebei Province Medical Science Research Key Project (No. 20210276).

Conflicts of interest

The authors indicated no potential conflicts of interest.

Author contributions

All authors contributed to data acquisition and interpretation and reviewed and approved the final version of this manuscript.

Data availability statement

Not applicable.

Ethical approval

Not applicable.

References

1. Ali AT. Risk factors for endometrial cancer. Ceska Gynekol. 2013;78(5):448-459.
2. Zhao H, Jiang Y, Liu Y, et al. Endogenous estrogen metabolites as biomarkers for endometrial cancer via a novel method of liquid chromatography-mass spectrometry with hollow fiber liquid-phase microextraction. Horm Metab Res. 2015;47(2):158-164.
3. Li F, Fu Y, Li JY, et al. Association between catechol-*O*-methytransferase activity and the development and progression of endometrial cancer. Tumor (Chinese). 2012;32(2):119–123.
4. Yuan W, Yu Y, Li J, et al. Estrogen metabolite 2-methoxyestradiol prevents hypertension in deoxycorticosterone acetate-salt rats. Cardiovasc Drugs Ther. 2013;27(1):17-22.
5. Zhang Q, Ma Y, Cheng YF, et al. Involvement of reactive oxygen species in 2-methoxyestradiol-induced apoptosis in human neuroblastoma cells. Cancer Lett. 2011;313(2):201-210.
6. Rajkumar SV, Richardson PG, Lacy MQ, et al. Novel therapy with 2-methoxyestradiol for the treatment of relapsed and plateau phase multiple myeloma. Clin Cancer Res. 2007;13(20):6162-6167.
7. Sweeney C, Liu G, Yiannoutsos C, et al. A phase II multicenter, randomized, double-blind, safety trial assessing the pharmacokinetics, pharmacodynamics, and efficacy of oral 2-methoxyestradiol capsules in hormone-refractory prostate cancer. Clin Cancer Res. 2005;11(18):6625-6633.
8. Parks M, Tillhon M, Donà F, et al. 2-Methoxyestradiol: new perspectives in colon carcinoma treatment. Mol Cell Endocrinol. 2011;331(1):119-128.
9. Li L, Heldin NE, Grawé J, et al. Induction of apoptosis or necrosis in human endometrial carcinoma cells by 2-methoxyestradiol. Anticancer Res. 2004;24(6):3983-3990.
10. Lakhani NJ, Sparreboom A, Dahut WL, et al. Determination of the antiangiogenesis agent 2-methoxyestradiol in human plasma by liquid chromatography with ultraviolet detection. J Chromatogr B Analyt Technol Biomed Life Sci. 2004;806(2):289-293.
11. O'Connor KA, Brindle E, Shofer JB, et al. Statistical correction for non-parallelism in a urinary enzyme immunoassay. J Immunoassay Immunochem. 2004;25(3):259-278.
12. Falk RT, Xu X, Keefer L, et al. A liquid chromatography-mass spectrometry method for the simultaneous measurement of 15 urinary estrogens and estrogen metabolites: assay reproducibility and interindividual variability. Cancer Epidemiol Biomarkers Prev. 2008;17(12):3411-3418.
13. Yamashita K, Okuyama M, Watanabe Y, et al. Highly sensitive determination of estrone and estradiol in human serum by liquid chromatography-electrospray ionization tandem mass spectrometry. Steroids. 2007;72(11-12):819-827.
14. Zacharia LC, Dubey RK, Jackson EK. A gas chromatography/mass spectrometry assay to measure estradiol, catecholestradiols, and methoxyestradiols in plasma. Steroids. 2004;69(4):255-261.
15. Lee SH, Yang YJ, Kim KM, et al. Altered urinary profiles of polyamines and endogenous steroids in patients with benign cervical disease and cervical cancer. Cancer Lett. 2003;201(2):121-131.
16. Dubey RK, Tofovic SP, Jackson EK. Cardiovascular pharmacology of estradiol metabolites. J Pharmacol Exp Ther. 2004;308(2):403-409.
17. Lakhani NJ, Sparreboom A, Xu X, et al. Characterization of *in vitro* and *in vivo* metabolic pathways of the investigational anticancer agent, 2-methoxyestradiol. J Pharm Sci. 2007;96(7):1821-1831.
18. Xu X, Roman JM, Issaq HJ, et al. Quantitative measurement of endogenous estrogens and estrogen metabolites in human serum by liquid chromatography-tandem mass spectrometry. Anal Chem. 2007;79(20):7813-7821.
19. Kambhampati S, Rajewski RA, Tanol M, et al. A second-generation 2-Methoxyestradiol prodrug is effective against Barrett's adenocarcinoma in a mouse xenograft model. Mol Cancer Ther. 2013;12(3):255-263.
20. Pribluda VS, Gubish ER Jr, Lavallee TM, et al. 2-Methoxyestradiol: an endogenous antiangiogenic and antiproliferative drug candidate. Cancer Metastasis Rev. 2000;19(1-2):173-179.
21. Wakuda T, Iwata K, Iwata Y, et al. Perinatal asphyxia alters neuregulin-1 and COMT gene expression in the medial prefrontal cortex in rats. Prog Neuropsychopharmacol Biol Psychiatry. 2015;56:149-154.
22. Li L, Yang WW, Gao HY, et al. Expression of CYP450 1B1 and COMT protein in human endometrial cancer. J Pract Gynecol Obstet (Chinese). 2012;28(3):215-217.
23. Zhang Z, Zhou D, Lai Y, et al. Estrogen induces endometrial cancer cell proliferation and invasion by regulating the fat mass and obesity-associated gene via PI3K/AKT and MAPK signaling pathways. Cancer Lett. 2012;319(1):89-97.

DOI 10.1007/s10330-021-0510-0
Cite this article as: Zhao HH, Li JY, Liu Y, et al. Association of 2-methoxyestradiol levels with the occurrence and development of endometrial cancer in humans. Oncol Transl Med. 2022;8(4):191–195.

Oncology and Translational Medicine
DOI 10.1007/s10330-022-0574-4

August 2022, Vol. 8, No. 4, P196–P200

ORIGINAL ARTICLE

One-stage limb Pelnac® reconstruction after removal of skin cancer: safety, efficacy, and aesthetic outcomes

Jia Shi[1], Min Gao[1], Haijun Zhu[1], Weiwei Lu[2] (✉)

[1] Department of Plastic Surgery, The Central Hospital of Wuhan, Tongji Medical College, Huazhong University of Science and Technology, Wuhan 430014, China
[2] Department of Orthopaedics, Tongji Hospital, Tongji Medical College, Huazhong University of Science and Technology, Wuhan 430030, China

Abstract

Objective To assess the outcomes of one-stage limb reconstruction after removal of skin cancers defect.

Methods This prospective study was conducted from September 2017 to January 2020 and included 15 patients. All patients underwent extensive tumor resection and one-stage Pelnac® reconstruction of large skin defects, and regular postoperative follow-up was scheduled. At the 6-month follow-up, tumor recurrence and scar quality was assessed using the Vancouver Scar Scale (VSS). None of the patients exhibited infection, wound necrosis, hematoma, seroma, or recurrence.

Results All the skin grafts were well accepted by the patients. Nine patients reported normal or near-normal sensory function, while six reported slight sensory loss. No cases of significant functional loss were observed. We enrolled 10 men and 5 women with a mean age of 63.9 years (range: 46–78 years). The mean follow-up duration was 20.6 months (range: 12–36 months). The skin tumors were located on the feet (n = 4), forearms (n = 3), and legs (n = 8). The malignant tumors included malignant melanomas (13.3%), basal cell carcinomas (33.3%), and squamous cell carcinomas (53.3%). The mean operative time was 40.7 min. Two patients underwent radiotherapy. The average length of hospital stay was 2.6 days. The mean skin defect area was 33.2 cm^2 (range: 16.6–51.6 cm^2). The patient satisfaction score (regarding the aesthetic appearance of the grafted area) was 79.7/100, and the VSS score was 3.8.

Conclusion Pelnac® dermal templates facilitate efficient and reliable reconstruction of skin defects after skin cancer resection.

Received: 10 May 2022
Revised: 5 July 2022
Accepted: 21 July 2022

Key words: skin cancer; Pelnac®; large-scale skin reconstruction

Large-scale skin reconstruction after major tumor resection is challenging for both orthopedic and plastic surgeons [1–3]. Unlike traumatic tissue loss, the defect area may be large, and the muscle, tendon, and periosteal tissues may have to be removed. In addition, the risk of tumor recurrence and likely subsequent therapy (adjuvant or neoadjuvant radiation) must be considered prior to surgery [3]. Treating cancer-related tissue defects is critically important for functional and aesthetic rehabilitation, elimination of scar contractures, and prevention of severe disability. The surgeon must consider the patient's age and general status, skin defect area, planned adjuvant treatment, comorbidities (such as diabetes or infection), and cosmesis [4]. This is especially important in older patients with locally advanced cancers, systemic diseases, or a history of skin tumor recurrence. Skin grafts or free flaps have traditionally been used to cover large soft tissue defects after oncological demolition [5–6]. Conventional flaps include muscular, myofascial, myocutaneous, and fasciocutaneous flaps [7–10]. However, these are associated with donor site morbidity, unreliability, and extended operating times [11]. Flap surgery is frequently difficult in older patients, those with systemic diseases and/or limited donor sites, and those undergoing adjuvant or neoadjuvant radiation therapy [12, 13]. Short operating time, brief hospitalization, and low

✉ Correspondence to: Weiwei Lu. Email: 215285906@qq.com

complication rates are important. Artificial dermis is an effective and reliable alternative with few complications when the use of traditional skin grafts or free flaps are restricted. The artificial dermis has been used for various surgical reconstructions for over two decades [14]. However, few reports on the use of the dermis for the one-stage reconstruction of complex cancer-related soft tissue defects have been reported.

This prospective study enrolled 15 patients with full-thickness defects and exposed bones or tendons (i.e., wide and deep wounds) who underwent one-stage full-skin reconstruction using an artificial dermis (Pelnac®; Gunze, Kyoto, Japan). We evaluated the efficacy, safety, and aesthetic outcomes.

Patients and methods

This prospective study was conducted between September 2017 and January 2020. The inclusion criterion was wound defects after enlarged skin resection. Early tumors (stages I and II) are the best candidates for a one-stage procedure. Advanced cases requiring more extensive surgery and a more complicated tumor-related treatment schedule, which will significantly delay the healing process, are not suitable for this treatment. The exclusion criteria were diabetes, heavy smoking, infected wound, and poor compliance, all of which affect wound healing. This study was approved by the ethics committee of Tongji Medical College, Huazhong University of Science and Technology, China. Informed consent was obtained from all the patients. The China Food and Drug Administration has approved the artificial dermis, Pelnac®, for clinical use.

Data were collected for 15 patients who underwent skin cancer enlarged resection and one-stage large skin reconstruction using an artificial dermal matrix, including their age, sex, and wound area (Table 1). None of the patients were lost to follow-up. There were 10 men and 5 women, with a mean age of 63.9 (range: 46–78, std: 10.4) years. The malignant tumors included malignant melanoma (13.3%), basal cell carcinoma (53.3%), and squamous cell carcinoma (33.3%). The mean area of skin loss was 33.2 (range: 16.6–51.6, std: 9.9) cm^2.

All operations were performed in a standard sterile environment. The first stage involved extensive tumor resection according to recognized guidelines. If the bone was exposed, Kirschner wires were used to create small holes on the bony surface to induce punctate bleeding. If the skin cancer had infiltrated the bone, osteotomy was performed to access the bleeding points. The second stage involved the application of an artificial dermis (Pelnac®), which was used to cover the wounds following the manufacturer's protocol. After immersion in saline for 15 s, the Pelnac® template was trimmed to the shape and size of the wound to achieve tension-free closure. Next, the Pelnac® template was sutured to the surrounding skin using 4/0 Prolene sutures. Small drainage holes were created in the outer layer to facilitate exudation. The Pelnac® template was inspected every 2–3 days. At approximately 3–4 weeks, based on the wound area and depth, new vascularized skin usually formed, so the outer layer of the Pelnac® template could be peeled off. The type of tumor, size of the wound defect, length of hospitalization, operative time, healing time, and surgical complications were recorded (Table 2).

During the follow-up (minimum 12 months), patient satisfaction with appearance was rated on a 100-point scale, with normal skin as the reference. Scar quality was evaluated using the Vancouver Scar Scale (VSS), which includes four items (pigmentation, pliability, vascularity, and height) [15]. Higher scores indicate more severe scarring. Sensory recovery was evaluated based

Table 1 Postoperative data collected

ID	Age (years)	Sex	Wound side	Subjective satisfaction with the aesthetic appearance	Sensation (A: near normal;B: slight loss;C: significant loss)	The vancouver Scar Scale value
1	46	F	Foot	90	A	2
2	49	M	Leg	85	A	3
3	56	M	Forearm	85	A	3
4	65	M	Leg	80	B	4
5	78	F	Foot	80	A	4
6	67	M	Forearm	85	B	4
7	69	F	Leg	75	A	3
8	51	M	Leg	80	A	3
9	55	M	Foot	90	A	4
10	76	M	Forearm	75	B	3
11	68	F	Leg	80	A	4
12	76	M	Leg	75	B	5
13	74	M	Foot	70	B	5
14	67	F	Leg	65	B	6
15	61	M	Leg	80	A	4

on patient responses as "normal or near-normal," "slight loss," "significant loss," or "complete loss" compared with the contralateral uninjured area or the normal tissue next to the wound (Table 2).

Results

The average follow-up period was 20.6 (range: 12–36, std: 7.9) months. The average time from placing the Pelnac® template to recovery was 37.5 (range: 28–56, std: 7.8) days. No infections, hematomas, or seromas were observed in any patient during the Pelnac® phase. Only one patient who received adjuvant radiation therapy experienced mild neodermal ulceration that healed spontaneously without any residual deficit. All the skin grafts were obtained. No tumor recurrence was observed. Patient satisfaction and VSS scores were assessed by a surgeon who was not involved in the treatment. The average patient satisfaction score for the aesthetic appearance of the grafted area was 79.7 (range: 65–90, std: 7.2), while the average VSS score was 3.8 (range: 2–6, std: 1.0). Nine patients reported normal or near-normal sensory function, six reported slight sensory loss, and none reported significant loss (Table 2). The clinical case is shown in Fig. 1.

The patients included 10 (66.7%) men and 5 (33.3%) women. The mean patient age was 63.9 (range: 46–78, std: 10.4) years. The mean follow-up period was 20.6 (range: 12–36, std: 7.9) months. The tumors included malignant melanomas (13.3%), basal cell carcinomas (53.3%), and squamous cell carcinomas (33.3%). The tumor sites were the legs ($n = 8$), forearms ($n = 3$), and feet ($n = 4$).

The mean area of skin loss was 33.2 (range: 16.6–51.6, std: 9.9) cm^2. The mean operating time was 40.7 (range: 30–59, std: 7.7) min. The average length of hospital stay was 2.6 (range: 2–4, std: 0.6). The mean healing time was 37.5 (range: 28–56, std: 7.8) days. The mean VSS score was 3.8 (range: 2–6, std: 1.0), indicating satisfactory cosmetic results (flat, pliable graft with normal pigmentation and vascularization not fixed to the underlying bone) in all patients.

Discussion

Larger soft tissue defects often require split-thickness skin grafts or local, regional, or fasciocutaneous flaps [16–17]. Autologous skin flaps remain the major reconstruction option for large, full-thickness soft tissue defects [9, 18]. Pelnac® (Gunze, Kyoto, Japan), first described by Suzuki *et al.* [19], is an acellular bilayer dermal substitute derived from collagen. The lower layer is a porous, three-dimensional atelocollagen matrix that serves as a scaffold supporting epidermal cell growth, and the upper layer is made of semipermeable silicone and serves as a temporary epidermis that protects against infection and mechanical trauma [20–21]. The dermal matrix of porcine type I collagen is nearly identical to that of human collagen; it is not perceived as an antigen, and the rejection rate is low [22]. The dermal collagen matrix is gradually replaced by endogenous collagen during healing, and a new vascularized skin usually forms. Replacement occurs gradually according to wound size, depth, and radiotherapy status. Prolonged and complicated procedures can compromise wound healing. In all of our patients, Pelnac® successfully covered complex wounds with exposed bones or tendons. The cosmetic results were good, and all outcomes were satisfactory.

Pelnac® has been used to treat traumatic wounds

Table 2 Preoperative clinical data of the patients

ID	Tumor type	Skin loss (cm^2)	Operation time (min.)	Length of hospitalization (days)	Healing time (days)	Complication	Follow -up (months)
1	BC	16.6	30	1+1	28	No	12
2	BC	24.4	32	1+1	35	No	12
3	BC	28.6	35	1+1	36	No	15
4	SC	36.0	40	1+2	42	No	24
5	MM	32.5	41	1+1	32	No	24
6	SC	40.4	45	1+2	45	No	36
7	SC	28.8	38	1+1	30	No	12
8	BC	30.1	40	1+2	33	No	18
9	BC	19.6	31	1+1	28	No	12
10	BC	37.9	42	1+2	36	No	24
11	BC	27.0	41	1+1	32	No	18
12	SC	42.5	48	1+2	45	No	24
13	MM	48.4	50	1+2	45	No	24
14	SC	51.6	59	1+3	56	Mild neodermal ulceration	36
15	BC	34.2	39	1+2	39	No	18

BC, basal cell carcinoma; SC, squamous cell carcinoma; MM, malignant melanoma

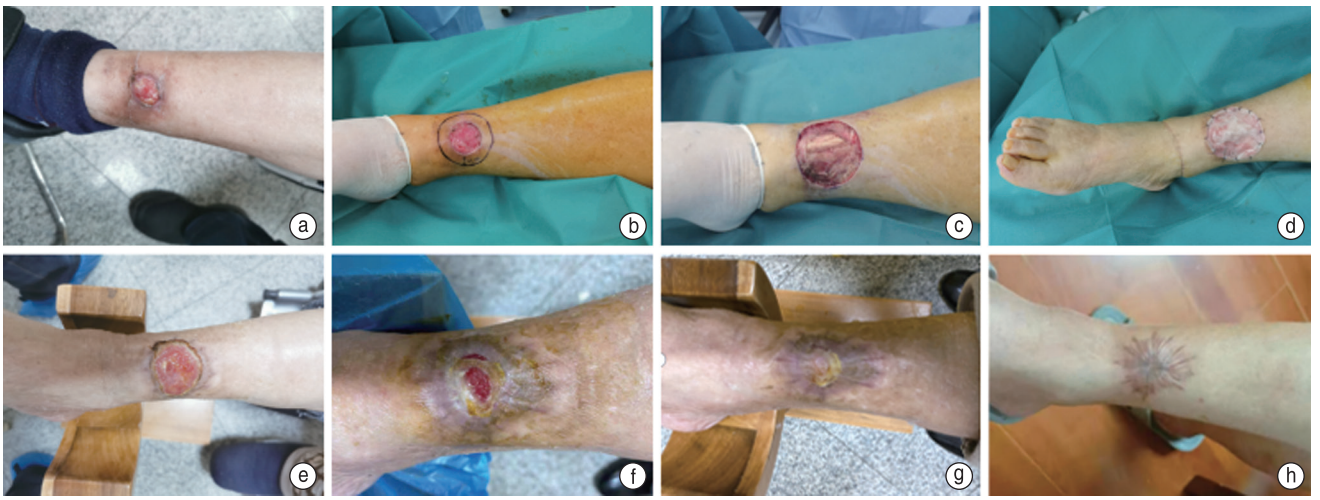

Fig. 1 A clinical case of a 69-year-old woman with recidivate SC at the right leg underwent wide excision and reconstruction with Pelnac®. (a) Preoperative view; (b, c) Wide and deep excision of tumors with soft-tissue defect (28.8 cm^2) and bone and tendon exposure; (d) Pelnac® coverage; (e) Wound bed outer layer of the Pelnac® template peeled off; (f, g) Wound healing on the 15th and 30th day after the Pelnac® template was peeled off; (h) At the follow-up (12 months), the patient achieved an acceptable aesthetic appearance (75%) and a satisfying functional recovery

and burn scars, including wounds created by removing giant nevi and ulcer repair [14, 23–29]. However, no study has evaluated one-stage application after large tumor resection. The application is simple, and it is possible to cover large defects. Moreover, no donor site morbidity was observed. The major disadvantage is that the healing time is longer than that after placement of traditional autologous skin flaps for large and deep wound [18, 30–31]. However, we found that Pelnac® was effective, providing durable coverage via a simple and well-tolerated procedure without donor site morbidity. In addition, early detection of local tumor recurrence is possible, and unlike autologous skin flaps, Pelnac® preserves the original surgical margins. Thus, the wound can be temporarily closed, resulting in pathological results [32]. Using an artificial dermis does not preclude skin graft placement if one-step surgery is insufficient. A high-quality surgical bed is essential for the vascularization of the artificial dermis. In six (40%) of our patients, Pelnac® was applied directly to the bone, with satisfactory results. As some studies have found that Pelnac® triggered peripheral neoangiogenesis in the dermal matrix of an avascular wound bed [26], we used a Kirschner wire to drill the bony surface and induce punctate bleeding. This improved the reliability and efficiency of the simple and safe operation.

Although the results are encouraging, caution is needed when wounds are infected, treating patients with diabetes, heavy smokers, patients receiving radiotherapy, and those on long-term glucocorticoids. Two of our patients received radiation after surgery; one exhibited mild new-onset skin necrosis that healed spontaneously without residual deficits. The dermal substitute provided excellent support, and the new skin was pliable and aesthetically acceptable.

Conclusion

Reconstruction of a large area of skin after cancer resection remains challenging. To our knowledge, this is the first report to evaluate one-stage Pelnac® reconstruction of complex wounds following cancer resection. Although auto skin grafting is a reliable reconstruction method, it is invasive, may cause complications in the donor area, and may be associated with aesthetic complications and a high failure rate. In our clinical series, the application of Pelnac® resulted in satisfactory cosmetic outcomes with low morbidity, few complications, and good patient satisfaction. We believe that this artificial dermis is a reliable alternative for reconstructing complex wounds after cancer resection. Further research with histological evidence and an increased number of cases is needed to strengthen these findings.

Acknowledgments

Not applicable.

Funding

Not applicable.

Conflicts of interest

The authors indicated no potential conflicts of interest.

Author contributions

All authors contributed to data acquisition and interpretation and reviewed and approved the final version of this manuscript.

Data availability statement

Not applicable.

Ethical approval

Not applicable.

References

1. Baker BG, Oudit D. The modified bipedicled flap for reconstruction of oncological skin defects of the trunk and extremities. J Plast Reconstr Aesthet Surg. 2020;73:913-920.
2. Ratycz MC, Lender JA, Gottwald LD. Multiple dorsal hand actinic keratoses and squamous cell carcinomas: a unique presentation following extensive UV nail lamp use. Case Rep Dermatol. 2019;11(3):286-291.
3. Ker H, Al-Murrani A, Rolfe G, et al. WOUND study: A cost-utility analysis of negative pressure wound therapy after split-skin grafting for lower limb skin cancer. J Surg Res. 2019;235:308-314.
4. Global Burden of Disease Child and Adolescent Health Collaboration, Kassebaum N, Kyu HH, et al. Child and Adolescent Health From 1990 to 2015: Findings From the Global Burden of Diseases, Injuries, and Risk Factors 2015 Study. JAMA Pediatr. 2017;171(6):573-592.
5. Okada A, Pereira DD, Montag E, et al. Optimizing outcomes in free flap breast reconstruction in the community hospital setting: A stepwise approach to DIEP/SIEA flap procedures with banking a hemiabdominal flap. J Reconstr Microsurg. 2017;33(7):474-482.
6. Nowacki M, Pietkun K, Jundziłł A, et al. Use of adipose-derived stem cells to support topical skin adhesive for wound closure: A preliminary report from animal in vivo study. Biomed Res Int. 2016;2016:2505601.
7. Lee Y, Woo SH, Kim YW, et al. Free flaps for soft tissue reconstruction of digits. Hand Clin. 2020;36(1):85-96.
8. Lim JX, Chung KC. VY advancement, thenar flap, and cross-finger flaps. Hand Clin. 2020;36(1):19-32.
9. Segal KL, Nelson CC. Periocular reconstruction. Facial Plast Surg Clin North Am. 2019;27(1):105-118.
10. Bradford BD, Lee JW. Reconstruction of the forehead and scalp. Facial Plast Surg Clin North Am. 2019;27(1):85-94.
11. Jo DI, Yang HJ, Kim SH, et al. Coverage of skin defects without skin grafts using adipose-derived stem cells. Aesthetic Plast Surg. 2013;37(5):1041-1051.
12. Global Burden of Disease Cancer Collaboration, Fitzmaurice C, Abate D, et al. Global, Regional, and National Cancer Incidence, Mortality, Years of Life Lost, Years Lived With Disability, and Disability-Adjusted Life-Years for 29 Cancer Groups, 1990 to 2017: A Systematic Analysis for the Global Burden of Disease Study. JAMA Oncol. 2019;5(12):1749-1768.
13. Wang L, Wu F, Liu C, et al. Low-level laser irradiation modulates the proliferation and the osteogenic differentiation of bone marrow mesenchymal stem cells under healthy and inflammatory condition. Lasers Med Sci. 2019;34(1):169-178.
14. De Francesco F, Busato A, Mannucci S, et al. Artificial dermal substitutes for tissue regeneration: comparison of the clinical outcomes and histological findings of two templates. J Int Med Res. 2020;48(8):300060520945508.
15. Dantzer E, Queruel P, Salinier L, et al. Dermal regeneration template for deep hand burns: clinical utility for both early grafting and reconstructive surgery. Br J Plast Surg. 2003;56(8):764-774.
16. Markeson D, Pleat JM, Sharpe JR, et al. Scarring, stem cells, scaffolds and skin repair. J Tissue Eng Regen Med. 2015;9(6):649-668.
17. Onesti MG, Fino P, Fioramonti P, et al. Reconstruction after skin cancer excision through a dermal induction template: our experience. Int Wound J. 2016;13(2):198-203.
18. Leedy JE, Janis JE, Rohrich RJ. Reconstruction of acquired scalp defects: an algorithmic approach. Plast Reconstr Surg. 2005;116(4):54e-72e.
19. Suzuki S, Kawai K, Ashoori F, et al. Long-term follow-up study of artificial dermis composed of outer silicone layer and inner collagen sponge. Br J Plast Surg. 2000;53(8):659-666.
20. Hao Z. Application of Pelnac® Artificial Dermis Combined with VSD in the Repair of Limb Wounds. J Invest Surg. 2020;33(7):642-643.
21. Liu T, Qiu C, Ben C, et al. One-step approach for full-thickness skin defect reconstruction in rats using minced split-thickness skin grafts with Pelnac overlay. Burns Trauma. 2019;7:19.
22. Keyes JT, Lockwood DR, Utzinger U, et al. Comparisons of planar and tubular biaxial tensile testing protocols of the same porcine coronary arteries. Ann Biomed Eng. 2013;41(7):1579-1591.
23. Hashemi SS, Mohammadi AA, Kabiri H, et al. The healing effect of Wharton's jelly stem cells seeded on biological scaffold in chronic skin ulcers: A randomized clinical trial. J Cosmet Dermatol. 2019;18(6):1961-1967.
24. Lou X, Xue H, Li G, et al. One-stage pelnac reconstruction in full-thickness skin defects with bone or tendon exposure. Plast Reconstr Surg Glob Open. 2018;6(3):e1709.
25. Lv Z, Wang Q, Jia R, et al. Pelnac® artificial dermis assisted by VSD for treatment of complex wound with bone/tendon exposed at the foot and ankle, A prospective study. J Invest Surg. 2020;33(7):636-641.
26. Lembo F, Cecchino LR, Parisi D, et al. Utility of a new artificial dermis as a successful tool in face and scalp reconstruction for skin cancer: analysis of the efficacy, safety, and aesthetic outcomes. Dermatol Res Pract. 2020;2020:4874035.
27. Suzuki S, Morimoto N, Yamawaki S, et al. A case of giant naevus followed up for 22 years after treatment with artificial dermis. J Plast Reconstr Aesthet Surg. 2013;66(8):e229-233.
28. Harish V, Raymond AP, Maitz PK. Reconstruction of soft tissue necrosis secondary to cryoglobulinaemia. J Plast Reconstr Aesthet Surg. 2014;67(8):1151-1154.
29. Lv Z, Yu L, Wang Q, et al. The use of dermal regeneration template for treatment of complex wound with bone/tendon exposed at the forearm and hand, a prospective cohort study. Medicine (Baltimore). 2019;98(44):e17726.
30. Zeng RX, He JY, Zhang YL, et al. Experimental study on repairing skin defect by tissue-engineered skin substitute compositely constructed by adipose-derived stem cells and fibrin gel. Eur Rev Med Pharmacol Sci. 2017;21(3 Suppl):1-5.
31. Rogers-Vizena CR, Lalonde DH, Menick FJ, et al. Surgical treatment and reconstruction of nonmelanoma facial skin cancers. Plast Reconstr Surg. 2015;135(5):895e-908e.
32. Laitinen MK, Parry MC, Le Nail LR, et al. Locally recurrent chondrosarcoma of the pelvis and limbs can only be controlled by wide local excision. Bone Joint J. 2019;101-B(3):266-271.

DOI 10.1007/s10330-022-0574-4
Cite this article as: Shi J, Gao M, Zhu HJ, et al. One-stage limb Pelnac® reconstruction after removal of skin cancer: safety, efficacy, and aesthetic outcomes. Oncol Transl Med. 2022;8(4):196-200.

Oncology and Translational Medicine
DOI 10.1007/s10330-022-0549-9
August 2022, Vol. 8, No. 4, P201–P208

CASE REPORT

Primary malignant melanoma of the esophagus successfully treated with camrelizumab: A case report and literature review*

Gaoyang Lin[1], Xin Zheng[2], Fuman Wang[1], Daijun Xing[2], Yufeng Cao[2] (✉)

[1] Department of Cardiothoracic Surgery, The Affiliated Qingdao Hiser Hospital of Qingdao University (Qingdao Hospital of Traditional Chinese Medicine), Qingdao 266033, China
[2] Department 3 of the Cancer Center, The Affiliated Qingdao Hiser Hospital of Qingdao University (Qingdao Hospital of Traditional Chinese Medicine), Qingdao 266033, China

Abstract

An 83-year-old Chinese woman presented with a 3-month history of dysphagia. She also had a history of hypertension, type 2 diabetes, fundus hemorrhage, and cataract but no history of cutaneous, ocular, or other-site melanomas. Upper gastrointestinal tract angiography revealed gastritis and duodenal diverticulum; thus, an endoscopic review was recommended. Enhanced computed tomography of the chest and upper abdomen revealed the following: (1) Esophageal space-occupying lesions and mediastinal lymph node enlargement (considering the high possibility of esophageal cancer, further endoscopy was recommended) and (2) A small amount of right pleural effusion, with no significant lymph node infiltration or distant metastasis. Esophagoscopy identified a bulge mass blocking the esophagus from 23 to 30 cm from the incisors. The upper mass had a spherical clustering, while the lower mass significantly festered. Pathological biopsy samples were obtained from the esophagus 23 and 28 cm from the incisors. Tissue biopsy showed proliferation of large round tumor cells and melanocytes. Immunohistochemistry showed positive findings for HMB45 and MelanA; partially positive findings for S100, CK7, CK5/6, CAM5.2, LCA, P63, and TTF-1; and negative findings for Syn. The Ki-67 positivity index was approximately 60%. Based on these findings, the patient was diagnosed with malignant esophageal melanoma with enlarged mediastinal lymph nodes. She was then treated with five cycles of camrelizumab therapy combined with chemotherapy from October 18, 2019, to May 5, 2020. Gastroscopy review following two courses of combination therapy revealed that the esophagus was 23–25 cm away from the incisors, and there were two continuous uplifted and beaded masses that had a smooth and black surface, with each of them having a length and diameter of approximately 1 cm. Melanosis of the mucosa around the lumen was observed at 40 cm from the incisors to the cardia; the dentate margin was clear; and the cardia had no stenosis. The patient then received five courses of combination therapy and became consistently stable after partial remission. No severe adverse events related to the immunotherapy were recorded. Camrelizumab may be a viable treatment option for patients with PMME. Additional evidence from future clinical trials and research is necessary to fully validate our findings.

Received: 10 January 2022
Revised: 26 April 2022
Accepted: 21 May 2022

Key words: primary malignant melanoma of the esophagus; PD-1 mAb; camrelizumab; immunotherapy

Melanoma is the fifth most common cancer in the United States and accounts for 5.6% of newly diagnosed cancers [1]. It is characterized by uncontrolled proliferation of melanocytes mainly found in the epidermis and constitutes 91.2% of all melanomas [2]. The non-cutaneous forms of primary melanoma include ocular and mucosal lesions and represent 5.2% and 1.3% of all melanomas, respectively [2–3]. The mucosal subtypes arise most commonly in the head and neck and far less commonly in the gastrointestinal and urogenital tracts [2]. In particular, primary esophageal melanoma is exceedingly rare and accounts for 0.5% of newly identified primary melanomas [4]. Primary malignant melanoma of the esophagus (PMME) is a much extremely rare disease accounting for

✉ Correspondence to: Yufeng Cao. Email: lingaoyanglynn@126.com
* Supported by a grant from the Qingdao 2020 Medical Scientific Research Guidance Plan (No. 2020-WJZD036).

0.1%–0.2% of all malignant esophageal tumors and 0.5% of all non-cutaneous melanomas [5–6]. It is highly aggressive with a high potential for metastasis. Almost half of patients with PMME have distant metastasis upon diagnosis, and the 5-year survival rate is between 2.2% and 37.5% [7–10]. The diagnosis of PMME should be based on the combination of morphological examination, pathological examination, and immunohistochemistry findings [8]. The main treatment remains to be radical resection of the tumor. However, the optimal adjuvant therapies for PMME have not yet been established [8]. Patients with PMME tend to have a poorer response to chemotherapies than do those with other melanomas, and previous studies have indicated that the currently available treatment is insufficient. The clinicopathological characteristics of PMME have been rarely reported, and no comprehensive treatment strategy has been established because of the lack of cases and strong evidence. Recently, immunotherapy has been the preferred choice for unresectable or metastatic melanomas, and as a result, the prognosis of patients with cutaneous metastatic melanoma has improved. Camrelizumab is a fully humanized IgG4 programmed death 1 (PD-1) immune checkpoint inhibitor antibody. It has been shown to yield a more favorable survival benefit in previously untreated patients with metastatic melanoma not harboring a BRAF/C-KIT/NRAS mutation [11]. Herein, we report the case of an elderly patient with PMME and multiple mediastinal lymph node enlargement who was successfully treated with camrelizumab without recurrence.

Case presentation

An 81-year-old Chinese woman visited the Zhengzhou Puyang People's Hospital on September 10, 2019 and presented with a 1-month history of dysphagia and consequently, weight loss. She also had a history of type 2 diabetes for 20 years, fundus hemorrhage and cataract for many years, and hypertension for 10 years but no family or medical history of other-site melanomas. On October 1, 2019, the patient visited the Liaocheng People's Hospital. Considering the presence of esophageal occupancy, gastritis, and duodenal diverticulum based on the upper gastrointestinal tract angiography findings, an endoscopic review was recommended. Enhanced computed tomography (CT) of the chest and upper abdomen (Fig. 1) conducted on October 8, 2019 upon visit to the Affiliated Qingdao Hiser Hospital of Qingdao University revealed the following: (1) esophageal space-occupying lesions and mediastinal lymph node enlargement (considering the possibility of esophageal cancer, further endoscopy was recommended) and (2) a small amount of right pleural effusion. Gastroscopy (Fig. 2) revealed that the esophagus was 23 cm from the portal bump or blocked the lumen, and the mass continued until 30 cm from the portal. The upper mass had a spherical clustering, while the lower mass showed significant ulceration. Pathological biopsy samples were obtained from the esophagus 23 and 28 cm from the incisors. Immunohistochemistry showed positive findings for HMB45 and MelanA; partially positive findings for S100, CK7, CK5/6, CAM5.2, LCA, P63, and TTF-1; and negative findings for Syn. The Ki-67 positivity index was approximately 60%. Based on these findings, the patient was diagnosed with malignant esophageal melanoma (Fig. 3). Considering the specific situation of the patient, her family refused surgery and further genetic testing. A total of five cycles of immune checkpoint inhibitor therapy combined with chemotherapy were administered from October 18, 2019, to May 5, 2020. According to the National Comprehensive Cancer Network (NCCN) guidelines for malignant melanoma treatment and based on the dominant effect of the latest domestic PD-1 mAb of camrelizumab beads in the treatment of malignant melanoma, she was started on intravenous administration of camrelizumab (200 mg, once every 3 weeks; Jiangsu Hengrui Pharmaceutical Co., Ltd., S20190027) + dacabzine (0.3 g, 1–5 days every 3 weeks; Nanjing Pharmaceutical Factory Co., Ltd., H32026231) + cisplatin (20 mg, 1–5 days; 65 mg/m^2, every 3 weeks; Qilu Pharmaceutical Co., Ltd., H20023460) + vincristine (1 mg, 1–2 days; 1.2 mg/m^2, every 3 weeks; Zhejiang Hanzheng Pharmaceutical Co., Ltd., H20043326). During chemotherapy, one to two degrees of nausea, vomiting, and loss of appetite were observed; meanwhile, no obvious myelosuppression and skin capillary hyperplasia were noted. The regimen was adjusted during cycle 4 owing to severe gastrointestinal reactions as follows: camrelizumab (200 mg, 1 day before chemotherapy, every 3 weeks; Jiangsu Hengrui Pharmaceutical Co., Ltd., S20190027) + dacabzine (0.3 g, 1–5 days every 3 weeks; Nanjing Pharmaceutical Factory Co., Ltd., H32026231) + nedaplatin (30 mg, 1–3 days; 60 mg/m^2, every 3 weeks; Qilu Pharmaceutical Co., Ltd., H20050563) + vindesine (4 mg, once every 3 weeks; Shandong Luoxin Pharmaceutical Group Co., Ltd., H20067018). During cycle 4, grade 1 fatigue was the only adverse event observed, and the partial treatment response was maintained for only 15 days. However, all treatments were discontinued for approximately 100 days owing to the nationwide coronavirus disease outbreak in 2019. Thereafter, cycle 5 was continued (protocol versus cycle 4). No severe immunotherapy-related adverse events (irAEs) were recorded. Eating limitations were significantly reduced after cycle 1 therapy combined with chemotherapy and gradually disappeared after cycle 3; thereafter, the patient gained weight. Gastroscopy (Fig. 4) conducted after two cycles of treatment on December 4, 2019 revealed the following: The esophagus was 23–25

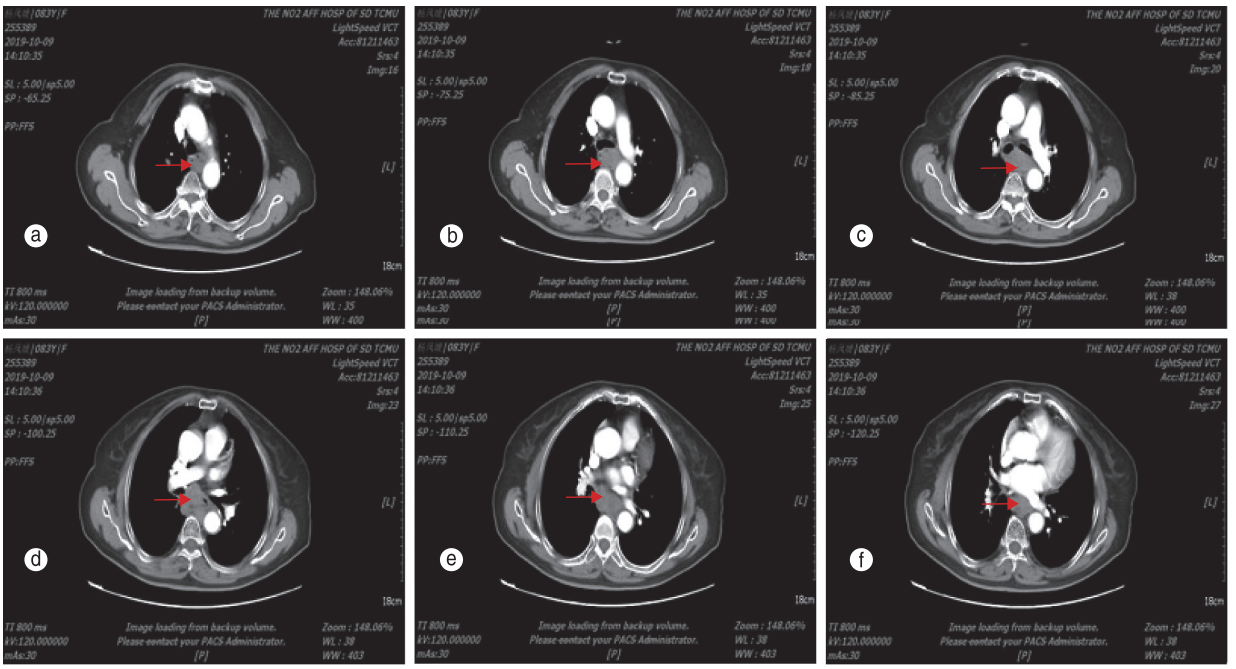

Fig. 1 CT enhancement of chest + upper abdomen on December 9, 2019 shown: esophagel occupying lesions, the lumen was significantly narrow and mediastinal lymph node enlargement (the red arrow shows); pleural effusion on the right side (small amount)

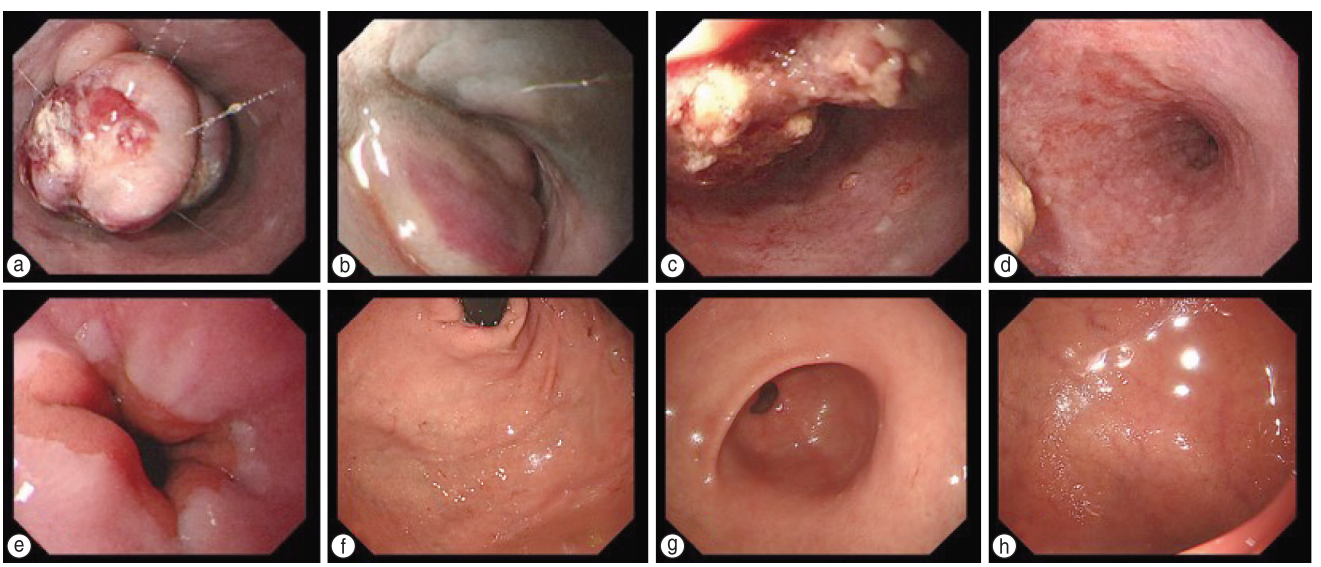

Fig. 2 Gastroscopy shown: (a) incisor to esophagus 23 cm (b) incisor to esophagus 23 cm, (c)incisor to esophagus 28 cm, (d)incisor to esophagus 30 cm, (e) dentate margin, (f) fundus ventriculi, (g) sinuses ventriculi, (h) duodenal bulb; The esophagus from the incisor 23 cm bulge mass block lumen, lumen stenosis, the endoscope is blocked, the mass continued to the esophagus 30 cm from the incisor, the upper segment of the mass is cluster spherical, bright surface sense, local surface ulceration with bleeding, the lower mass ulceration is obvious, covered with moss. From 35 cm from the portal to the cardia, the tooth line is clear and the cardia is not narrow. The gastric floor mucosa is congested and edema, clear, extended after inflation, and the mucus lake is clear and medium. The gastric is curved. Gagastric sinus mucosa congestion and oedema. The door is round, comfortable contraction. The duodenal bulb and lower mucosa are smooth and smooth without stenosis. The esophagus was taken on biopsy 23 cm from the inciaors and 28 cm from the mass,and the upper segment was more brittle and suffered more bleeding. The lower segment of the mass is hard, bleeding can be

cm from the incisors, with two continuous beaded-like bulge masses that had a smooth and black surface and a diameter of approximately 1 cm; melanosis of the mucosa around the lumen was observed at 40 cm from the incisors to the cardia; the dentate margin was clear; and the cardia had no stenosis. Endoscopic ultrasound ring scan (Fig. 5) revealed that at the esophageal bulge, there was a lesion of approximately 1 cm in diameter located in the mucosal

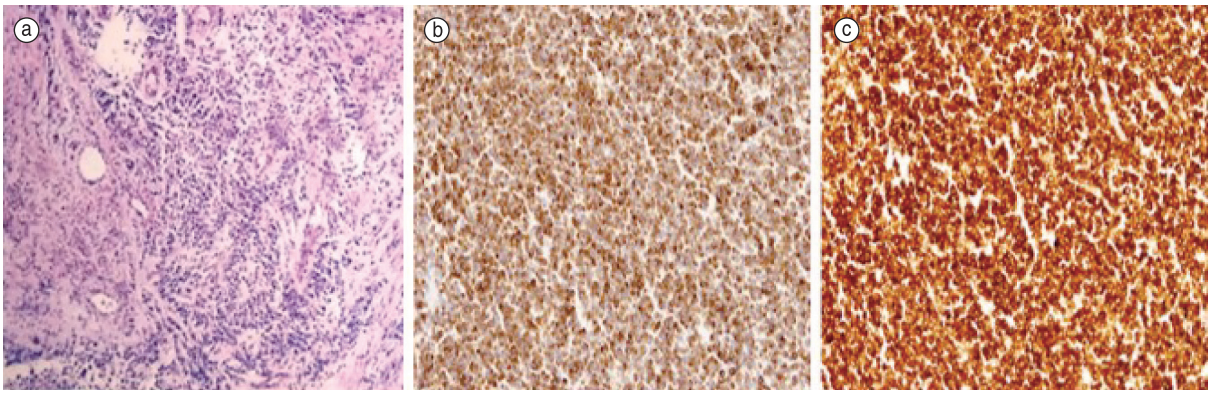

Fig. 3 (a) There was solid proliferation, and tumor cells had large round nuclei. Melanin pigmentation was sparse (HE staining × 100); (b) Tumor cells were difusely positive (HMB-45 immunostaining × 100); (c) Tumor cells were difusely positive (Melan-A immunostaining × 100)

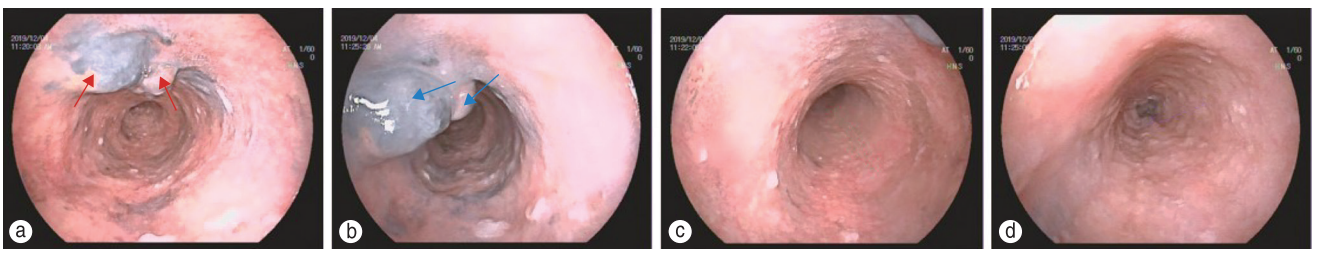

Fig. 4 Review occurred after 2 cycles of treatment on 4 December 2019, as indicated by gastroscopy: the esophagus is seen 23 to 25 cm from the incisors in two continuous bulge masses (red arrow), beaded-like, each raised about 1 cm in diameter, with a smooth black; from aisors 40 cm to the cardia with clear dentate margin (purple arrow) and no atenosis in the cardia (green arrow)

layer, and the echo was heterogeneous. CT (Fig. 6) after two cycles of treatment revealed a significantly better disease status reaching partial remission. CT (Fig. 7) after four cycles of treatment showed that the esophageal tumor continued to shrink; normal swallowing function returned; and the patient condition became stable.

Discussion

Malignant melanoma of the gastrointestinal tract is usually a metastasis from a primary cutaneous source. PMME is extremely rare, accounting for only 0.1%–0.2% of all tumors of the esophagus [12–13]. The incidence of malignant melanoma has increased over the past few decades, and approximately 132,000 individuals develop malignant melanoma each year worldwide [11]. Almost all malignant melanoma cases arise from the skin, and it is reported that only 1% of melanomas arise from the mucosa (head and neck, eyes, and genitourinary and alimentary tracts) [14]. PMME most commonly occurs in men, with a male-to-female sex ratio of 2:1, and the average age of onset is 60.5 years. The tumor is usually located in the middle and lower third of the esophagus (76.2%) [15–16]. Herein, we report a case of recurrent PMME successfully treated with camrelizumab. After the treatment, the difficulty in swallowing and weight loss symptoms dramatically decreased; the patient condition became stable and the survival rate increased; and no irAEs were observed. The patient received camrelizumab therapy for 5 months and showed no further signs of clinical disease progression. Although melanomas arising from the mucosa generally have a worse prognosis than those arising from cutaneous sites, no intrinsic risk factors and specific treatment options have been established. Furthermore, there is no evidence of a difference in sensitivity to camrelizumab therapy between skin and mucosal melanomas. Wang *et al.* [13] reported that in 76 patients, PMME occurred more commonly in men, with a male-to-female sex ratio of 2.17:1. The majority of patients with PMME are symptomatic on diagnosis, with dysphagia being the most common major symptom, as was observed in our case. Concerning the locations of PMME tumors, 92.1% are located in the middle and lower portions of the esophagus, while half of the tumors invade the muscularis propria or further. On endoscopy, PMME usually presents as a well-circumscribed, solid, polypoid tumor with black or purple pigmentation on the surface, sometimes accompanied by ulcers and bleeding [16–17]. In contrast, metastatic melanoma usually has multiple nodular lesions and may be distributed in various parts of the gastrointestinal tract [18]. However, some PMME cases present as a flat lesion [19] or as multinodular lesions that

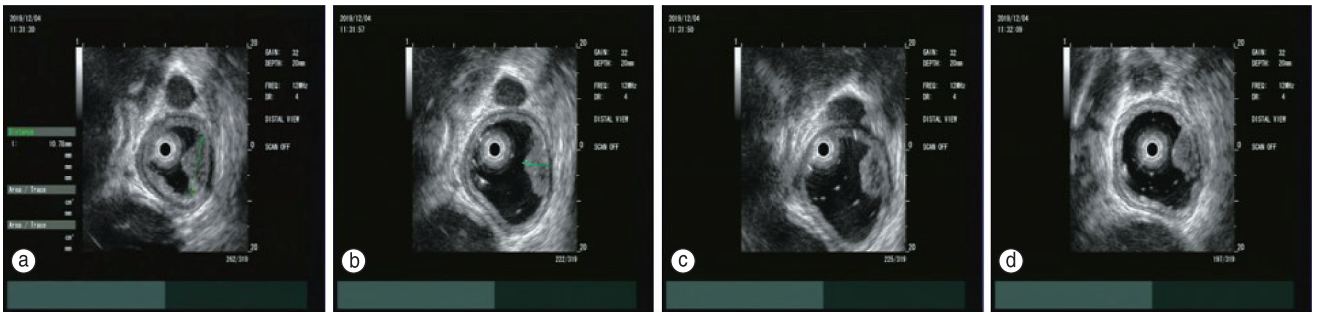

Fig. 5 Ultrasound endoscopic ring scan: At the esophagel bulge, see a lesion of about 1 cm in diameter, located in the mucosal layer, and the echo is heterogeneous

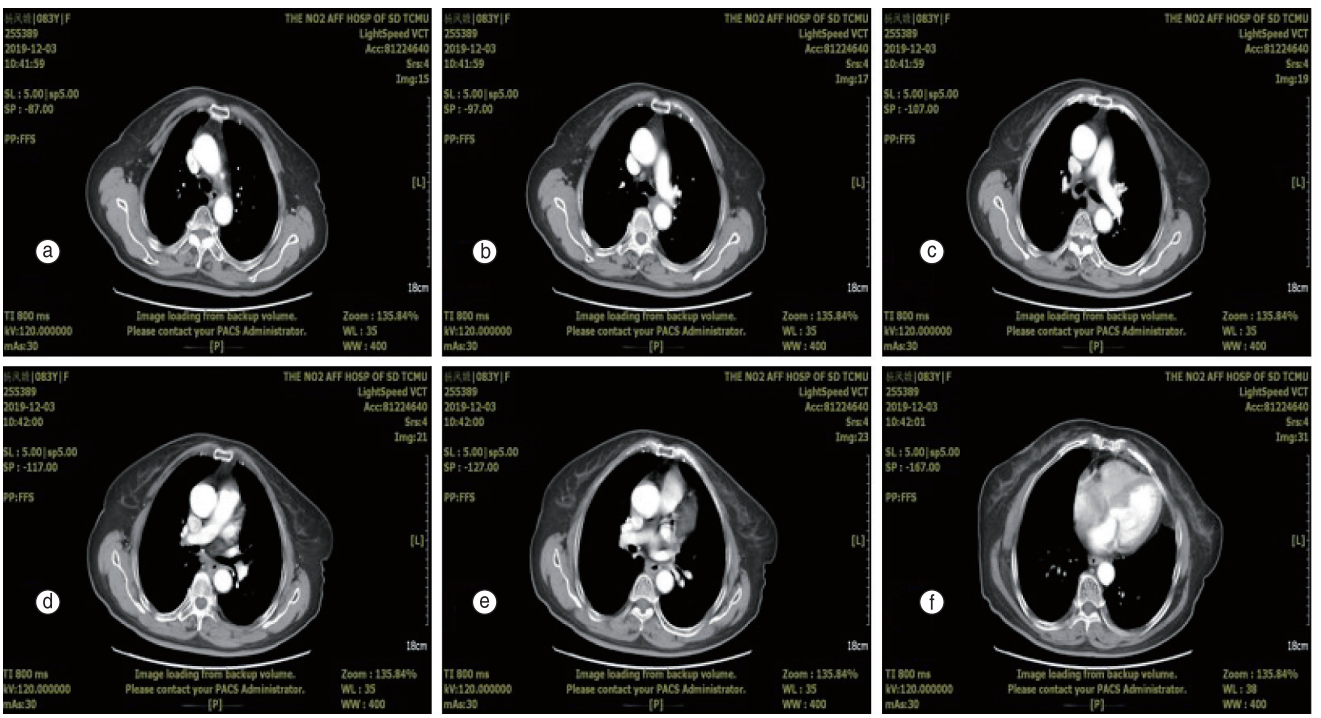

Fig. 6 CT after 2 cycles of treatmnet on December 3, 2019 shown: After esophageal melanoma chemotherapy, the review was significantly better than before, reaching partial remission. The eaophageal occupation decreased signififcantly compared with the previous one, and the mediastinal lymph nodes decreased significantly

are difficult to distinguish from metastatic lesions [20–21]. Surface pigmentation is characteristic of gastrointestinal melanoma. However, some melanomas lack melanin (i.e., the so-called amelanotic melanomas); these account for 10%–25% of all PMME cases and are extremely difficult to distinguish from other tumor types [22]. An accurate preoperative diagnosis of primary malignant melanoma is difficult to make from a biopsy specimen because the biopsy results are easily misinterpreted as indicating undifferentiated carcinoma. Repeated endoscopic biopsy may be required [23]. A definite diagnosis of melanoma depends on an immunohistochemical examination showing positive results for S100 protein, HMB45, and neuron-specific enolase [18].

Surgical resection is the most common treatment, with 77.6% of patients undergoing subtotal esophagectomy or esophagogastrostomy with lymph node dissection. Despite complete excision, recurrence occurred in 89.7% of patients in previous studies. In addition, the interval between primary surgery and recurrence was only 4.5 months [13]. The risk of recurrence is extremely high after an initial staging surgery, which likely reflects the aggressive characteristics of PMME and the important role of adjuvant therapy. Indeed, adjuvant therapy has been shown to increase recurrence-free survival (RFS) and to have varying effects on overall survival (OS) in patients with cutaneous melanoma [24]. A previous trial has suggested that temozolomide-based adjuvant

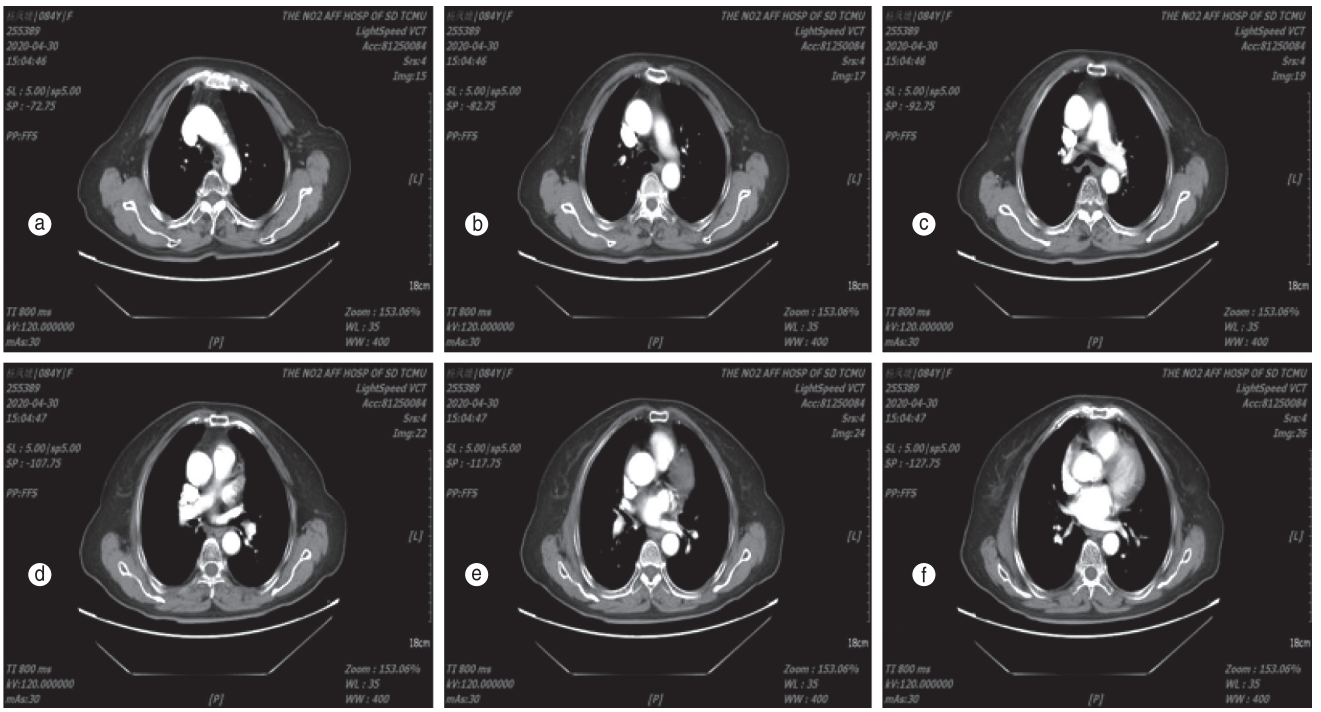

Fig. 7 After 4 cycles of treatment, the reexamination of CT on April 30, 2020 shown: esophageal tumor continued to shrink, and normal swallowing showed no uncomfortable symptoms, and the condition was stable

chemotherapy can improve both RFS and OS in patients with mucosal melanoma [25]. However, because of the rarity of PMME, optimal adjuvant therapies have not yet been established. Postoperative adjuvant chemotherapy may be considered for patients with PMME because it can significantly improve RFS. However, even with adjuvant chemotherapy, the RFS is still much lower in PMME than in other subtypes of mucosal melanoma [25]. A previous phase 3 randomized trial has suggested that adjuvant therapy with ipilimumab can treat stage III melanoma based on a significantly prolonged RFS [26]. In addition, CheckMate 238 showed that among patients undergoing resection of stage IIIB, IIIC, or IV melanoma, adjuvant therapy with nivolumab resulted in a significantly longer RFS and a lower rate of grade 3 or 4 adverse events than did adjuvant therapy with ipilimumab [27]. A previous open-label phase IB trial has shown that the combination of toripalimab with axitinib was tolerable and showed promising antitumor activity in patients with treatment-naive metastatic mucosal melanoma. The patients enrolled in this previous study were all Asians, and the combination therapy used must be validated in a randomized phase III trial that includes a non-Asian population before it can become a standard of care [28]. Camrelizumab combined with apatinib for advanced acral lentiginous melanoma (ALM) phase II research has achieved excellent efficacy is known as a landmark research on acroterminal malignant melanoma. In the initial treatment of metastatic ALM, apatinib combined with camrelizumab not only was safely tolerated but also improved anti-tumor activity and progression-free survival (PFS), benefitting OS. The most common type of melanoma in Asian populations is acroral melanoma. Meanwhile, the incidence of acral melanoma in European and American populations is less than 5%, and the effectivity rate of PD-1 mAb in acroral melanoma treatment is only approximately 14%. The objective response rate (ORR) of camrelizumab combined with apatinib was 22.2%; the DCR reached 77.8%; and the median PFS reached 8 months in patients with metastatic ALM [11]. Moreover, immunotherapy may be effective as adjuvant therapy for patients with PMME.

The role of systemic therapy for metastatic or unresectable PMME remains unclear. The first-line systemic therapy for melanoma is immunotherapy, including nivolumab, ipilimumab, and pembrolizumab, according to the NCCN guidelines. In previous studies, camrelizumab also showed a better therapeutic effect. The traditional cytotoxic chemotherapies have displayed very minimal efficacy against advanced-stage PMME. The overall response rate of chemotherapy in a previous cohort study was only 10.9%, with a short PFS of only 3 months [27]. Other studies have also shown unsatisfactory results of chemotherapy. Over the past decade, the introduction of novel therapies has drastically improved the survival of patients with advanced melanoma, and these therapies are broadly grouped into immune checkpoint inhibitors

(immunotherapy) and BRAF or MEK inhibitors (targeted therapy) [29]. Immune checkpoint inhibitors nivolumab, ipilimumab, and camrelizumab are novel treatment agents for malignant melanoma. These drugs have been reported to demonstrate a substantial clinical benefit for patients with metastatic melanoma, with an ORR of 31.0%–40.0% [30]. A number of previous case reports have suggested that the usefulness of immunotherapy with nivolumab for PMME may be comparable to that for melanoma of other organs. Patients with metastases at the time of diagnosis had a median survival duration of 15.8 months, whereas those who developed metastases later or had unresected stage III disease had an average survival duration of 22.8 months from the date of first diagnosis; the median OS from the first diagnosis was 18.5 months [31]. A nationwide study revealed that marked improvements in OS were associated with the use of targeted therapy and immunotherapy in patients with stage IV melanoma with an unknown primary site [29]. Pablizumab is the first PD-1 inhibitor approved for the treatment of advanced melanoma in China, bringing the treatment of melanoma in China into the era of immunotherapy. Melanoma in Chinese populations is mainly composed of acral and mucosal types; thus, it is necessary to further conduct clinical trials and develop original melanoma-specific immunotherapy drugs suitable for the Chinese population. These findings could be used as a basis in clinical practice and the treatment of PMME; however, more studies are required to prove the benefit.

Conclusion

In conclusion, PMME is an extremely rare but highly aggressive tumor. The special pattern of pigmentation should be recognized while performing endoscopy. The diagnosis of PMME requires careful pathological examination and exclusion of other possible origins in the entire body. Early detection and radical resection of the tumor are critical to ensure favorable outcomes. The effect of adjuvant chemotherapy and radiotherapy is uncertain, and data from large clinical multicenter long-term follow-up studies are lacking. With the continuous development and progress of radiotherapy equipment, precision radiotherapy may be an effective treatment strategy for primary malignant melanoma among patients with advanced or poor general state of malignancy. Novel therapies, including immunotherapy and targeted therapy, may improve the OS in patients with PMME. PD-1 inhibitors may represent a promising option for patients with advanced PMME. However, more evidence is needed from future clinical research to further validate their role.

Acknowledgments

Not applicable.

Funding

Supported by a grant from the Qingdao 2020 Medical Scientific Research Guidance Plan (No. 2020-WJZD036).

Conflicts of interest

The authors indicated no potential conflicts of interest.

Author contributions

Gaoyang Lin drafted the manuscript. Yufeng Cao and Xin Zheng treated the patient. Fuman Wang and Daijun Xing helped search articles. All authors have read and approved the manuscript for submission.

Data availability statement

The SEER dataset was used in the creation of this manuscript. All information of the case presentation was available from standard documentation in the patient's electronic medical record.

Ethical approval

Not applicable.

References

1. Howlader N, Noone AM, Krapcho M, et al. SEER Cancer Statistics Review (CSR), 1975-2016. National Cancer Institute. Update April, 2020 (Revision History). https://seer.cancer.gov/csr/1975_2016/
2. Chang AE, Karnell LH, Menck HR. The National Cancer Data Base report on cutaneous and noncutaneous melanoma: a summary of 84,836 cases from the past decade. The American College of Surgeons Commission on Cancer and the American Cancer Society. Cancer. 1998;83(8):1664-1678.
3. Simons M, Ferreira J, Meunier R, et al. Primary versus Metastatic Gastrointestinal Melanoma: A Rare Case and Review of Current Literature. Case Rep Gastrointest Med. 2016;2016:2306180.
4. Sabanathan S, Eng J, Pradhan GN. Primary malignant melanoma of the esophagus. Am J Gastroenterol. 1989;84(12):1475-1481.
5. Bisceglia M, Perri F, Tucci A, et al. Primary malignant melanoma of the esophagus: a clinicopathologic study of a case with comprehensive literature review. Adv Anat Pathol. 2011;18(3):235-252.
6. Archer HA, Owen WJ. Primary malignant melanoma of the esophagus. Dis Esophagus. 2000;13(4):320-323.
7. Volpin E, Sauvanet A, Couvelard A, et al. Primary malignant melanoma of the esophagus: a case report and review of the literature. Dis Esophagus. 2002;15(3):244-249.
8. Iwanuma Y, Tomita N, Amano T, et al. Current status of primary malignant melanoma of the esophagus: clinical features, pathology, management and prognosis. J Gastroenterol. 2012;47(1):21-28.
9. Zheng J, Mo H, Ma S, et al. Clinicopathological findings of primary esophageal malignant melanoma: report of six cases and review of literature. Int J Clin Exp Pathol. 2014;7(10):7230-7235.
10. Sabat J, Mannan R, Legasto A, et al. Long-term survivor of primary malignant melanoma of the esophagus treated with surgical resection. Int J Surg Case Rep. 2015;6C:182-185.

11. Wang X, Ji Q, Yan X, et al. The impact of liver metastasis on anti-PD-1 monoclonal antibody monotherapy in advanced melanoma: analysis of five clinical studies. Front Oncol. 2020;10:546604.
12. Liu L, Pan T, Wei X. et al. Primary malignant melanoma of the esophagus. Chinese-German J Clin Oncol. 2008;7(3):121-123.
13. Wang X, Kong Y, Chi Z, et al. Primary malignant melanoma of the esophagus: A retrospective analysis of clinical features, management, and survival of 76 patients. Thorac Cancer. 2019;10(4):950-956.
14. D'Angelo SP, Larkin J, Sosman JA, et al. Efficacy and safety of nivolumab alone or in combination with ipilimumab in patients with mucosal Melanoma: A Pooled Analysis. J Clin Oncol. 2017;35(2):226-235.
15. Chen H, Fu Q, Sun K. Characteristics and prognosis of primary malignant melanoma of the esophagus. Medicine (Baltimore). 2020;99(28):e20957.
16. Ishizaki M, Aibara Y, Furuya K. Primary malignant melanoma of the esophagogastric junction: Report of a case. Int J Surg Case Rep. 2013;4(8):700-703.
17. Iwanuma Y, Tomita N, Amano T, et al. Current status of primary malignant melanoma of the esophagus: clinical features, pathology, management and prognosis. J Gastroenterol. 2012;47(1):21-28.
18. Wong K, Serafi SW, Bhatia AS, et al. Melanoma with gastric metastases. J Community Hosp Intern Med Perspect. 2016;6(4):31972.
19. Ueyama H, Yao T, Matsumoto K, et al. Flat-type primary malignant melanoma of the esophagus. Endosc Int Open. 2016;4(6):E687-689.
20. Kouvaras S, Rokkas T, Goga H, et al. Multifocal Gastrointestinal Melanoma. J Gastrointestin Liver Dis. 2019;28:237-240.
21. Zhou YB, Yuan Y, Hu B, et al. Image of the month: primary multifocal malignant melanoma of esophagus co-occurs with esophagogastric junction adenocarcinoma. Am J Gastroenterol. 2016;111(3):312.
22. Koga N, Kubo N, Saeki H, et al. Primary amelanotic malignant melanoma of the esophagus: a case report. Surg Case Rep. 2019;5(1):4.
23. Oshiro T, Shimoji H, Matsuura F, et al. Primary malignant melanoma of the esophagus arising from a melanotic lesion: report of a case. Surg Today. 2007;37(8):671-675.
24. Weber J, Mandala M, Del Vecchio M, et al; CheckMate 238 Collaborators. Adjuvant Nivolumab versus Ipilimumab in Resected Stage III or IV Melanoma. N Engl J Med. 2017;377(19):1824-1835.
25. Lian B, Si L, Cui C, et al. Phase II randomized trial comparing high-dose IFN-α2b with temozolomide plus cisplatin as systemic adjuvant therapy for resected mucosal melanoma. Clin Cancer Res. 2013;19(16):4488-4498.
26. Eggermont AMM, Chiarion-Sileni V, Grob JJ, et al. Adjuvant ipilimumab versus placebo after complete resection of stage III melanoma: long-term follow-up results of the European Organisation for Research and Treatment of Cancer 18071 double-blind phase 3 randomised trial. Eur J Cancer. 2019;119:1-10.
27. Coit DG, Thompson JA, Albertini MR, et al. Cutaneous Melanoma, Version 2.2019, NCCN Clinical Practice Guidelines in Oncology. J Natl Compr Canc Netw. 2019;17(4):367-402.
28. Sheng X, Yan X, Chi Z, et al. Axitinib in Combination With Toripalimab, a Humanized Immunoglobulin G4 Monoclonal Antibody Against Programmed Cell Death-1, in Patients With Metastatic Mucosal Melanoma: An Open-Label Phase IB Trial. J Clin Oncol. 2019;37(32):2987-2999.
29. Verver D, van der Veldt A, van Akkooi A, et al. Treatment of melanoma of unknown primary in the era of immunotherapy and targeted therapy: A Dutch population-based study. Int J Cancer. 2020;146(1):26-34.
30. Robert C, Long GV, Brady B, et al. Nivolumab in previously untreated melanoma without BRAF mutation. N Engl J Med. 2015;372(4):320-330.
31. Rochefort P, Roussel J, de la Fouchardière A, et al. Primary malignant melanoma of the esophagus, treated with immunotherapy: a case report. Immunotherapy. 2018;10(10):831-835.

DOI 10.1007/s10330-022-0549-9
Cite this article as: Lin GY, Zheng X, Wang FM, et al. Primary malignant melanoma of the esophagus successfully treated with camrelizumab: A case report and literature review. Oncol Transl Med. 2022;8(4):201-208.

Patriotism | Innovation | Practicality | Commitment | Coordination | Cultivation

Xiaoping Chen

Academician of the Chinese Academy of Sciences
Professor of Surgery at Tongji Hospital
Affiliated with Tongji Medical College of HUST

"Exceptional skills" Pushing the boundaries and saving lives. Unmatched contributions

"Never give another thought
to time, money,
gains, or losses."